# NACA



# RESEARCH MEMORANDUM



## BOUNDARIES OF SUPERSONIC AXISYMMETRIC FREE JETS

By Eugene S. Love, Mildred J. Woodling,
and Louise P. Lee

Langley Aeronautical Laboratory
Langley Field, Va.



WASHINGTON

October 5, 1956

V





NATIONAL ADVISORY COMMITTEE FOR AERONAUTICS

RESEARCH MEMORANDUM

# BOUNDARIES OF SUPERSONIC AXISYMMETRIC FREE JETS

By Eugene S. Love, Mildred J. Woodling,
and Louise P. Lee

## SUMMARY

Calculations have been made by the method of characteristics of 2960 boundaries of supersonic axisymmetric free jets exhausting from conically divergent nozzles into still air. The calculations cover jet Mach numbers from 1.5 to 3.0, ratio of specific heats of the jet from 1.115 to 1.667, divergence angles of the nozzle from $5^{\circ}$ to $20^{\circ}$, and jet static-pressure ratios from 1 to 10. The results are presented nondimensionally and in a form that facilitates practical use. Some random examples of the effects of the variables involved are shown, and the possibilities of the simulation of one jet by another are examined for jets exhausting into still air and into supersonic streams.

## INTRODUCTION

One of the important characteristics of free jets exhausting into still air is the shape of the jet boundary. Once the shape of the boundary is known, it may be applied to a number of problems for which the condition of constant pressure along the jet boundary is a permissible assumption. Some of these applications have been discussed and illustrated in reference 1. Perhaps the most direct applications occur in the design of airframe components to obtain jet clearance in the static thrust condition and in the assessment of the deflections of the external stream caused by a propulsive jet exhausting from an airplane flying at low to moderate subsonic speeds. Other applications occur in estimating the performance of ejectors having near-constant pressure mixing and in the estimation of pressure on the base annulus separating an exhausting jet from an external supersonic stream. (See ref. 1.)

In reference 1 several calculations were made by the method of characteristics to obtain primarily the shape of the jet boundary, and it was shown that the theoretical nonviscous boundaries agreed satisfactorily with observed experimental boundaries over the region of principal interest, namely, from the nozzle exit to the vicinity of the

maximum diameter of the free jet within the first wavelength. Beyond the maximum diameter, turbulent diffusion significantly affects the boundary shape and generally permits simplified assumptions to be made of the shape. The theoretical boundaries of reference 1 included a few calculations for conically divergent nozzles in which the effects of nozzle divergence angle and ratio of specific heats of the jet were examined for certain arbitrarily chosen initial conditions. The purpose of this paper is to extend the theoretical calculations of boundary shapes for jets exhausting from conically divergent nozzles and to present these boundary shapes in a form convenient for practical use. These boundaries cover the following range of variables: jet Mach numbers from 1.5 to 3.0, jet static-pressure ratios from 1 to 10, nozzle divergence angles from $5^\circ$ to $20^\circ$, and ratio of specific heats of the jet from 1.115 to 1.667.

## SYMBOLS

See figure 1 for clarification of symbols.

| | |
|---|---|
| $M_j$ | jet Mach number; value at nozzle lip immediately ahead of exit |
| $p_j$ | jet static pressure; value at nozzle lip immediately ahead of exit |
| $p_\infty$ | ambient static pressure |
| $r_j$ | radius of jet exit |
| $x$ | distance from plane of nozzle exit measured parallel to jet axis |
| $y$ | perpendicular distance from jet axis |
| $\gamma_j$ | ratio of specific heats of jet |
| $\delta_j$ | initial inclination of free jet boundary at jet exit |
| $\theta_N$ | conical divergence angle or exit angle of nozzle measured with respect to jet axis |

Subscripts:

| | |
|---|---|
| j | jet |
| N | nozzle |

o value at $\theta_N = 0^\circ$

$\infty$ ambient

## CALCULATIONS

### Scope

The calculations were made for all combinations of the following variables: values of $M_j$ of 1.5, 2.0, 2.5, and 3.0; values of $\gamma_j$ of 1.115, 1.200, 1.300, 1.400, and 1.667; values of $\theta_N$ of $5^\circ$, $10^\circ$, $15^\circ$, and $20^\circ$; and values of $\frac{p_j}{p_\infty}$ of 1 to 10 in increments of 0.25.

### Method

The method of characteristics was used throughout. The procedure was identical to that described in the section of appendix A of reference 1 entitled "Solution for Divergent Nozzles."

The leading characteristic lines (fig. 1) and the initial values for the characteristic lines from the center of expansion were computed manually. The characteristic nets were determined on a card-programed electronic calculator.

The calculations were proposed to be carried through only until the maximum diameter of the jet boundary was reached, since the shape beyond the maximum diameter has little practical value. It will be noted, however, that a number of the boundary calculations extend beyond the maximum diameter. This random extension results from a random continuance of the calculations; since these additional points on the boundary were available, they have been included. For those boundaries that extend well beyond the maximum diameter, the boundary shape in the neighborhood of the final calculated point on the boundary may be subject to small errors that the foldback method of characteristics can introduce in this region. (See appendix A of ref. 1.) A few of the boundary calculations at $M_j = 1.5$ were inadvertently terminated slightly short of the maximum diameter. In all the present calculations the first-family characteristic line determining the final point on the boundary had its origin on the leading-characteristic line (fig. 1). Consequently, the leading-characteristic line was terminated short of the jet axis, and the complications of calculations coming off the axis were not encountered. (See appendix A of ref. 1.) Inasmuch as the accuracy of the boundary calculations is closely related to the density of the characteristic net, some idea of the number of points contained in a typical

characteristic net (see fig. 1) may be of interest. For every increase in $\frac{p_j}{p_\infty}$ of 0.25, an additional characteristic line from the center of expansion was introduced. Thus, a relatively uniform accuracy was maintained as $\frac{p_j}{p_\infty}$ was increased. For example, at $M_j = 1.5$, $\theta_N = 15^\circ$, and $\gamma_j = 1.400$, there are 28 points in the calculation at $\frac{p_j}{p_\infty} = 1$ and 288 points in the calculation at $\frac{p_j}{p_\infty} = 10$.

The calculated boundaries are presented in discontinuous-slope form, which is compatible with the lattice-point characteristic method (that is, calculated points on boundary joined by straight lines). In practical application a smooth curve is, of course, fitted to the discontinuous-slope form of the boundary, particular care being given to maintain the initial inclination of the boundary.

## RESULTS

### Presentation of Boundaries

The 2960 calculated boundaries are presented in figures 2 to 5. Each group of boundaries corresponds to a variation of $\frac{p_j}{p_\infty}$ from 1 to 10 for a particular combination of $M_j$, $\theta_N$, and $\gamma_j$. The solid boundaries denote changes in $\frac{p_j}{p_\infty}$ of 1; the three dashed boundaries between the solid boundaries correspond to changes in $\frac{p_j}{p_\infty}$ of 0.25 and are also calculated not interpolated boundaries. For clarity, a number of the groups have insets covering the lower range of $\frac{x}{r_j}$ in which the ordinate $\frac{y}{r_j}$ is shown to twice scale. The order of presentation of these groups of boundaries is as follows:

| Figure | $M_j$ |
|---|---|
| 2 | 1.5 |
| 3 | 2.0 |
| 4 | 2.5 |
| 5 | 3.0 |

For figures 2 to 5, parts (a), (b), (c), and (d) are for $\theta_N$ of 5°, 10°, 15°, and 20°, respectively. Each figure subdivision contains five groups of boundaries corresponding to the five values of $\gamma_j$, and these five groups are presented in the order of ascending values of $\gamma_j$, that is, from $\gamma_j = 1.115$ to 1.667.

## Effects of Variables

The effect of increasing static-pressure ratio $\frac{p_j}{p_\infty}$ is obvious from figures 2 to 5. Effects of the other variables at a static-pressure ratio of 5 (arbitrarily chosen) are shown in figure 6. At this static-pressure ratio, the effect of increasing $M_j$ (fig. 6(a)) is to decrease the initial inclination of the boundary, to increase the maximum diameter of the free jet, and to move the maximum diameter farther away from the plane of the jet exit. The effect of increasing $\gamma_j$ (fig. 6(b)) is to decrease the initial inclination of the boundary, to decrease the maximum diameter of the free jet, and to move the maximum diameter closer to the plane of the jet exit. The effect of increasing $\theta_N$ (fig. 6(c)) is to increase the initial inclination of the boundary, to increase the maximum diameter of the free jet, and to move the maximum diameter closer to the plane of the jet exit. A brief examination at other values of $\frac{p_j}{p_\infty}$ indicated that these effects are apparently typical of all pressure ratios; however, there might be exceptions which were not disclosed by this examination.

## Simulation of One Jet Boundary by Another

In figures 2 to 6 it may be noted that the initial inclination of the boundary varies with every variable. When jet boundaries are simulated, the initial inclination is, perhaps, the most important property to be duplicated. (See refs. 1 and 2.) For this reason and because of the problems confronted in jet simulation, it is of interest to examine the degree of boundary simulation that may be achieved by simulating initial inclination only through a variation of $\frac{p_j}{p_\infty}$ only and, in addition, to determine whether complete simulation is possible through a variation of all variables.

In order to aid in the selection of values of $\frac{p_j}{p_\infty}$ that give the same initial inclination $\delta_j$, figure 7 has been prepared which gives the

variation with $\frac{p_j}{p_\infty}$ of the initial inclination for a jet exhausting from a nozzle having zero divergence angle (denoted by $\delta_{j_o}$). The value of $\delta_j$ at any finite value of $\theta_N$ is simply the sum of $\theta_N + \delta_{j_o}$.

Figure 8 presents some typical examples of boundary simulation. Random examples of the boundary simulation that may be expected by duplication of $\delta_j$ only are shown in figures 8(a) to 8(d). In these examples $M_j$ and $\theta_N$ remain constant and $\frac{p_j}{p_\infty}$ is allowed to vary so that the value of $\delta_j$ is the same for both values of $\gamma_j$. (See fig. 7.) In essence, a boundary given by an air jet ($\gamma_j = 1.400$, dashed boundary) is compared with a boundary given by a jet of another gas or by a heated air jet ($\gamma_j < 1.400$). The results indicate that the differences between the boundaries thus simulated can be attributed primarily to differences in $\gamma_j$ and that differences in $\gamma_j$ of the order of 0.1 or less create negligibly small differences in the boundary when the initial inclination is duplicated. This observation also implies that, insofar as the effects of boundary shape are concerned, air jets heated to the order of 2,500° R or lower can be satisfactorily simulated by cold air jets by altering the pressure ratio to give the same initial inclination. The results discussed in the appendix show that this observation may be extended to the case of supersonic jets exhausting into supersonic streams.

Figure 8(e) gives an example which illustrates the point that the boundary of any jet may be satisfactorily simulated by an air jet by allowing a freedom of choice of the variables for the air jet. Extremely large values of $\frac{p_j}{p_\infty}$ would, of course, produce exceptions. (It will be noted that the boundaries of figure 8 are, as before, given in the discontinuous-slope form. This form tends to exaggerate the differences in the lower range of $\frac{x}{r_j}$, particularly at the first calculated point on the boundary.)

Figure 8(f) illustrates that, for a particular value of $\gamma_j$, there are a number of combinations of $M_j$, $\theta_N$, and $\frac{p_j}{p_\infty}$ that produce essentially the same boundary.

## Interpolation and Extrapolation of Calculated Boundaries

Interpolation and cross-plotting can be used to obtain a reliable boundary within the range of any of the variables covered by these calculations.

The reliability of a boundary necessitating the use of extrapolation to cover a variable the magnitude of which places it outside the range of these calculations is not readily apparent. A cursory examination, however, gave the following indications. Extrapolations of $\frac{p_j}{p_\infty}$ should not exceed values of $\frac{p_j}{p_\infty}$ of about 14 and probably less; extrapolations below $\frac{p_j}{p_\infty} = 1$ are not recommended. Extrapolations to $\theta_N = 0^\circ$ are of particular interest since the nozzle having parallel flow at the exit is often encountered. This extrapolation may be made with good results as indicated by the example given in figure 9 where an extrapolated boundary for $\theta_N = 0^\circ$ is shown to be in good agreement with the calculated boundary for $\theta_N = 0^\circ$ from reference 1. Extrapolations to values of $\theta_N$ in excess of about $25^\circ$ are not recommended. Extrapolations of $M_j$ to $M_j = 1$ ($\theta_N = 0^\circ$) appear permissible, and extrapolations to $M_j \approx 3.5$ or slightly higher appear within reason. The necessity for extrapolations of $\gamma_j$ beyond the range of these calculations appears remote; however, should the need arise, the extrapolation could in all likelihood be made with confidence.

## CONCLUDING REMARKS

Calculations have been made by the method of characteristics of 2960 boundaries of supersonic axisymmetric free jets exhausting from conically divergent nozzles into still air. The calculations cover jet Mach numbers from 1.5 to 3.0, ratio of specific heats of the jet from 1.115 to 1.667, divergence angles of the nozzle from $5^\circ$ to $20^\circ$, and jet static-pressure ratios from 1 to 10. The results are presented nondimensionally and in a form that facilitates practical use. Some random examples of the effects of the variables involved are shown, and the possibilities of the simulation of one jet by another are examined for jets exhausting into still air and into supersonic streams.

Langley Aeronautical Laboratory,
National Advisory Committee for Aeronautics,
Langley Field, Va., June 22, 1956.

## APPENDIX

## JETS EXHAUSTING INTO SUPERSONIC STREAMS

Because of the negligibly small differences found in the boundaries of supersonic jets exhausting into still air for differences in $\gamma_j$ of the order of 0.1, provided the initial inclination is duplicated, an attempt was made to determine whether equally small differences in the boundary shape and, of equal importance, in the ambient wave interference field could be expected for supersonic jets exhausting into supersonic streams under the same conditions of simulation (identical $\delta_j$). At the outset, one might suspect that the effect of a given change in $\gamma_j$ would have less effect upon the jet-boundary shape for jets exhausting expansively into supersonic streams as compared with jets exhausting into still air at the same value of $\frac{p_j}{p_\infty}$. This suspicion arises for the following reasons. For the same value of $\frac{p_j}{p_\infty}$, the jet exhausting into the supersonic stream undergoes considerably less expansion than the jet exhausting into still air because of the pressure rise across the exit shock generated in the supersonic stream. Thus, effectively, the initial portion of the issuing jet flow for the jet exhausting into the supersonic stream resembles that which occurs for a jet exhausting into still air at a significantly lower value of $\frac{p_j}{p_\infty}$. In reference 1, it has already been shown that the lower the value of $\frac{p_j}{p_\infty}$, the less the effect of $\gamma_j$, and that at $\frac{p_j}{p_\infty} = 1$ changes in $\gamma_j$ greater than 0.4 have negligible effect upon the boundary shape of jets exhausting into still air.

A characteristic calculation has been made by Schäfer in reference 3 for a jet having $M_j = 2.37$, $\gamma_j = 1.405$, $\theta_N = 12.5^\circ$, and exhausting at $\frac{p_j}{p_\infty} \approx 8.9$ into an ambient stream having a Mach number of 3.24 and a ratio of specific heats of 1.405 (same as jet); the exterior surface ahead of the jet exit had a boattail angle of $9^\circ$. In reference 4, the isobars for this calculation have been computed and the calculation is presented in isobar-streamline form. (The values of some of the initial variables quoted in figure 13 of reference 4 contain slight errors which were corrected for this calculation.) The Schäfer calculation has been repeated with the initial variables remaining the same except for $\gamma_j$,

which was changed to 1.300, and $\frac{p_j}{p_\infty}$, which was reduced so that the initial inclination of the mixing boundary was duplicated. This new calculation was carried to the maximum diameter of the jet. The boundary shape and the interference isobars in the ambient stream obtained in this calculation could not be distinguished from those shown in reference 4. Thus, the conclusion drawn for jets exhausting into still air would appear to apply as well to jets exhausting into supersonic streams, namely, differences in $\gamma_j$ of the order of at least 0.1 create negligibly small differences when the initial inclination of the jet boundary is duplicated.

On the basis of the above conclusion, cold air jets may be expected to simulate the wave interference of other jets satisfactorily in the range of variables covered in reference 2 when the initial inclination is duplicated according to the curves of reference 2. (The results of reference 2 are for $\gamma_j = 9/7$ or 1.286; therefore, the cold-air-jet simulation amounts to a difference in $\gamma_j$ of the order of 0.1.) Furthermore, the curves of reference 1 giving initial inclination of the boundary and of the exit shock may be used to achieve simulation of the wave-interference field with cold air jets over a larger region of the interference field than was at first thought possible.

## REFERENCES

1. Love, Eugene S., and Grigsby, Carl E.: Some Studies of Axisymmetric Free Jets Exhausting From Sonic and Supersonic Nozzles Into Still Air and Into Supersonic Streams. NACA RM L54L31, 1955.

2. Love, Eugene S.: Initial Inclination of the Mixing Boundary Separating an Exhausting Supersonic Jet From a Supersonic Ambient Stream. NACA RM L55J14, 1956.

3. Schäfer, M.: Steady Supersonic Flows. Reps. and Translations No. 996, British M.A.P. Völkenrode. May 1, 1948.

4. Love, Eugene S.: Supersonic Wave Interference Affecting Stability. NACA RM L55L14a, 1956.

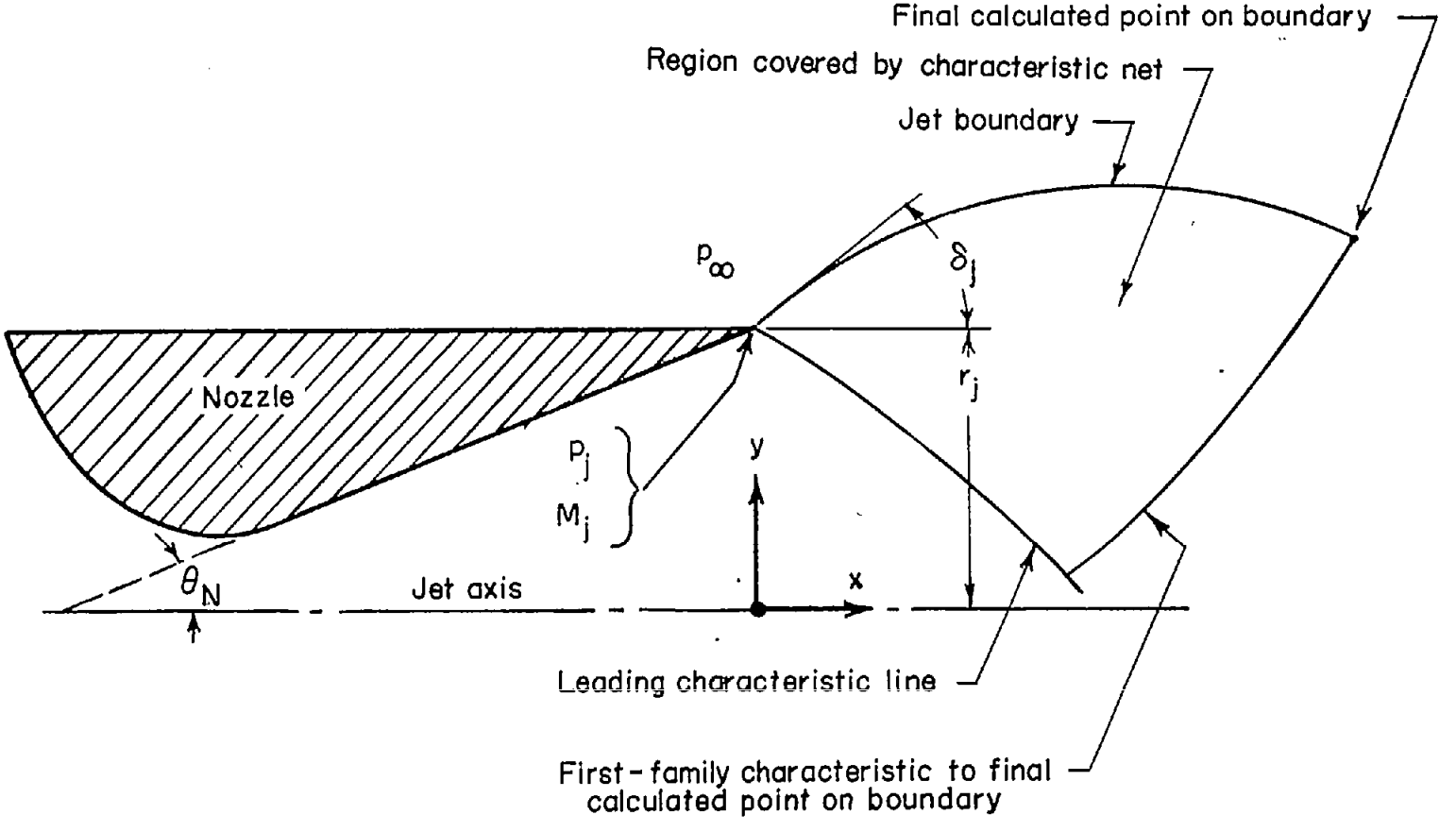


Figure 1.- Sketch of nozzle, jet boundary, and pertinent information.

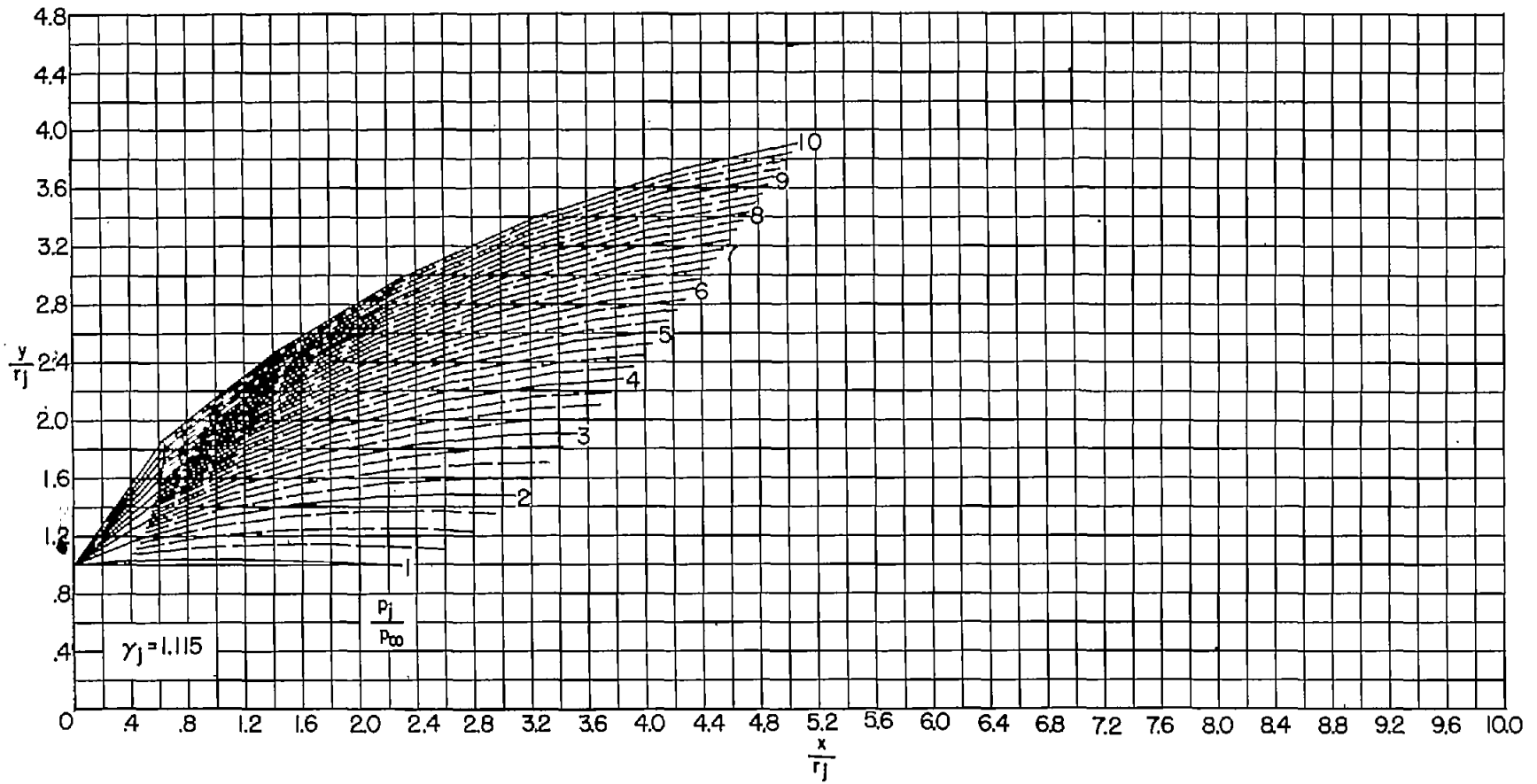


(a) $\theta_N = 5^\circ$.

Figure 2.- Jet boundaries at $M_j = 1.5$ for jet static-pressure ratios from 1 to 10. (Dashed boundaries denote changes in $p_j/p_\infty$ of 0.25.)

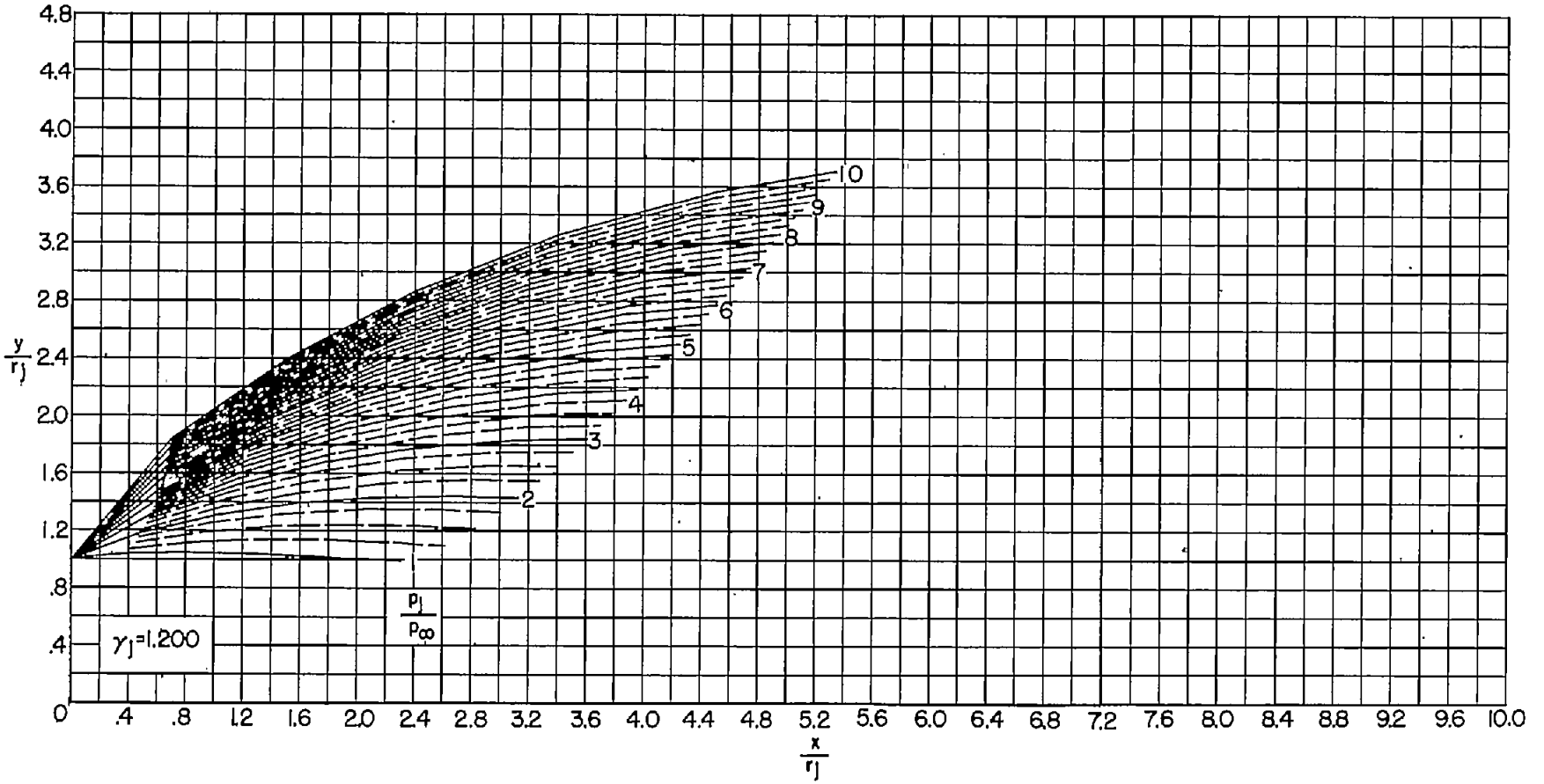


(a) $\theta_N = 5^\circ$. Continued.

Figure 2.- Continued.

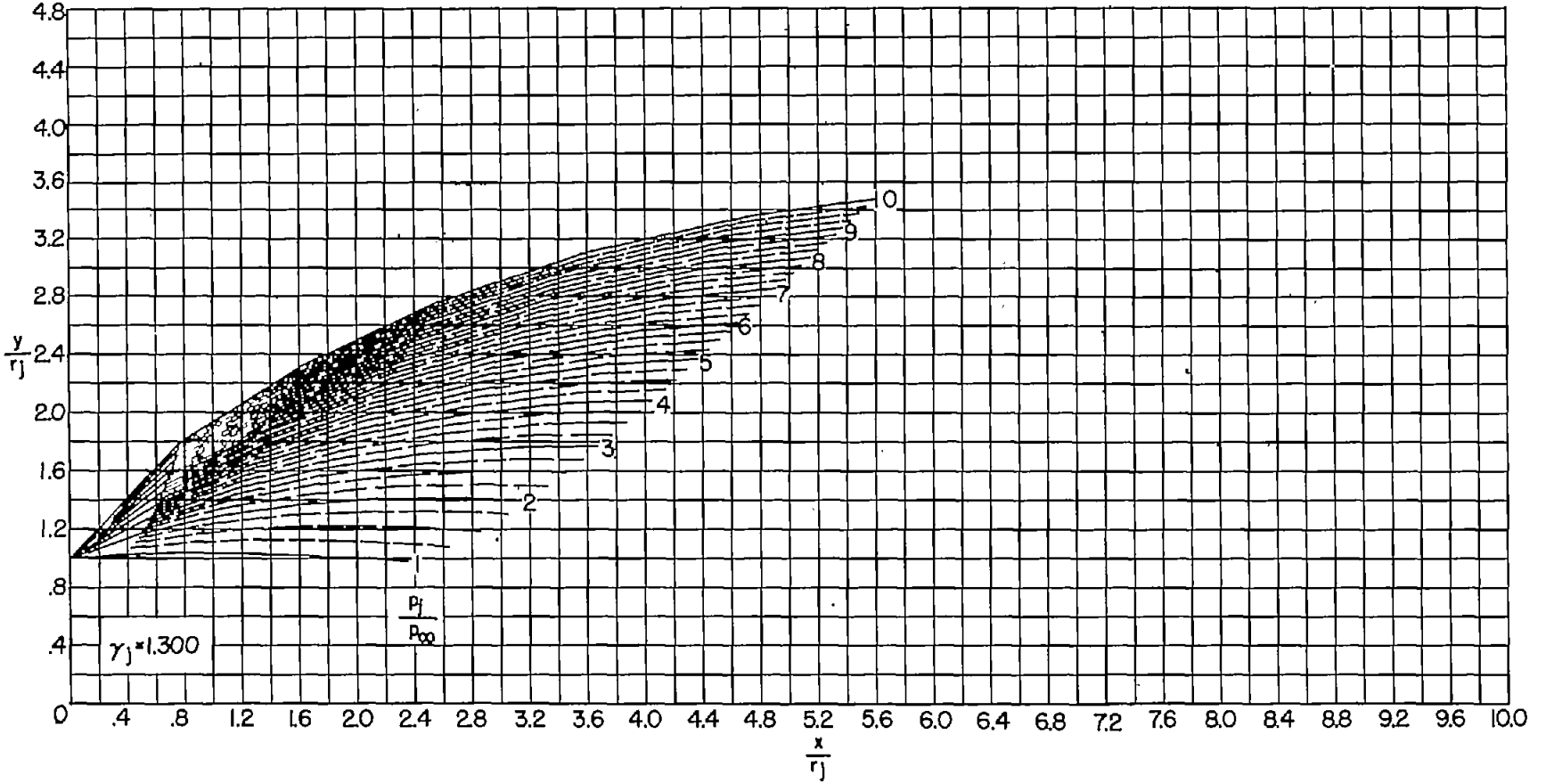


(a) $\theta_N = 5^\circ$. Continued.

Figure 2.- Continued.

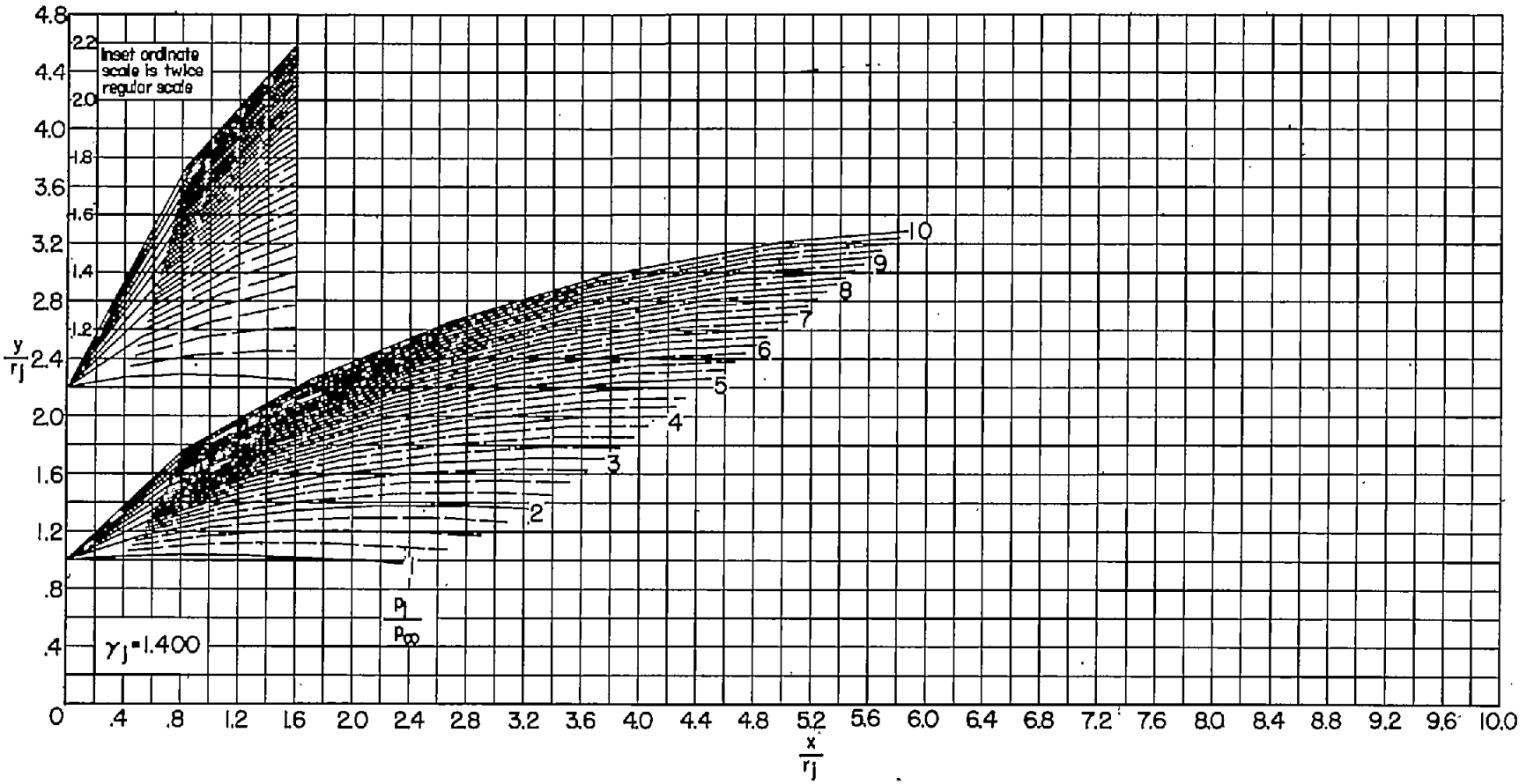


(a) $\theta_N = 5^\circ$. Continued.

Figure 2.- Continued.

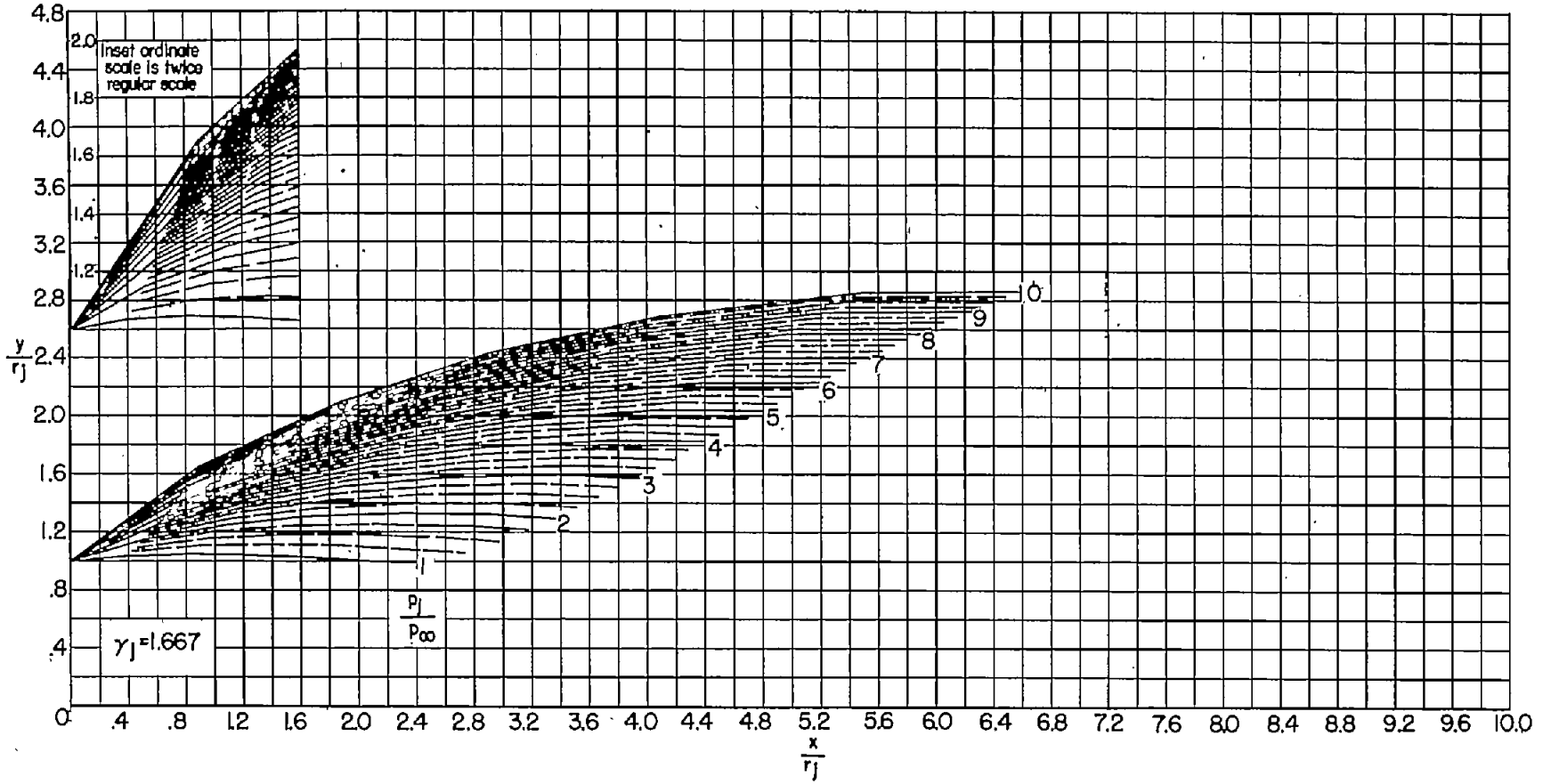


(a) $\theta_N = 5^\circ$. Concluded.

Figure 2.- Continued.

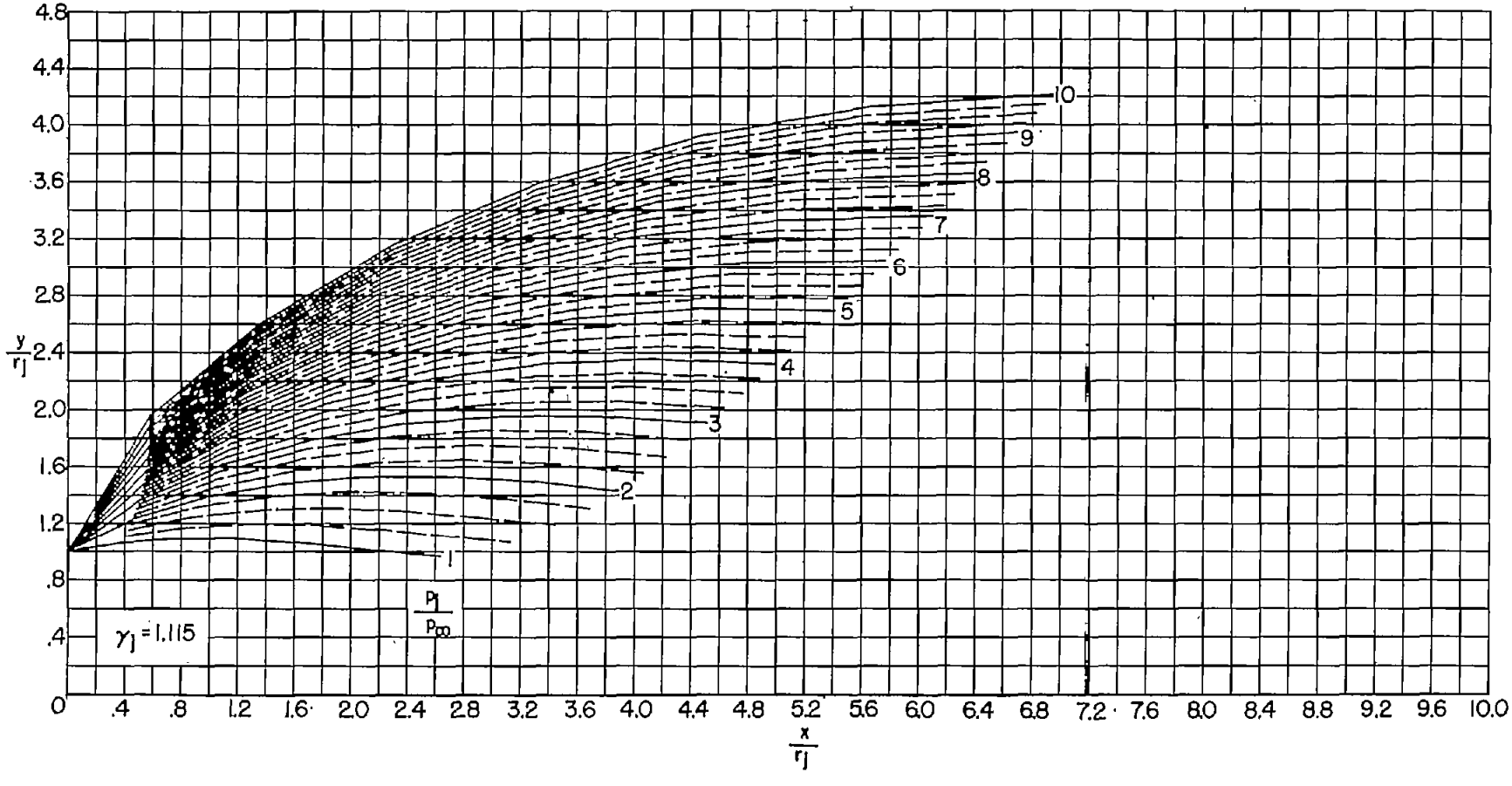


(b) $\theta_N = 10^\circ$.

Figure 2.- Continued.

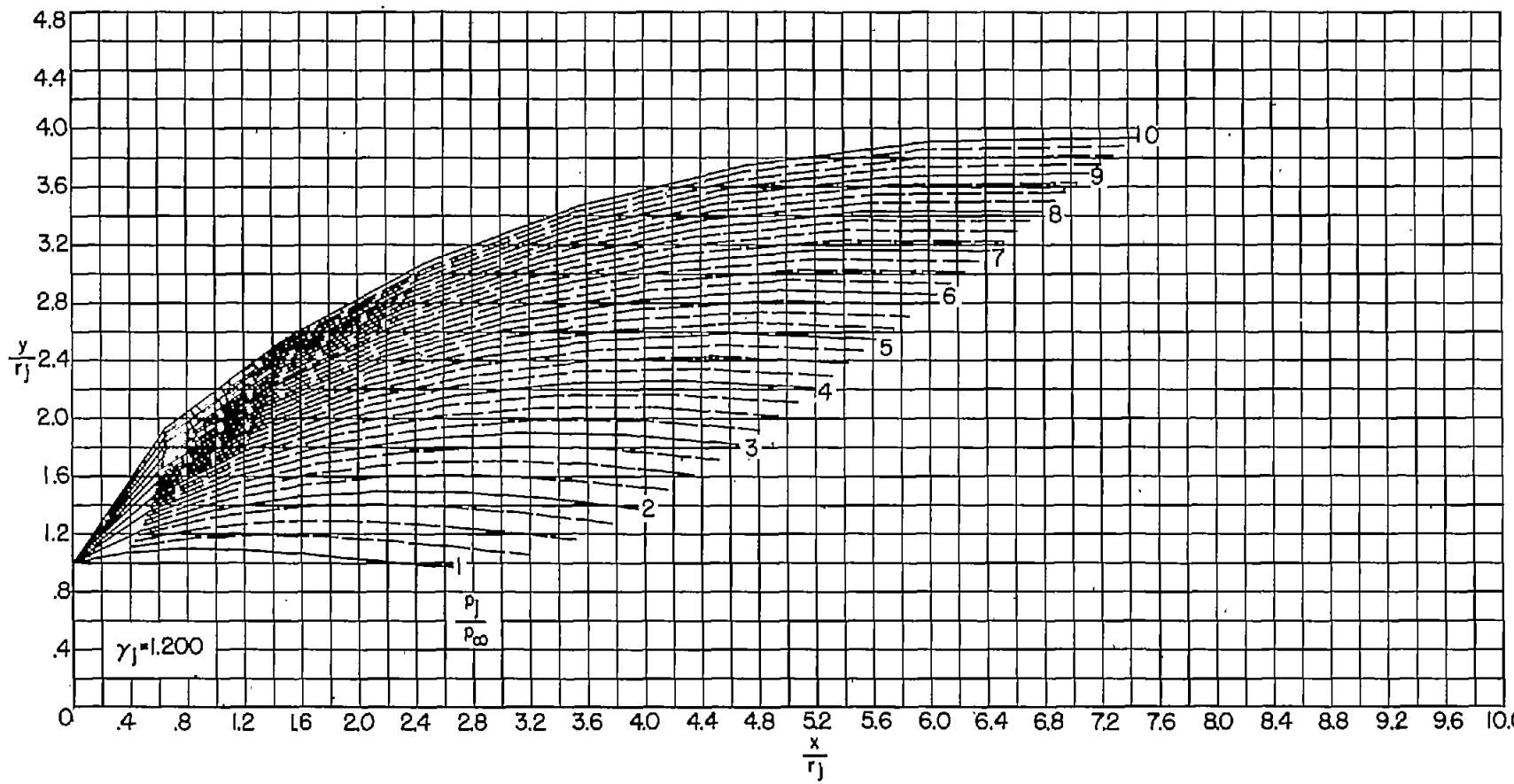


(b) $\theta_N = 10^\circ$. Continued.

Figure 2.- Continued.

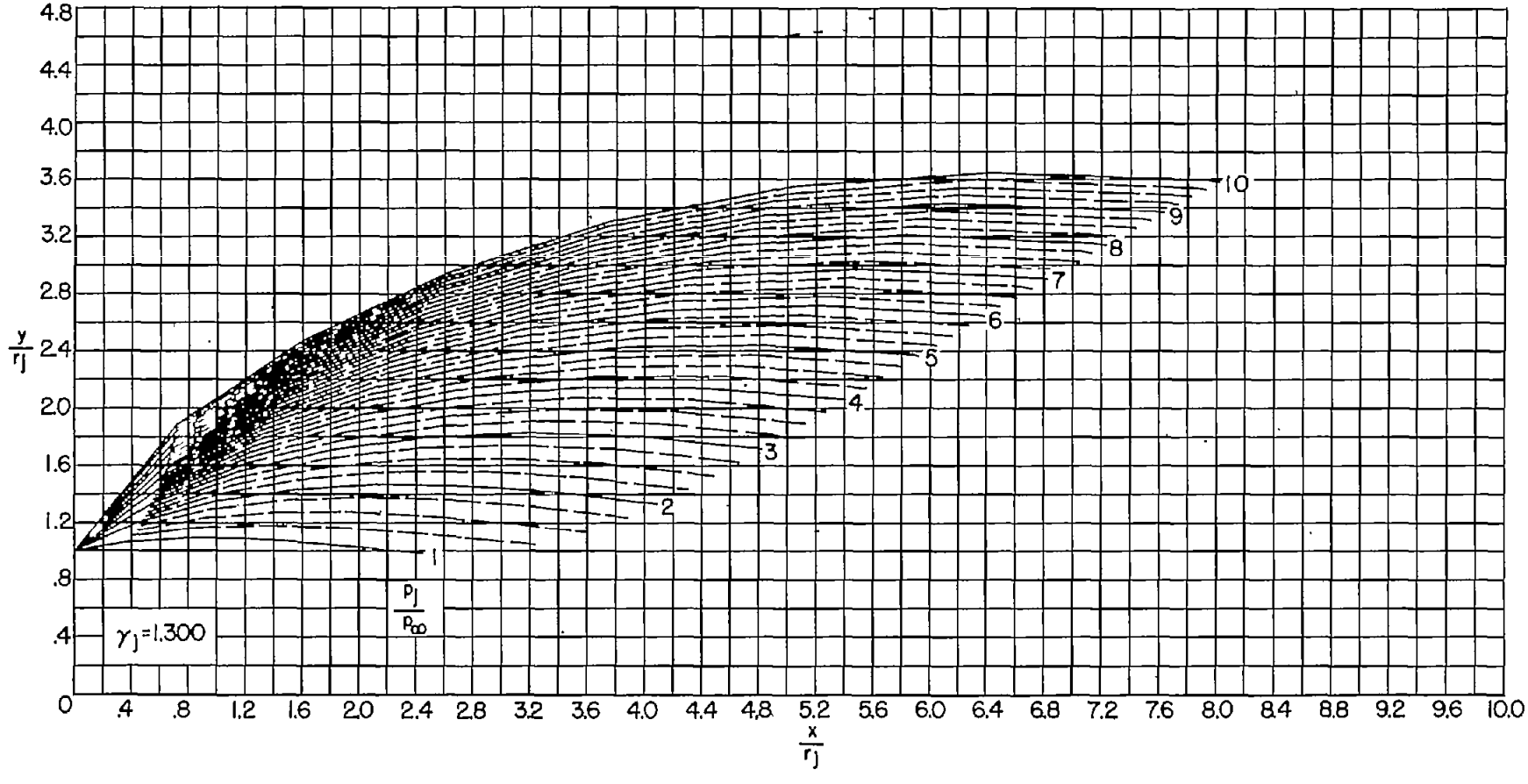


(b) $\theta_N = 10^\circ$. Continued.

Figure 2.- Continued.

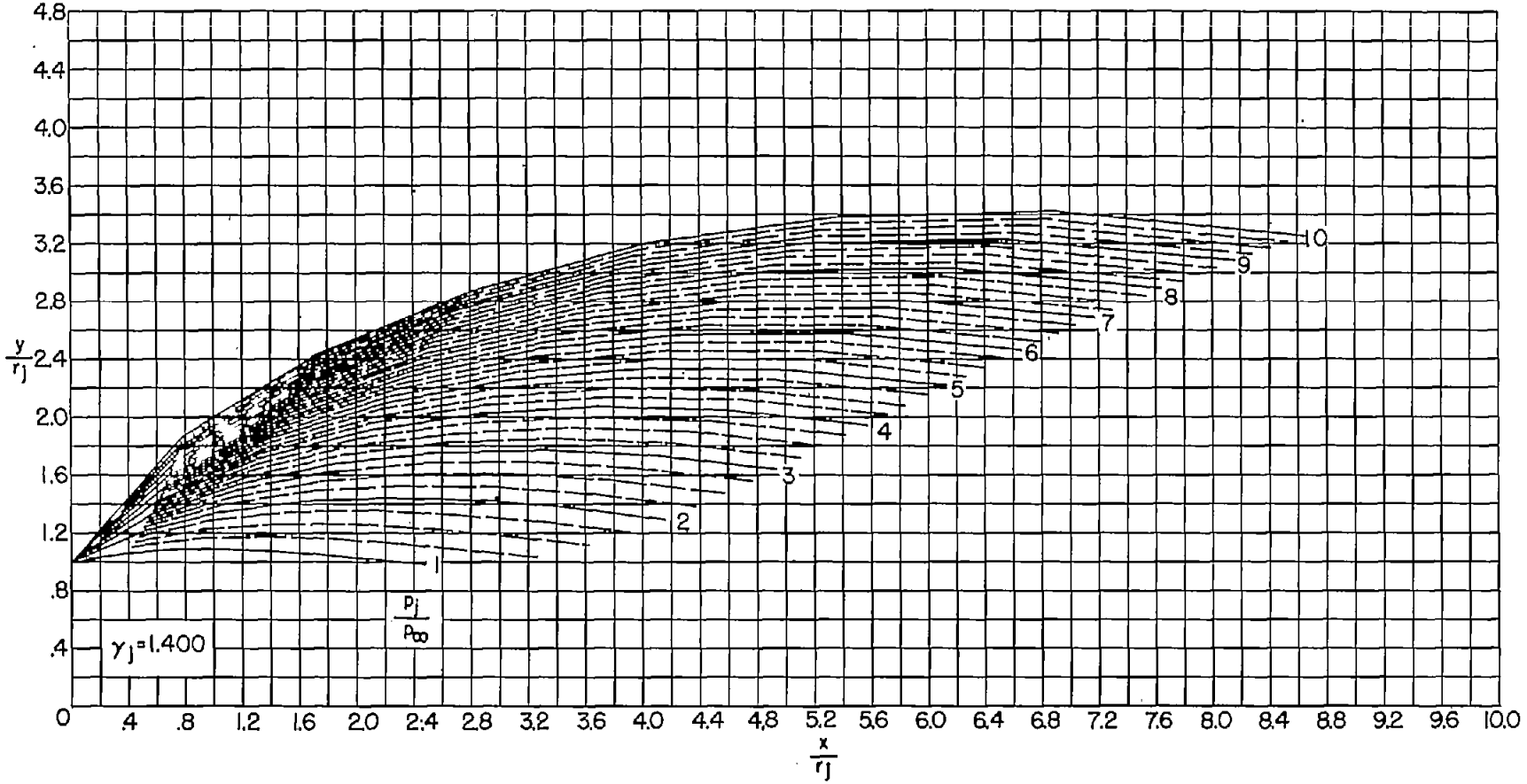


(b) $\theta_N = 10^\circ$. Continued.

Figure 2.- Continued.

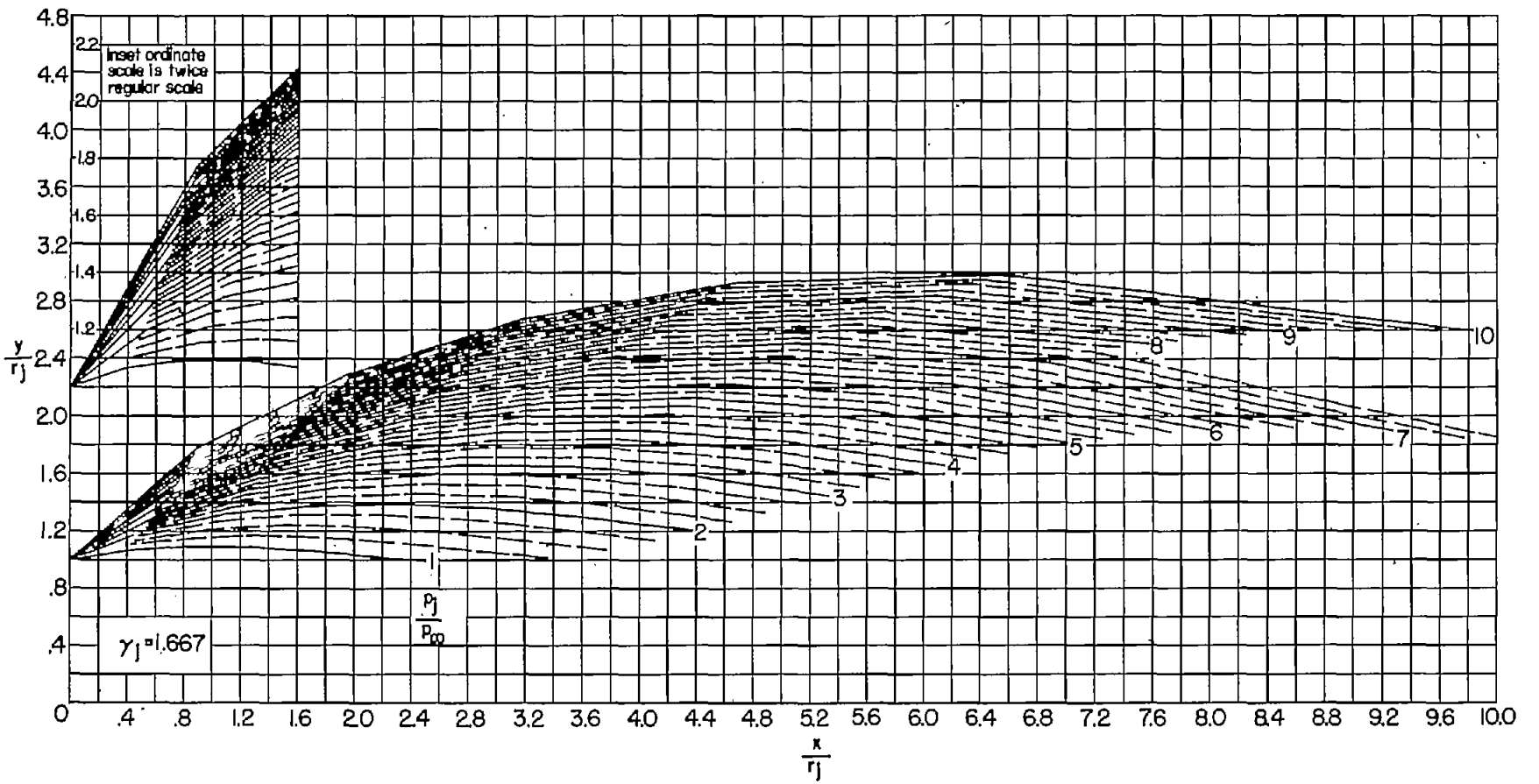


(b) $\theta_N = 10^\circ$. Concluded.

Figure 2.- Continued.

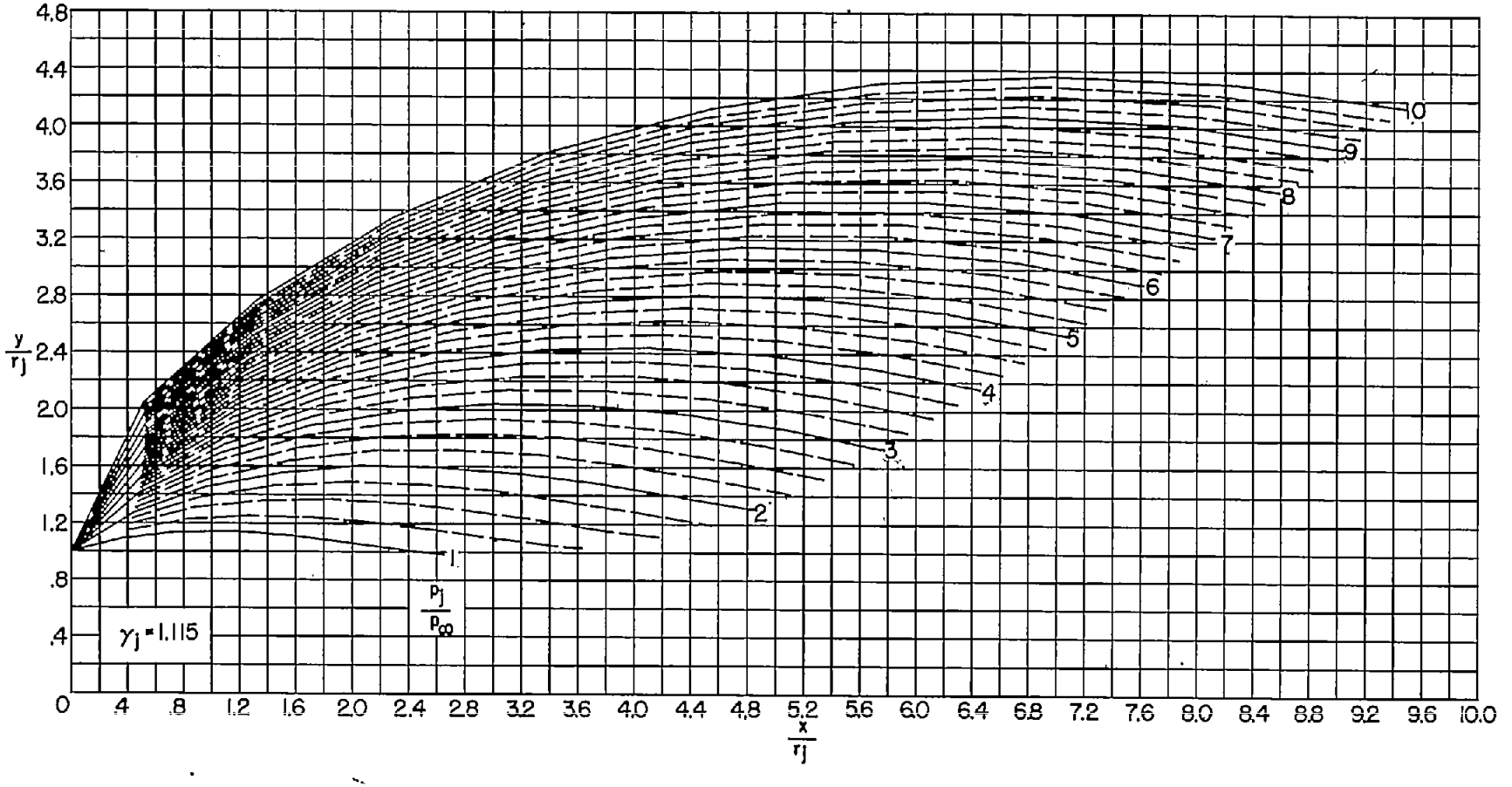


(c) $\theta_N = 15^\circ$.

Figure 2.- Continued.

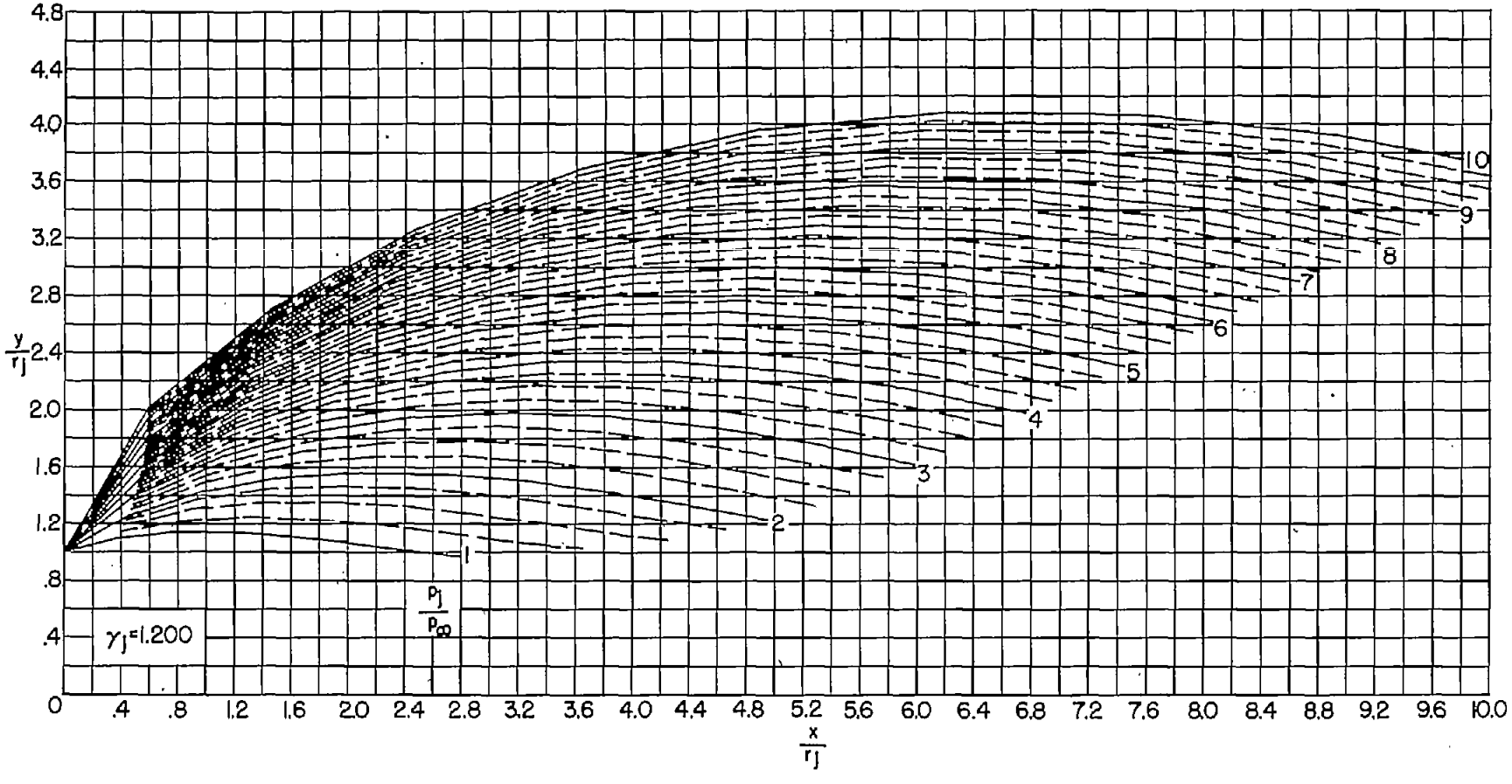


(c) $\theta_N = 15^\circ$. Continued.

Figure 2.- Continued.

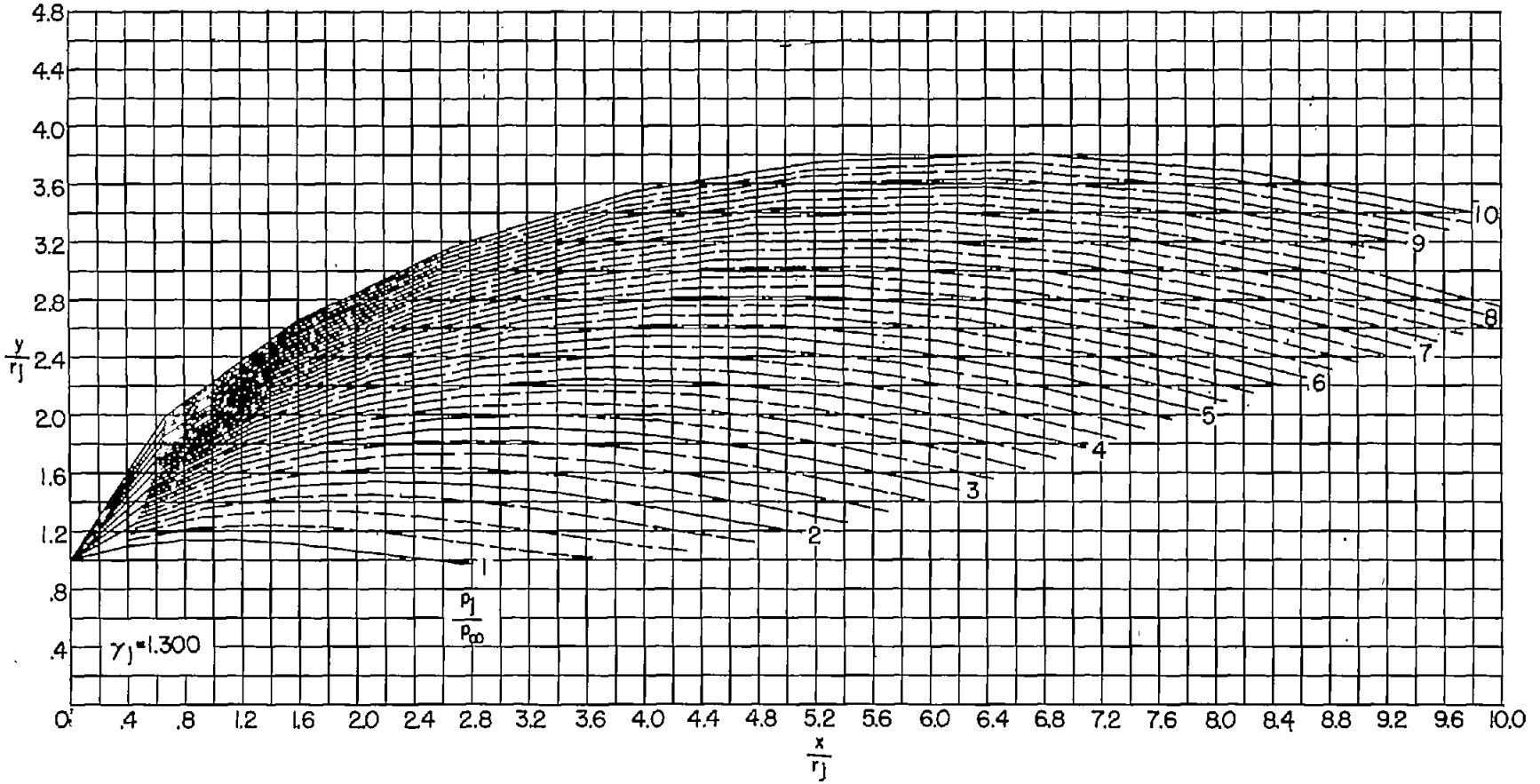


(c) $\theta_N = 15^\circ$. Continued.

Figure 2.- Continued.

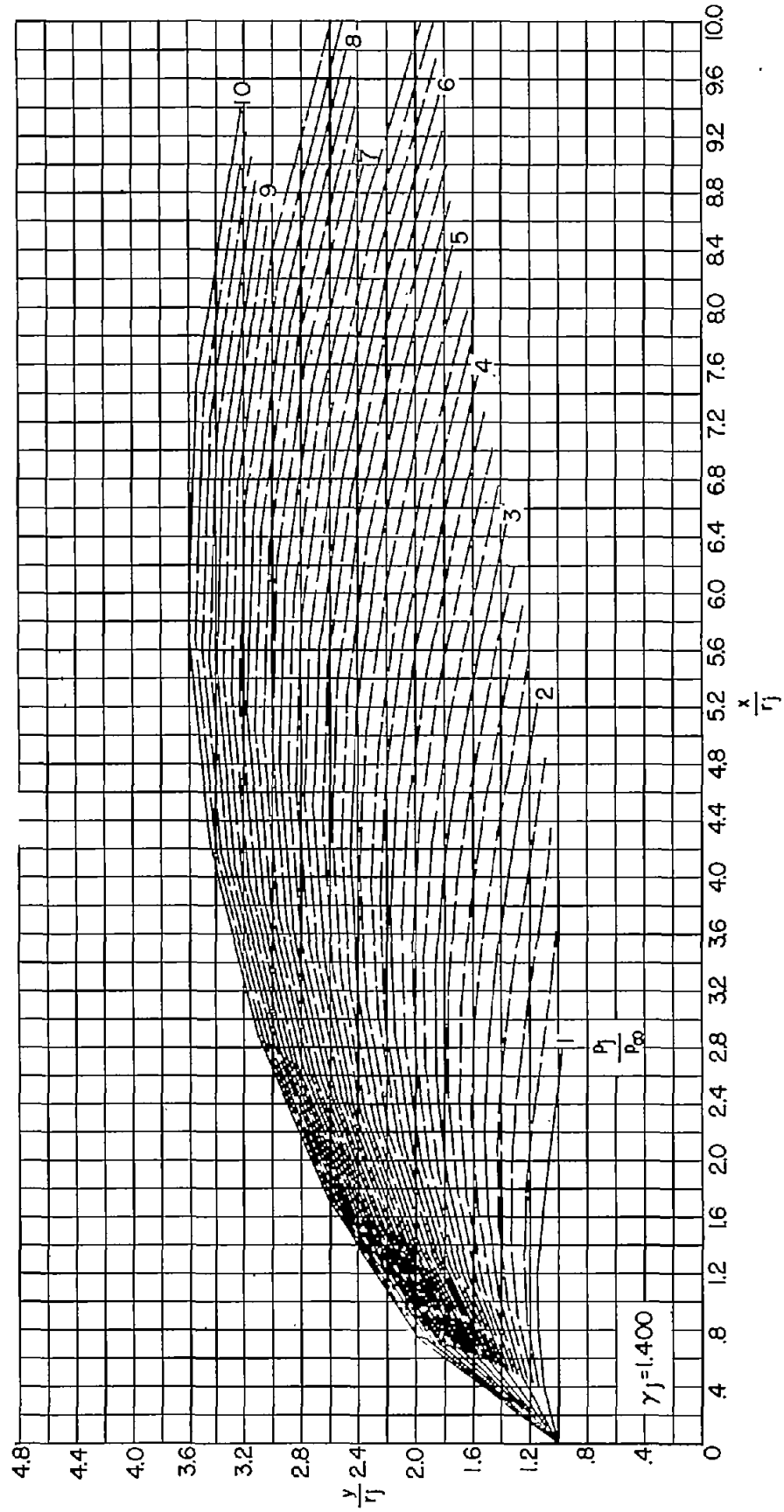


(c) $\theta_N = 15^\circ$. Continued.

Figure 2.- Continued.

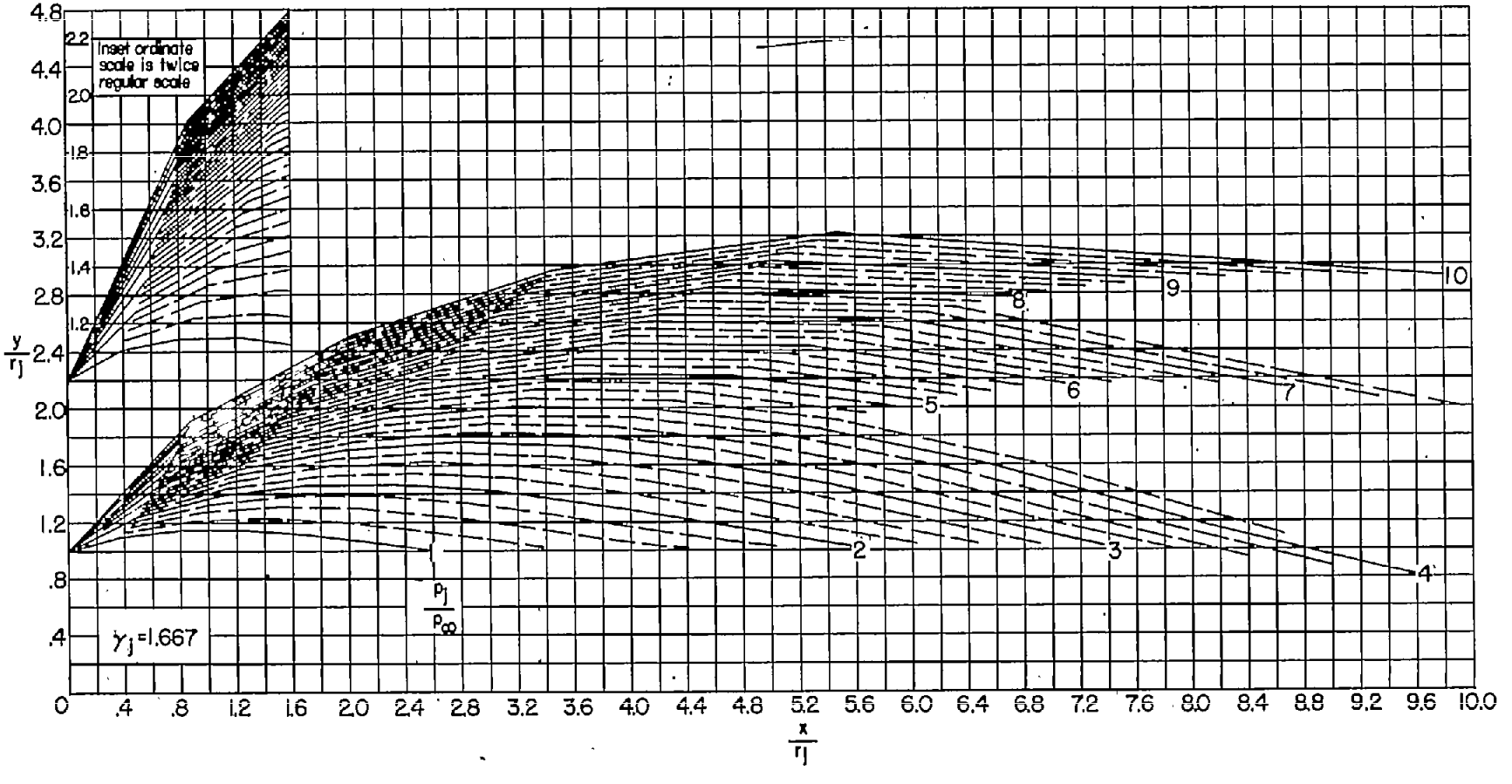


(c) $\theta_N = 15^\circ$. Concluded.

Figure 2.- Continued.

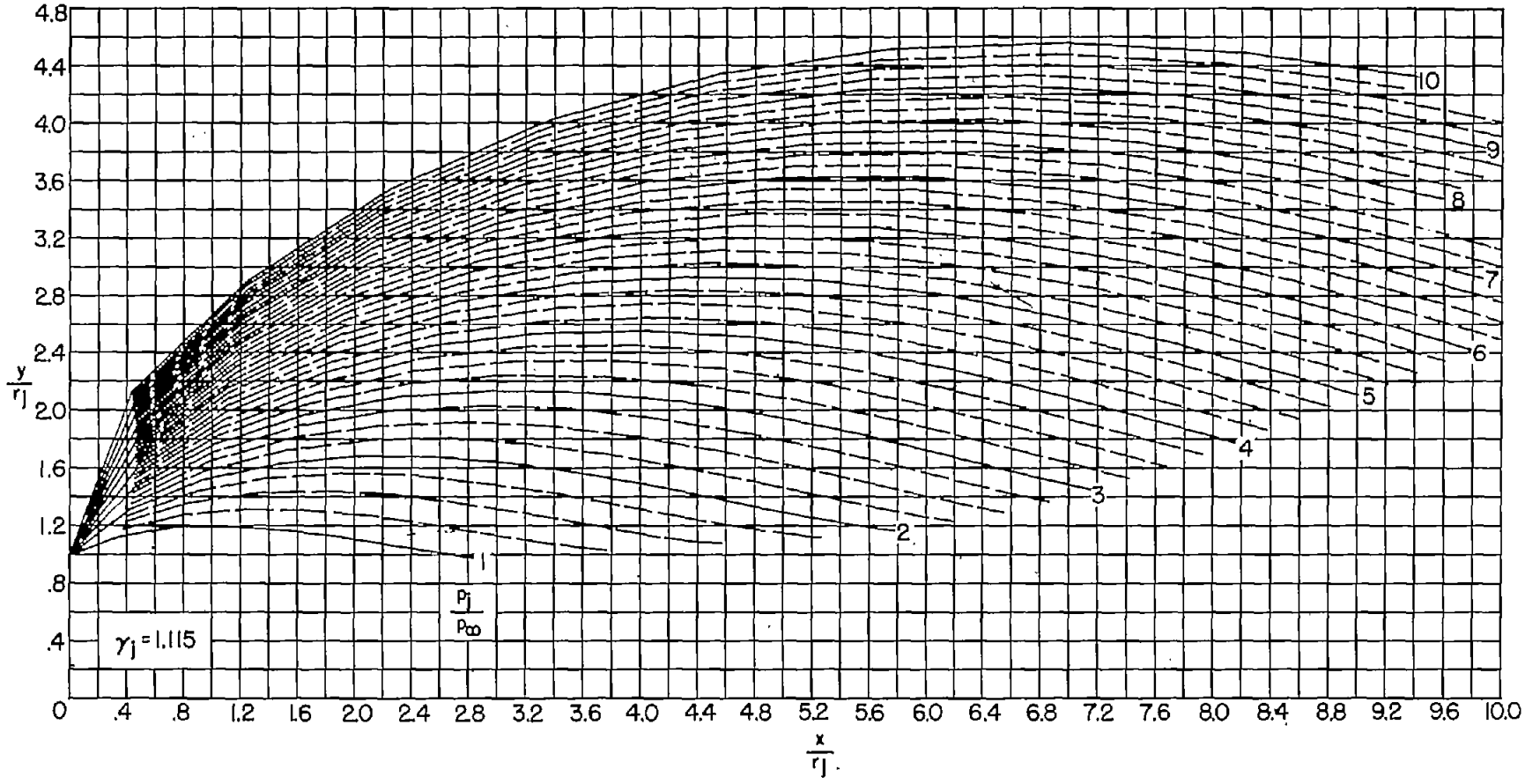


(d) $\theta_N = 20^\circ$.

Figure 2.- Continued.

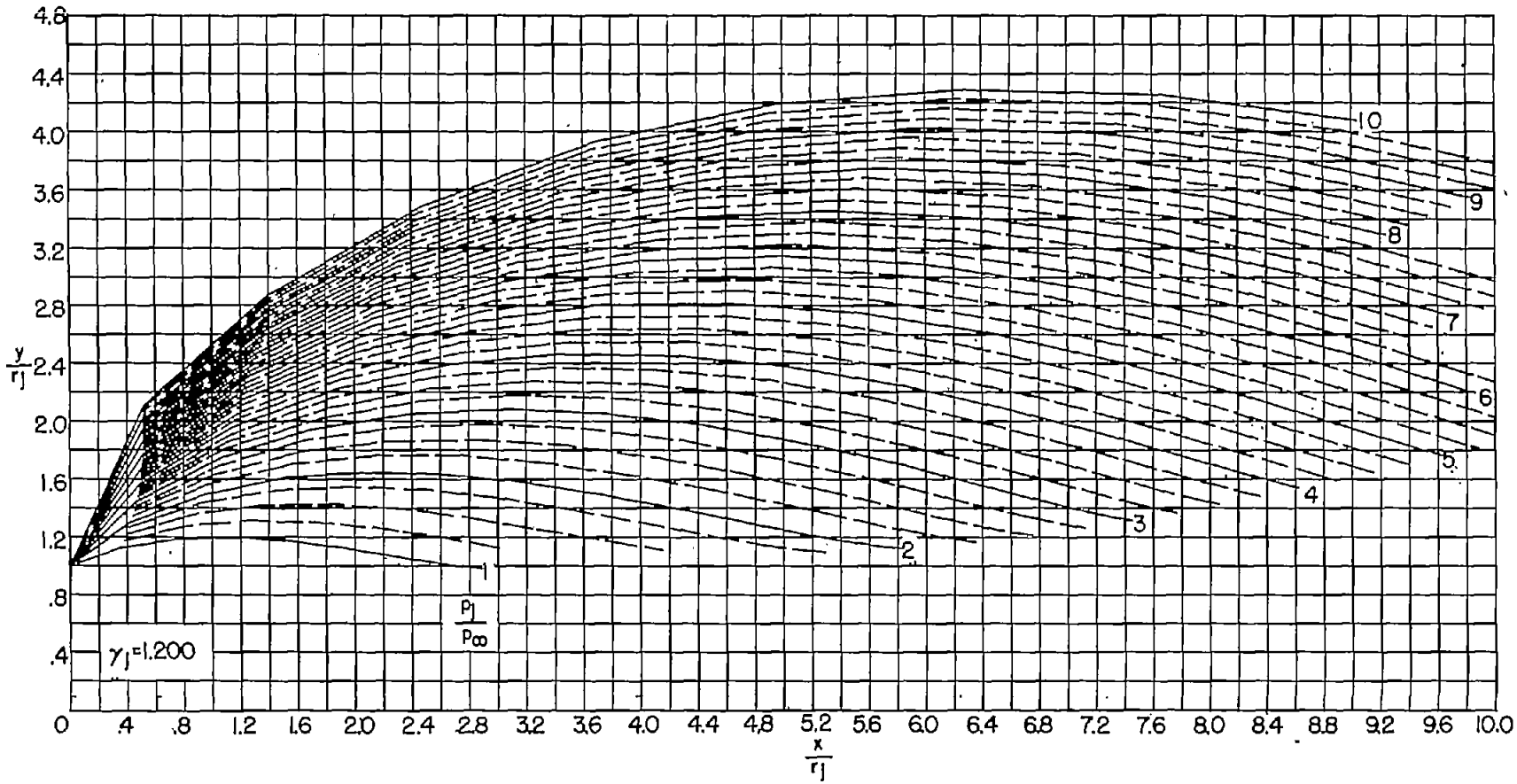


(d) $\theta_N = 20^\circ$. Continued.

Figure 2.- Continued.

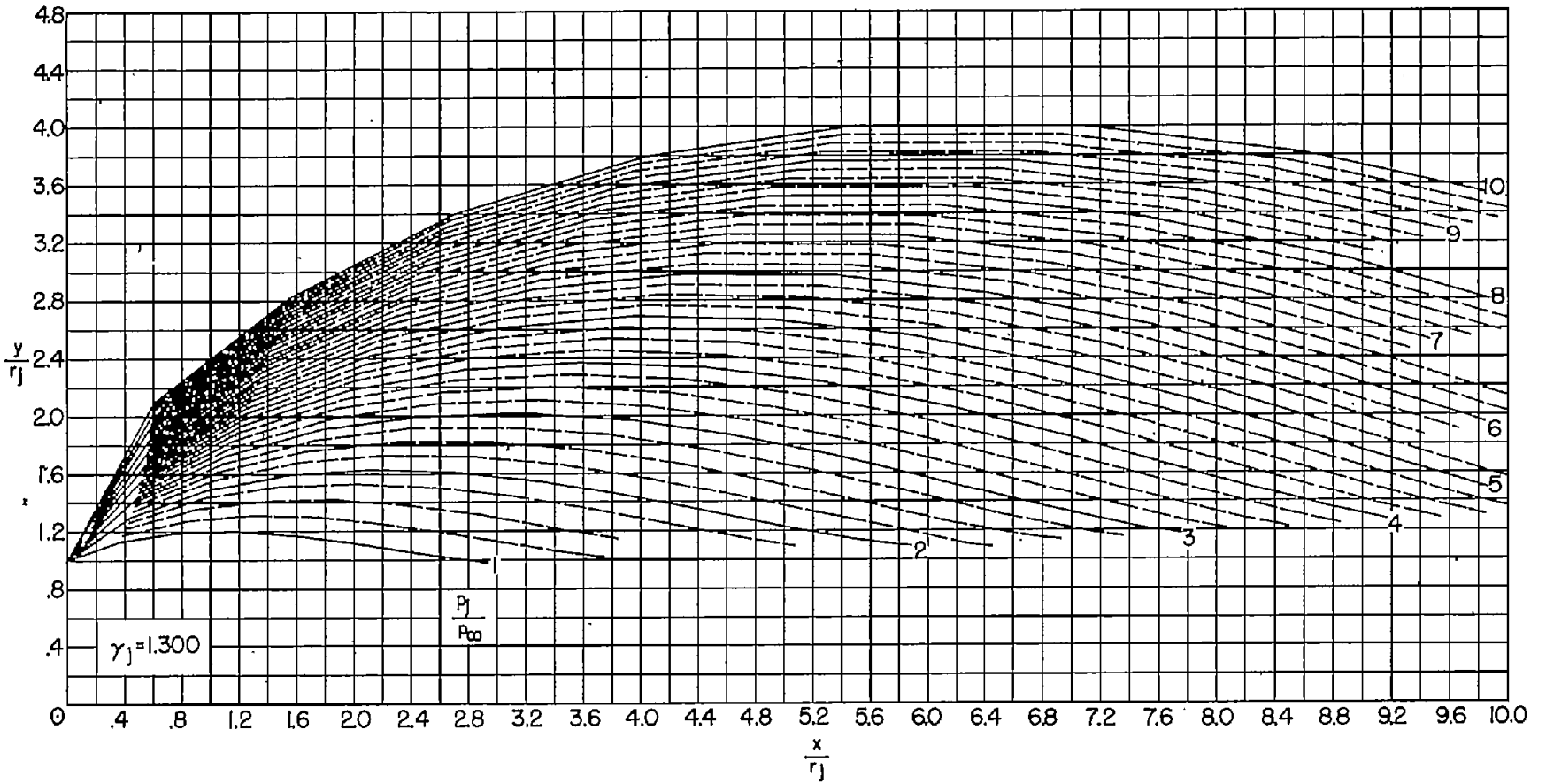


(d) $\theta_N = 20^\circ$. Continued.

Figure 2.- Continued.

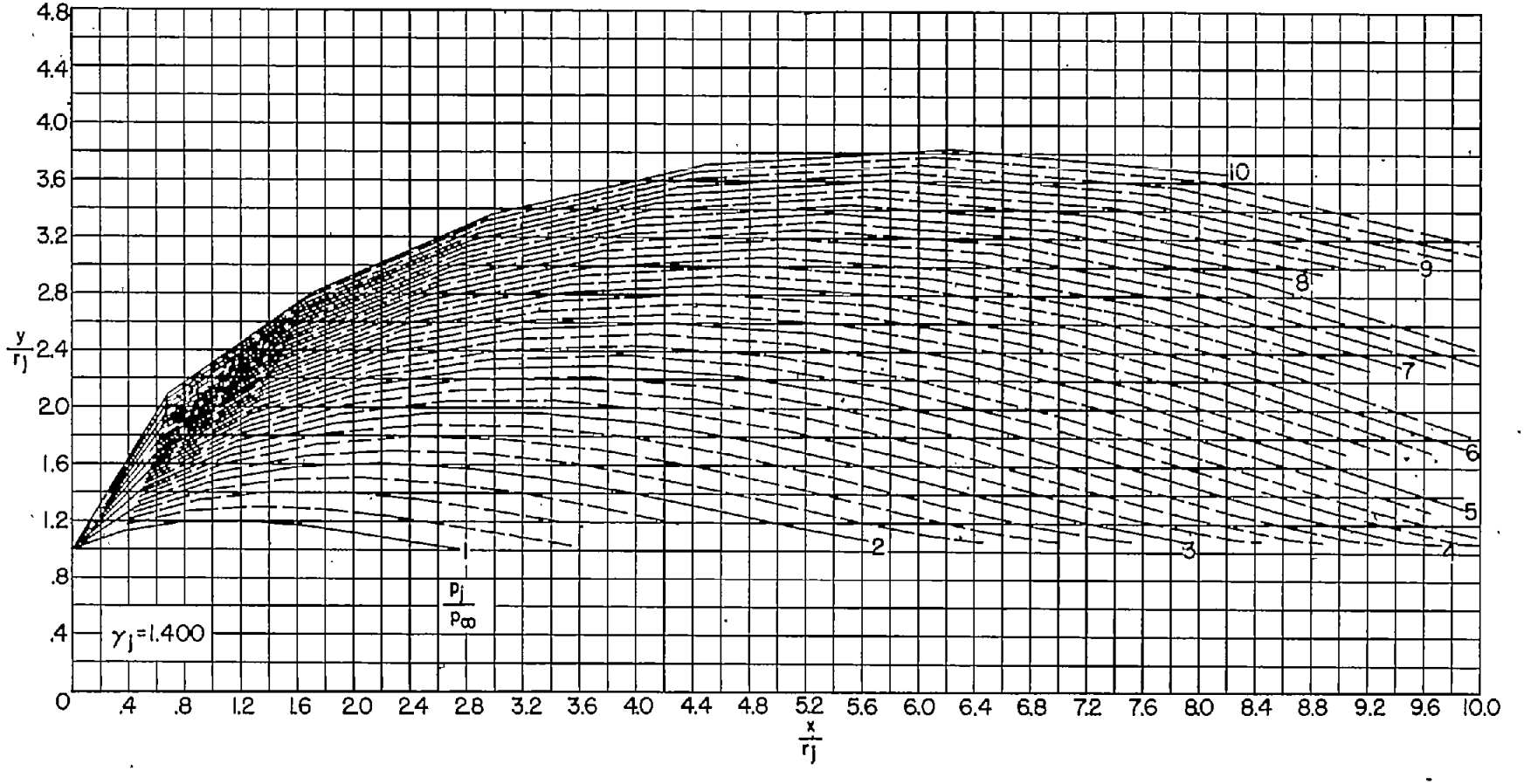


(d) $\theta_N = 20^\circ$. Continued.

Figure 2.- Continued.

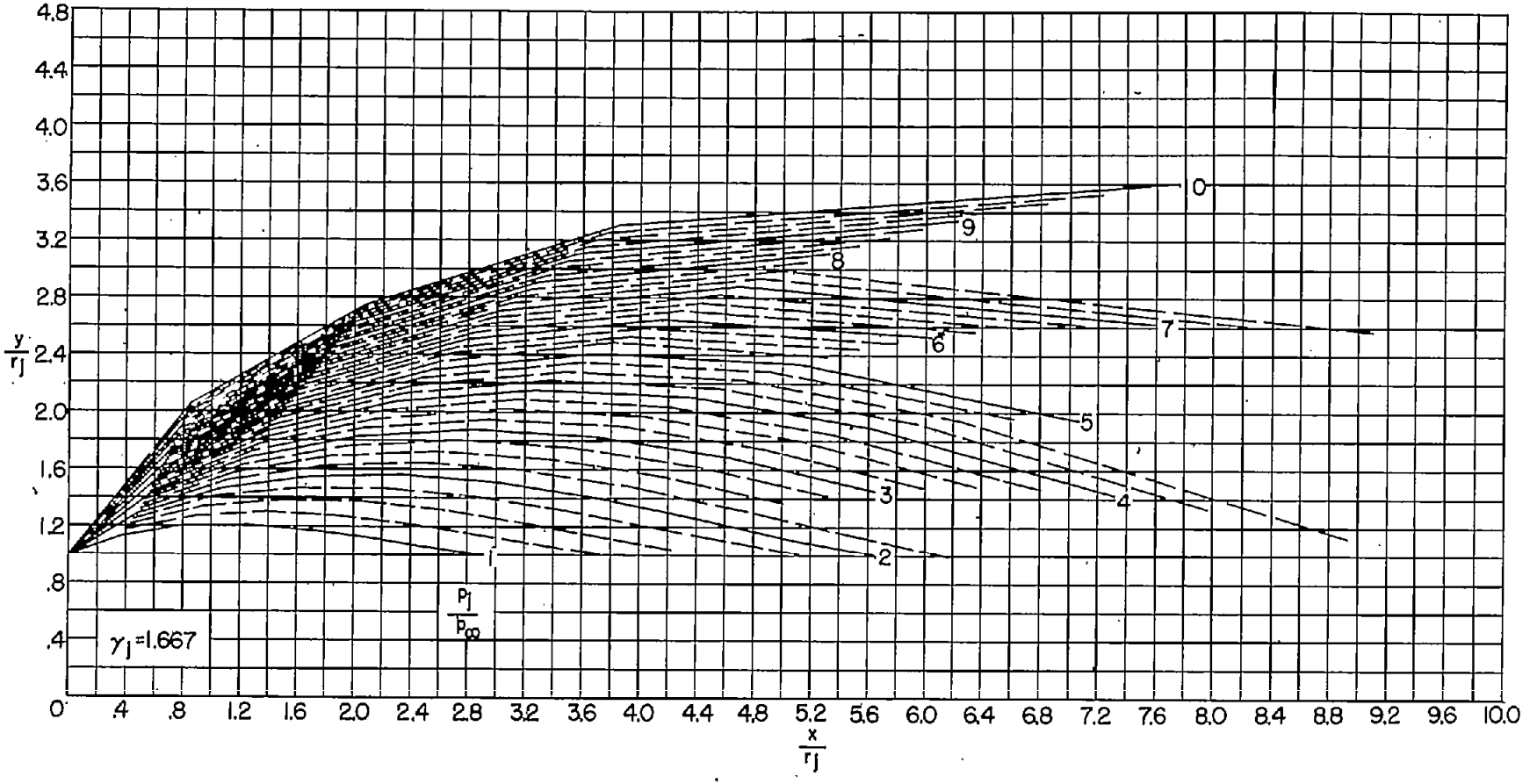


(d) $\theta_N = 20^\circ$. Concluded.

Figure 2.- Concluded.

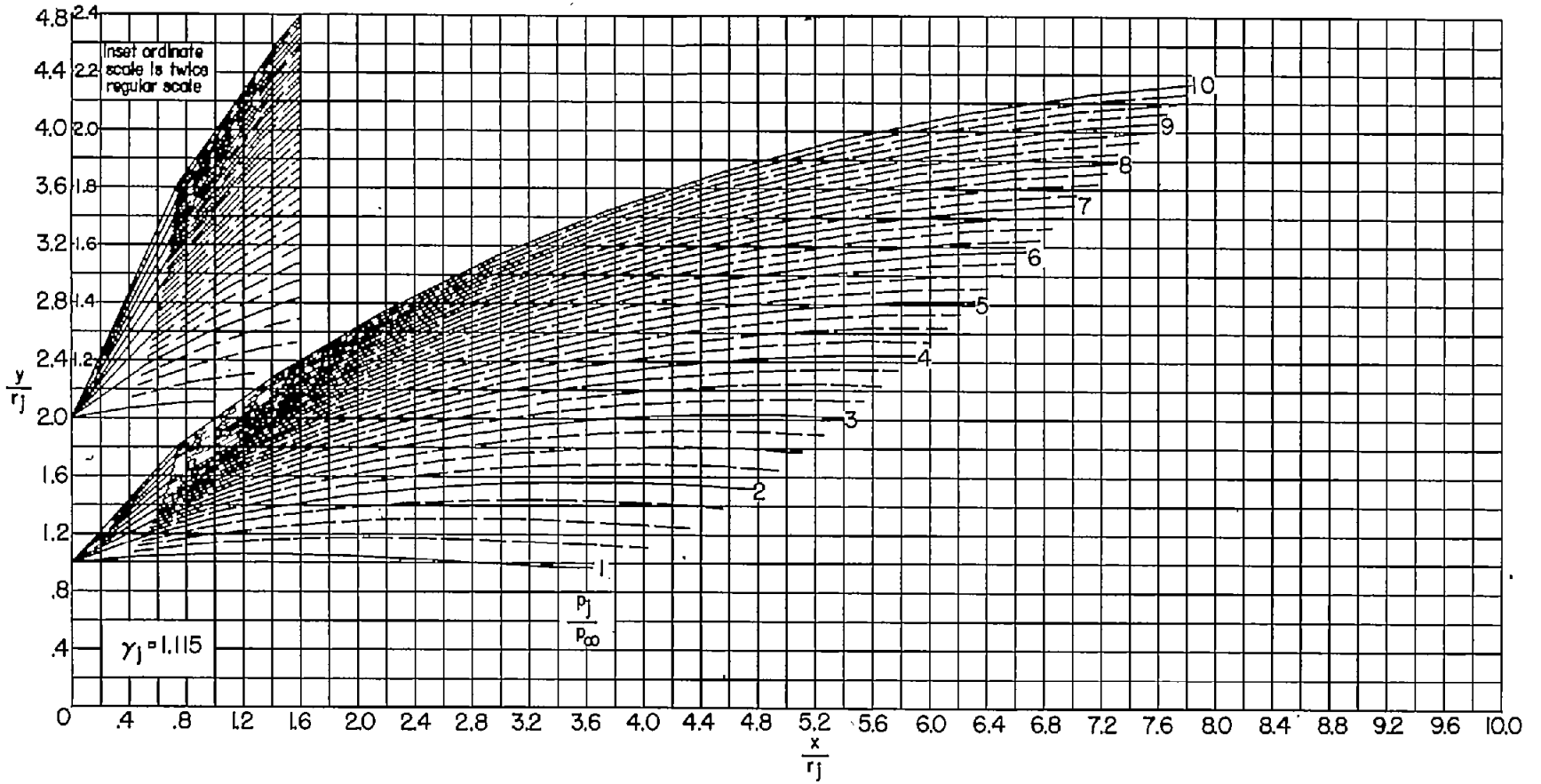


(a) $\theta_N = 5^\circ$.

Figure 3.- Jet boundaries at $M_j = 2.0$ for jet static-pressure ratios from 1 to 10. (Dashed boundaries denote changes in $p_j/p_\infty$ of 0.25.)

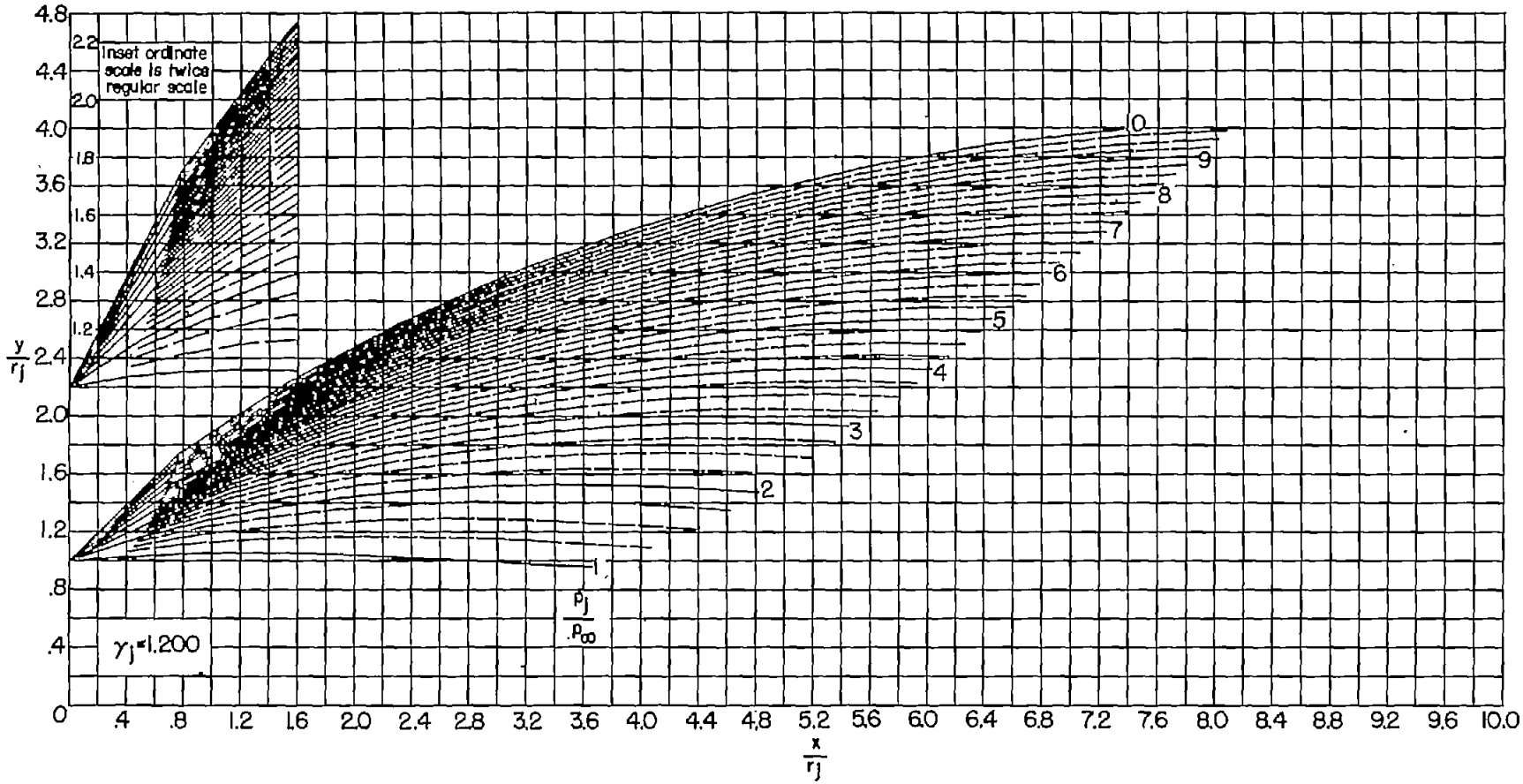


(a) $\theta_N = 5^\circ$. Continued.

Figure 3.- Continued.

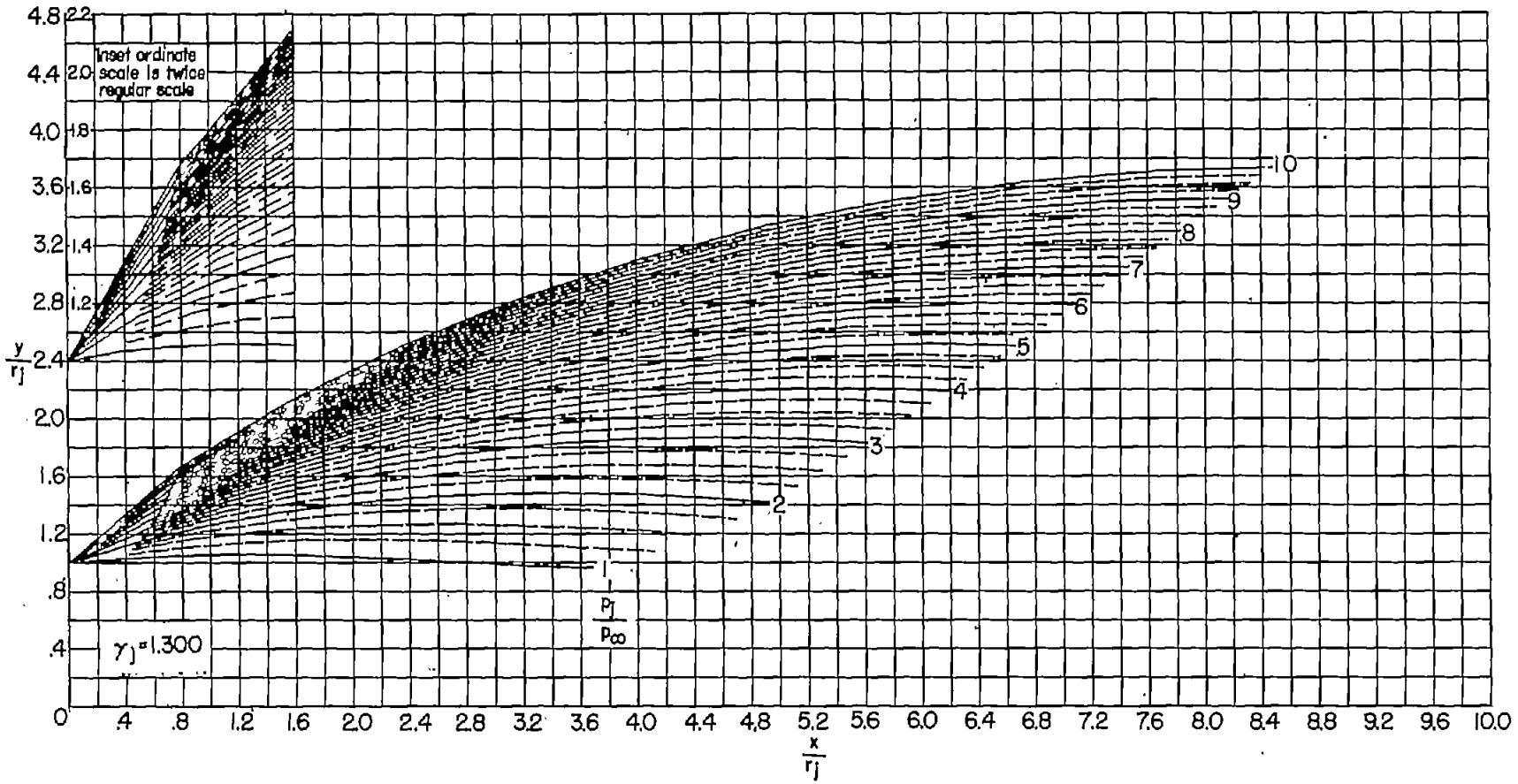


(a) $\theta_N = 5^\circ$. Continued.

Figure 3.- Continued.

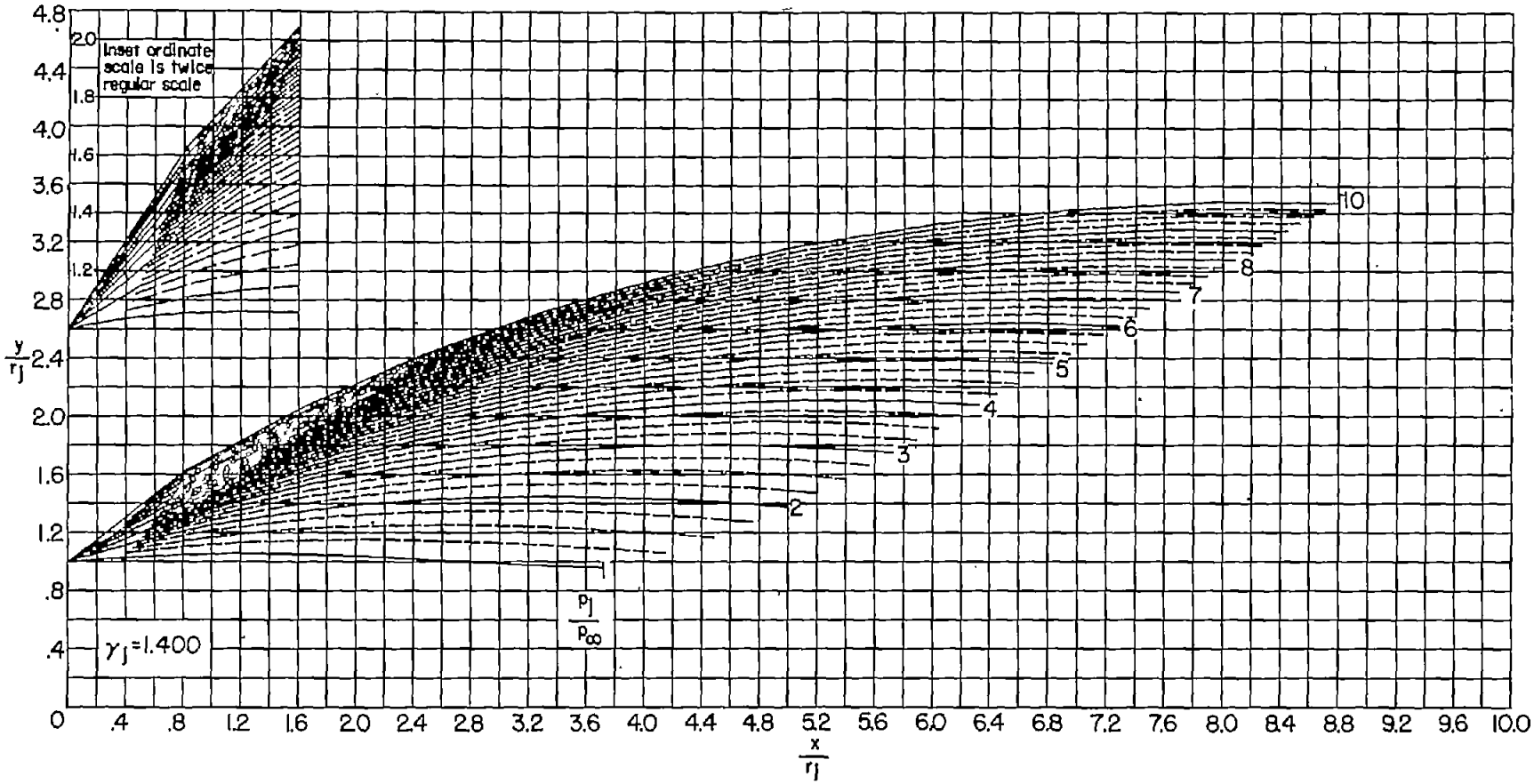


(a) $\theta_N = 5^\circ$. Continued.

Figure 3.- Continued.

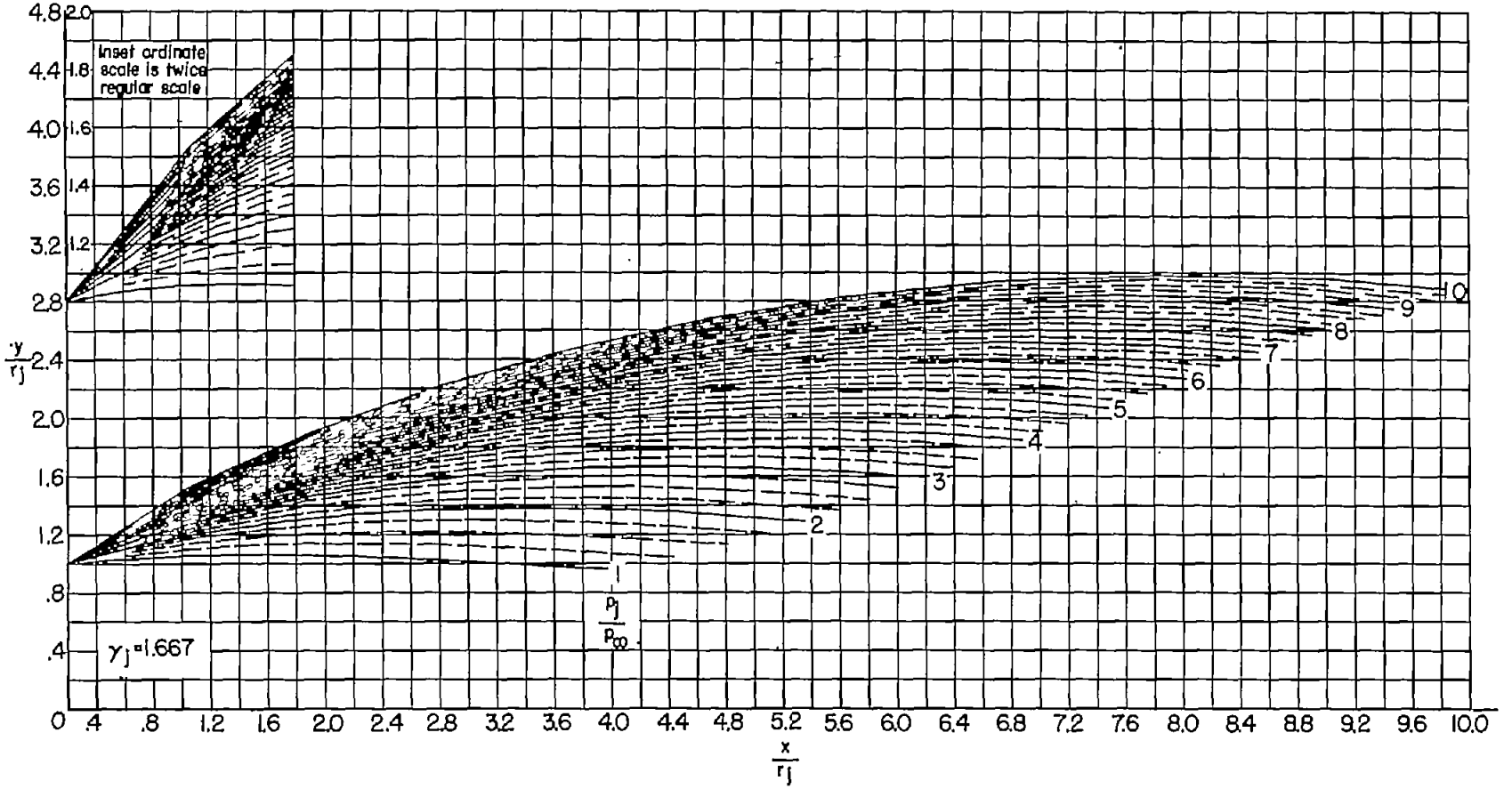


(a) $\theta_N = 5^\circ$. Concluded.

Figure 3.- Continued.

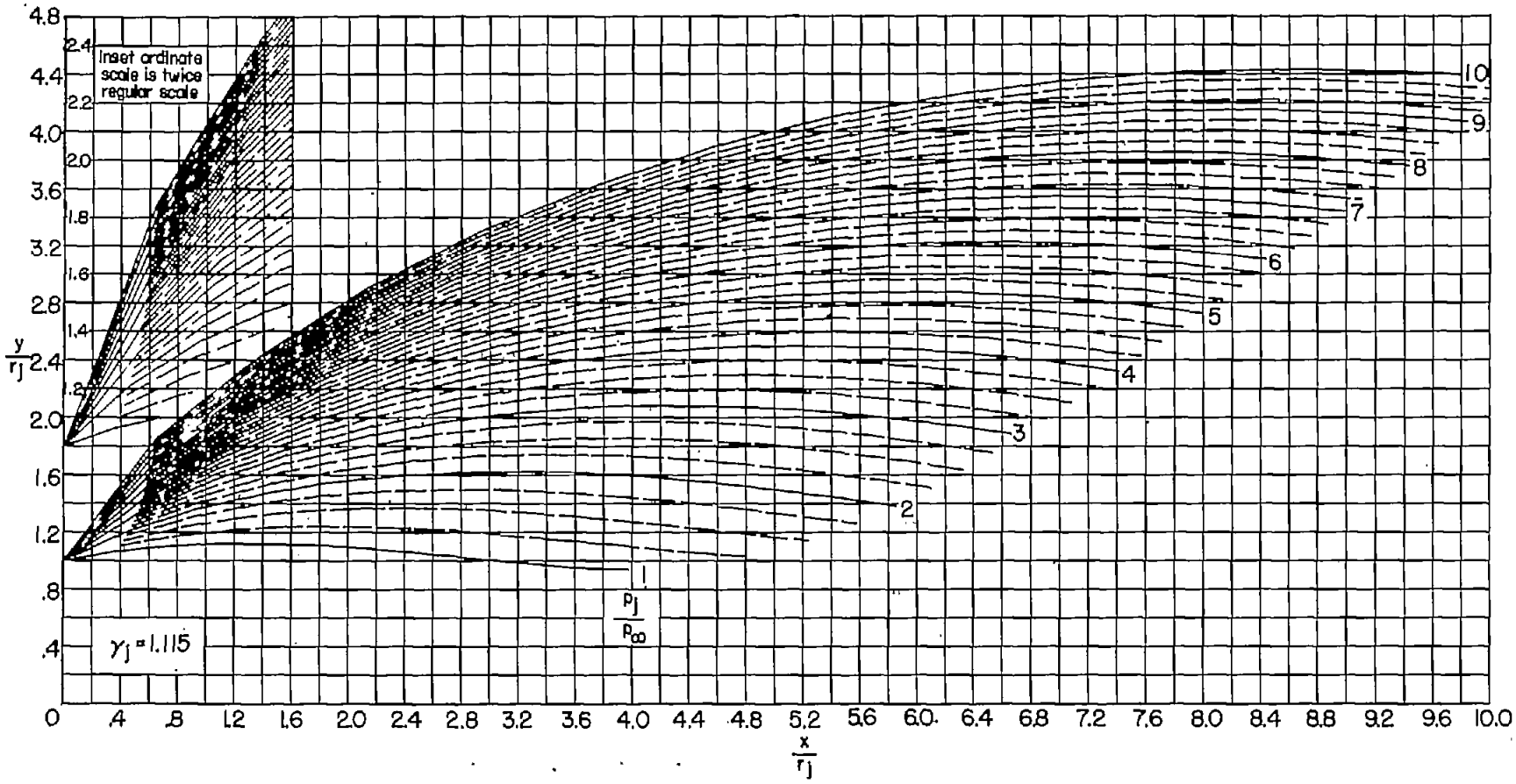


(b) $\theta_N = 10^\circ$.

Figure 3.- Continued.

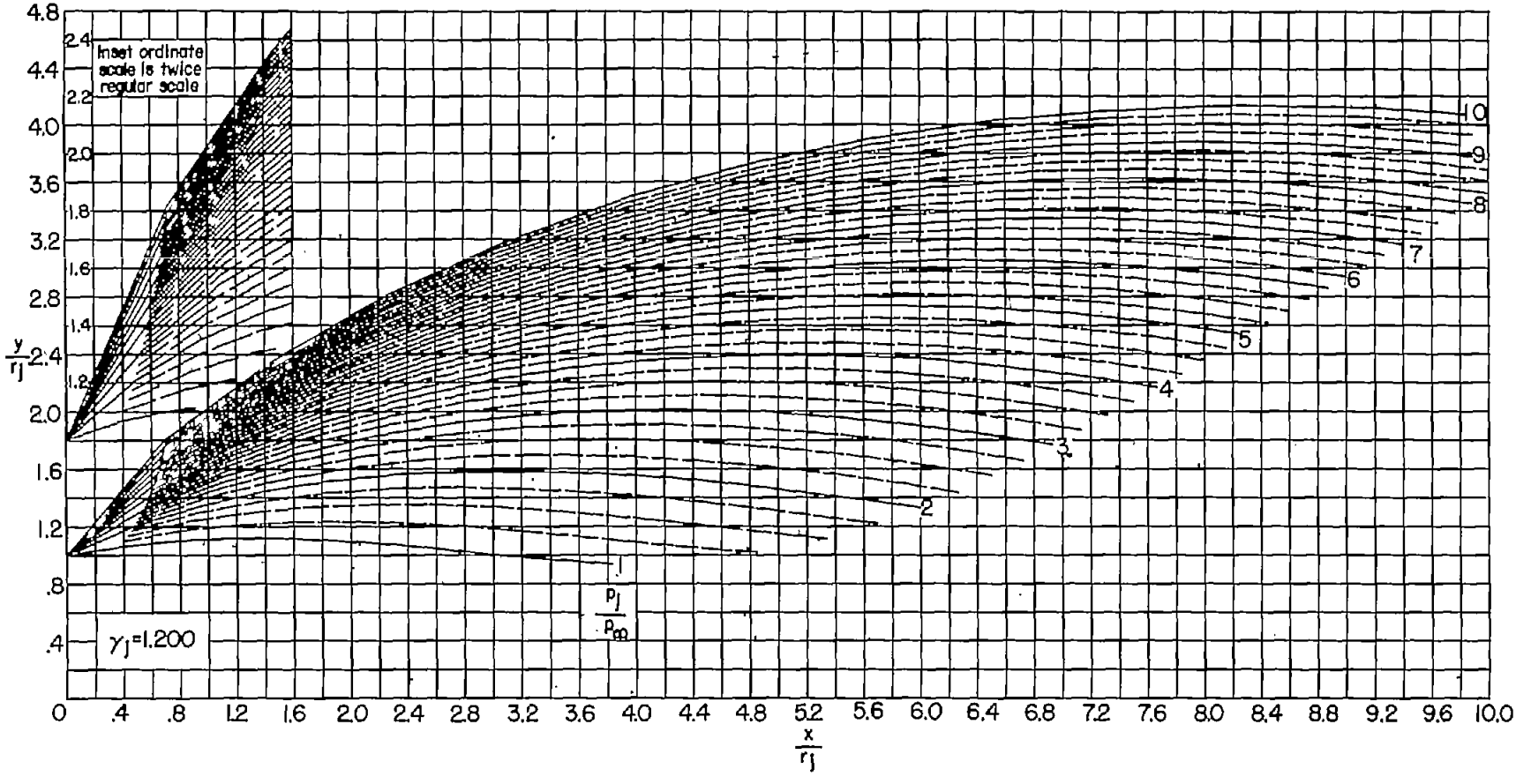


(b) $\theta_N = 10^\circ$. Continued.

Figure 3.- Continued.

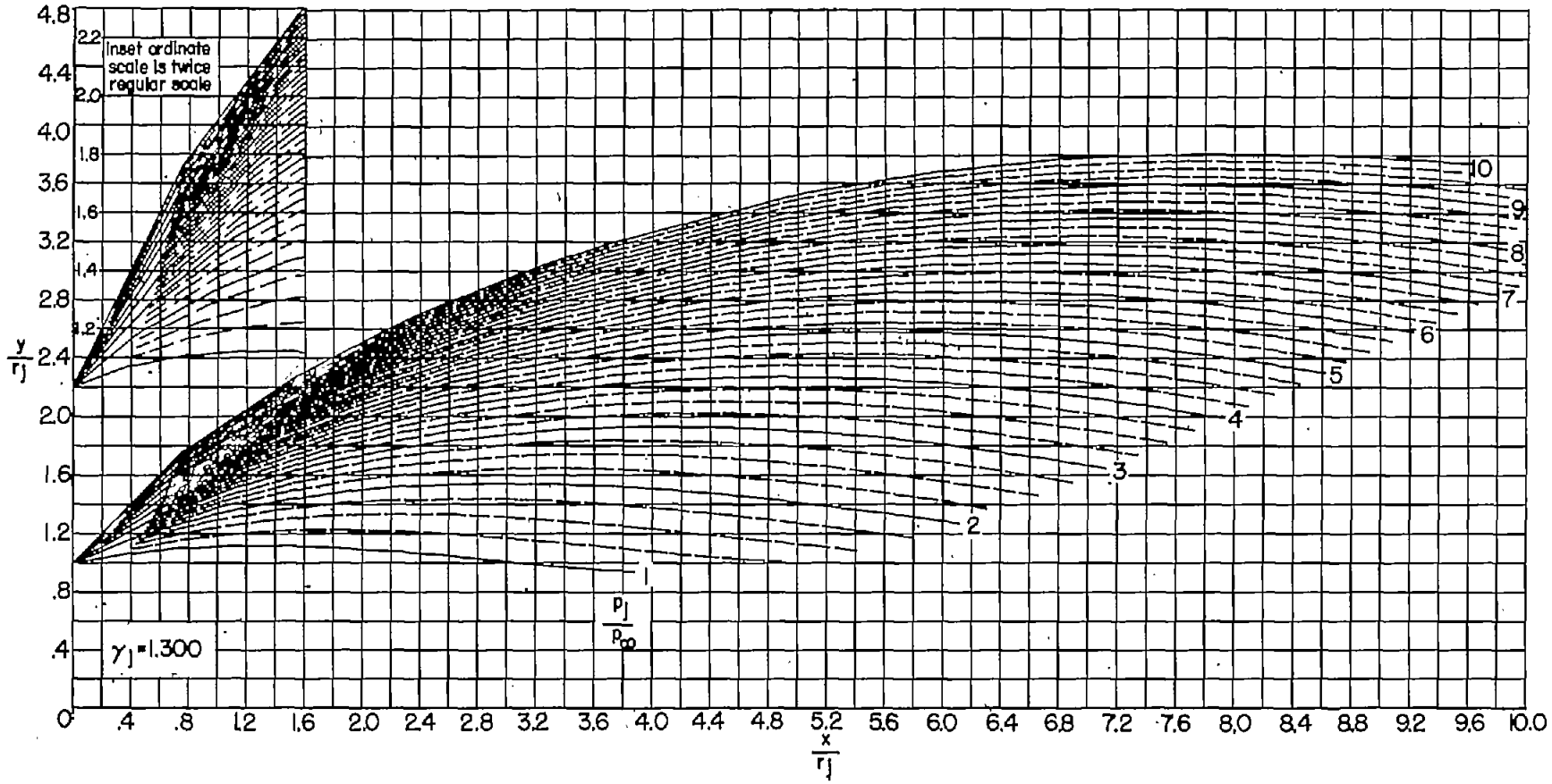


(b) $\theta_N = 10^\circ$. Continued.

Figure 3.- Continued.

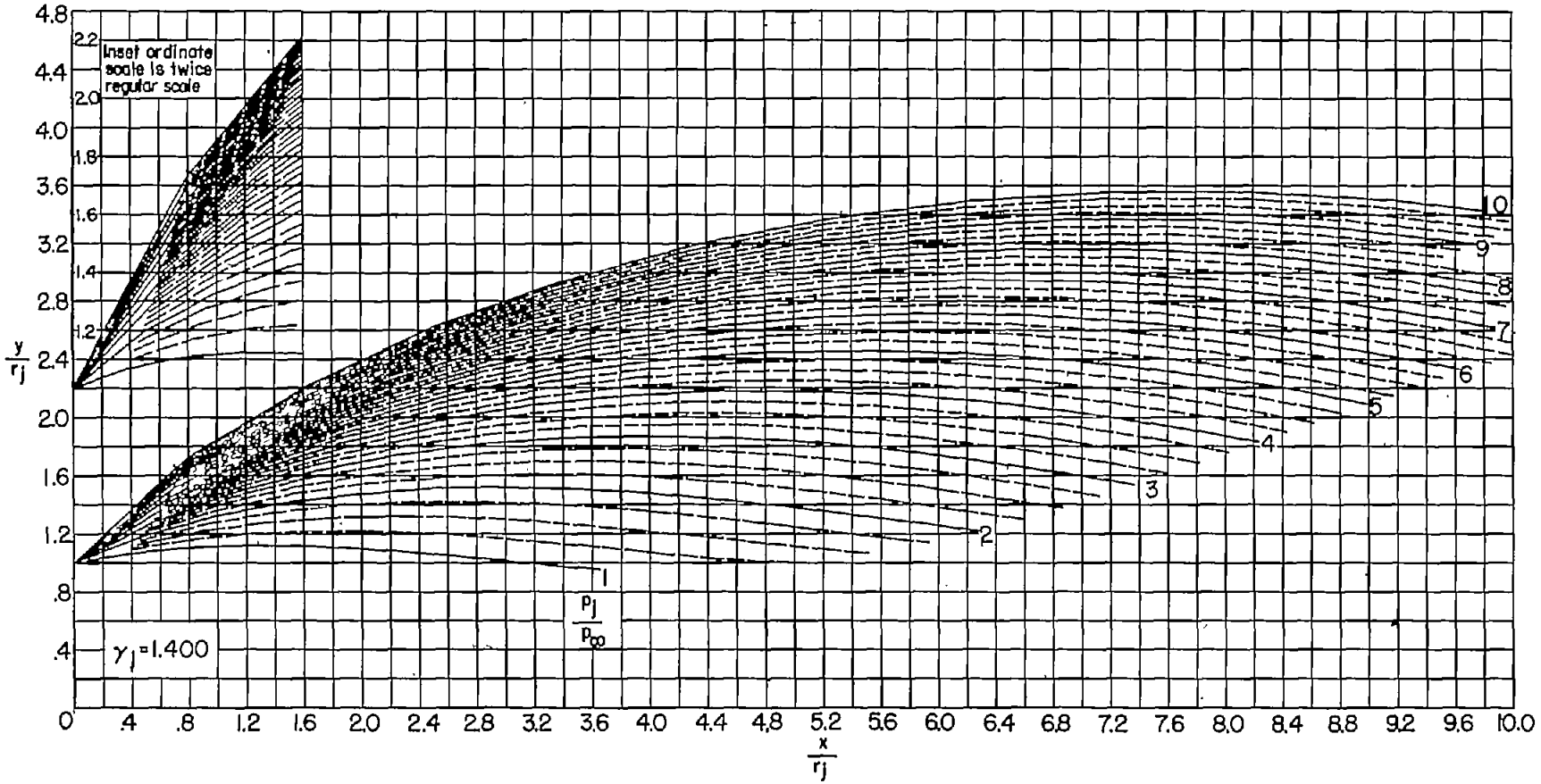


(b) $\theta_N = 10^\circ$. Continued.

Figure 3.- Continued.

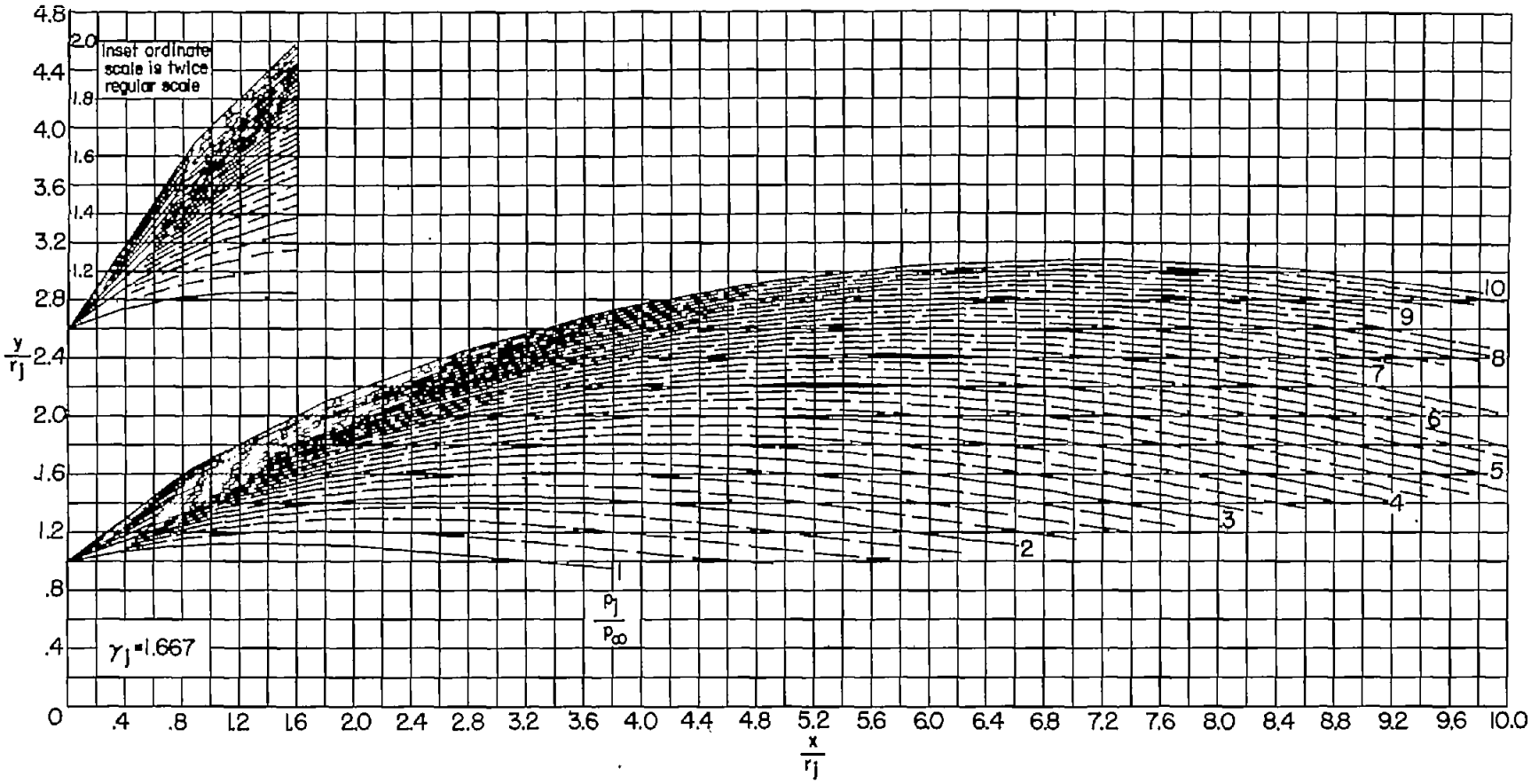


(b) $\theta_N = 10^\circ$. Concluded.

Figure 3.- Continued.

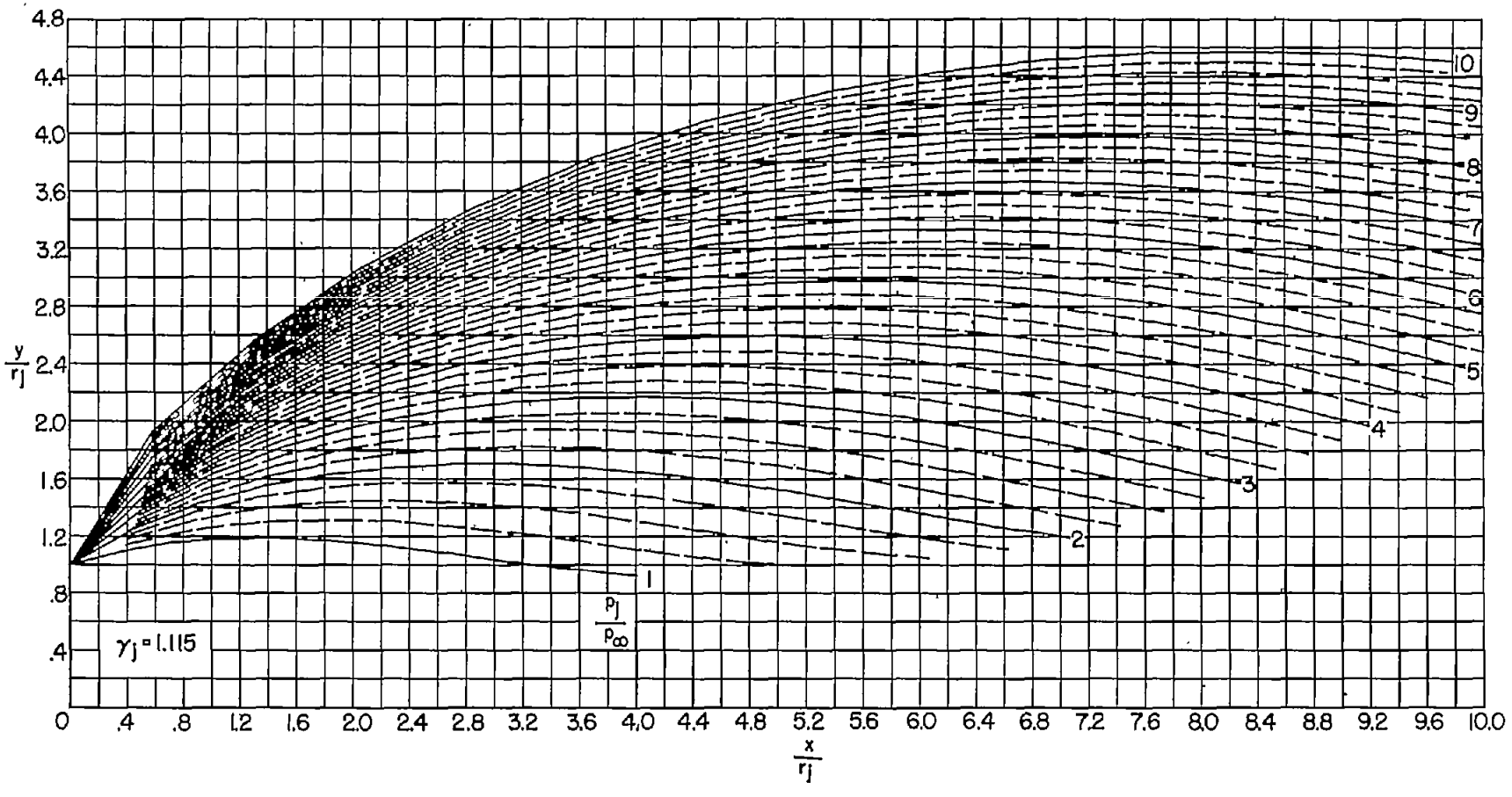


(c) $\theta_N = 15°$.

Figure 3.- Continued.

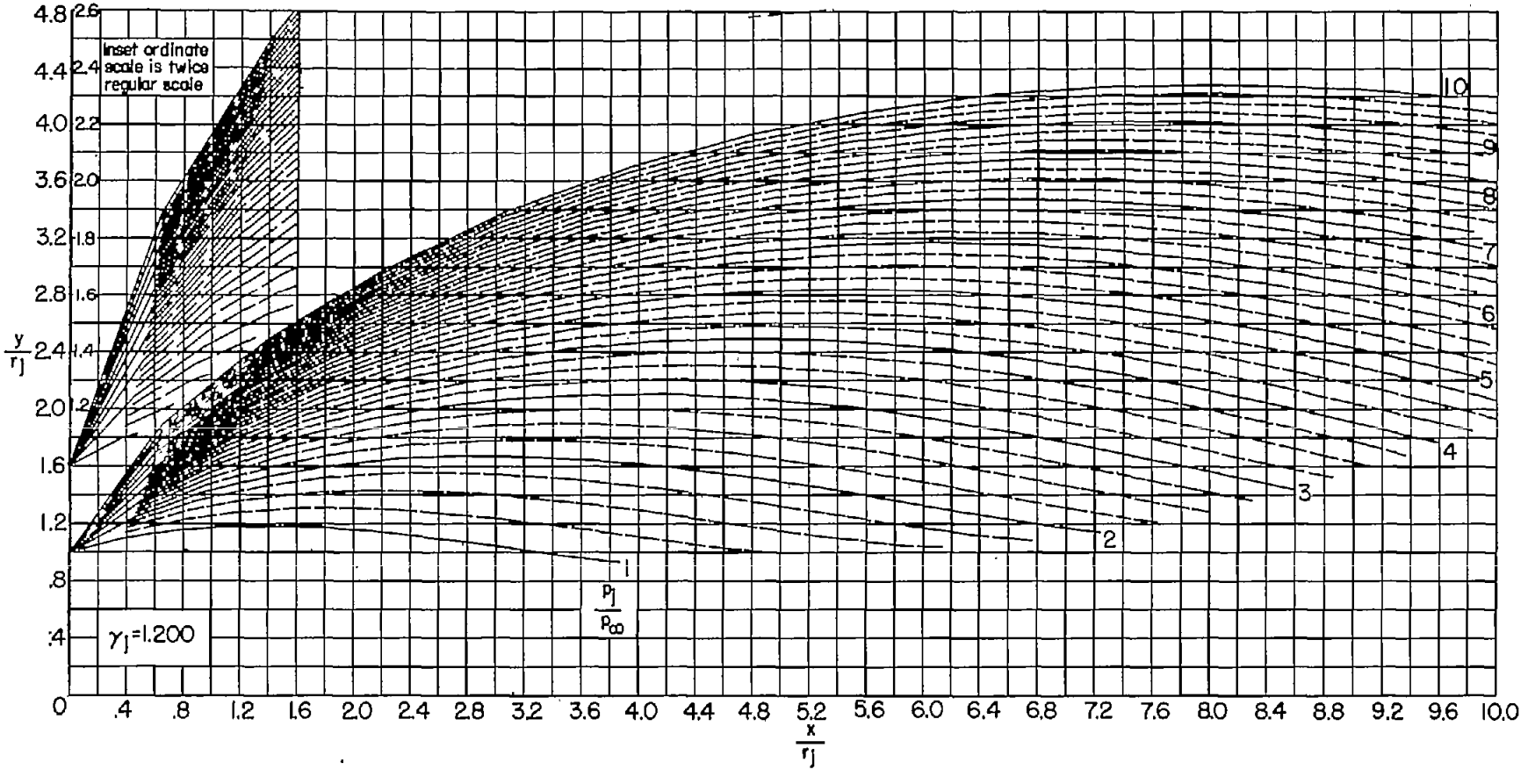


(c) $\theta_N = 15^\circ$. Continued.

Figure 3.- Continued.

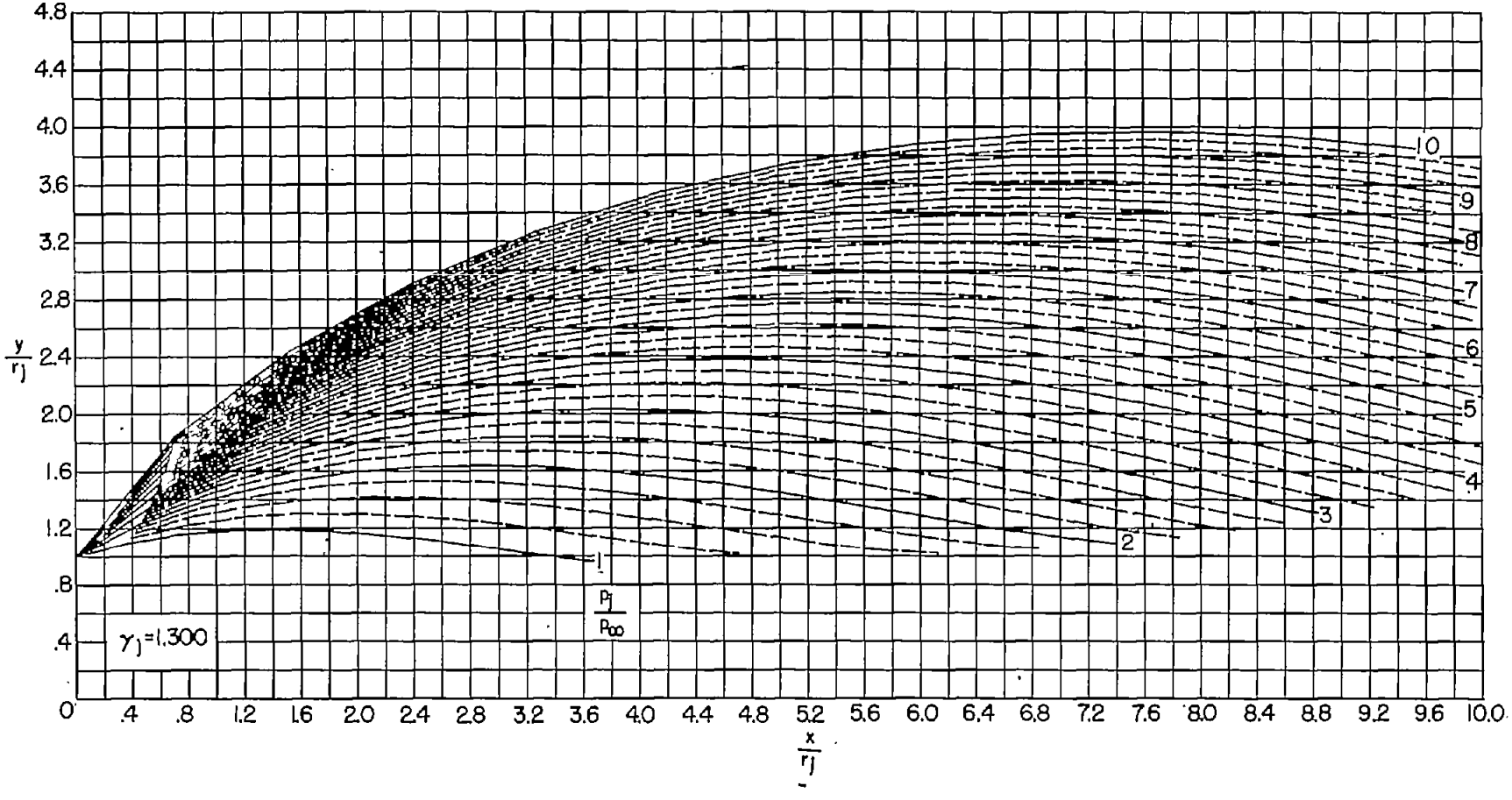


(c) $\theta_N = 15^\circ$. Continued.

Figure 3.- Continued.

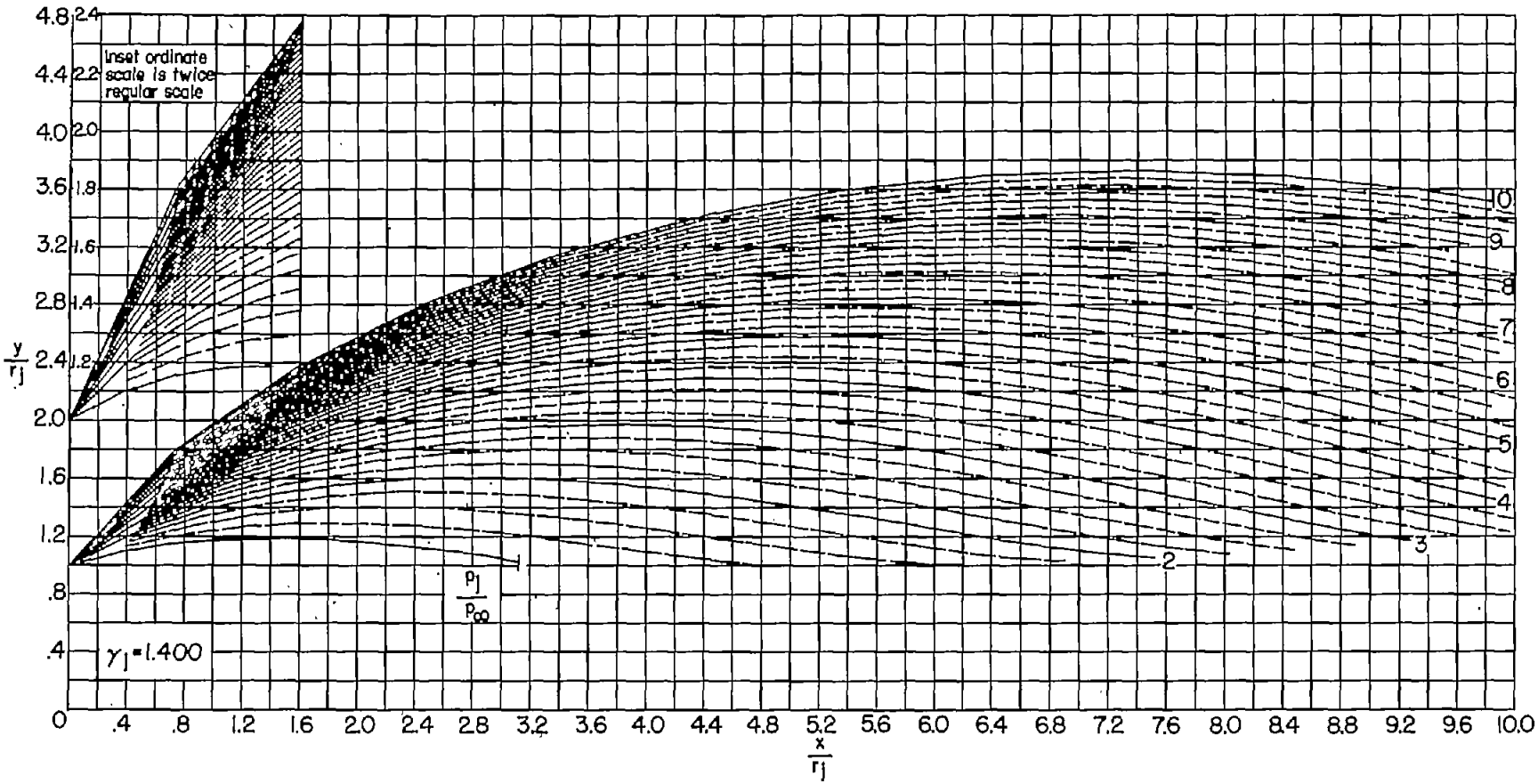


(c) $\theta_N = 15^\circ$. Continued.

Figure 3.- Continued.

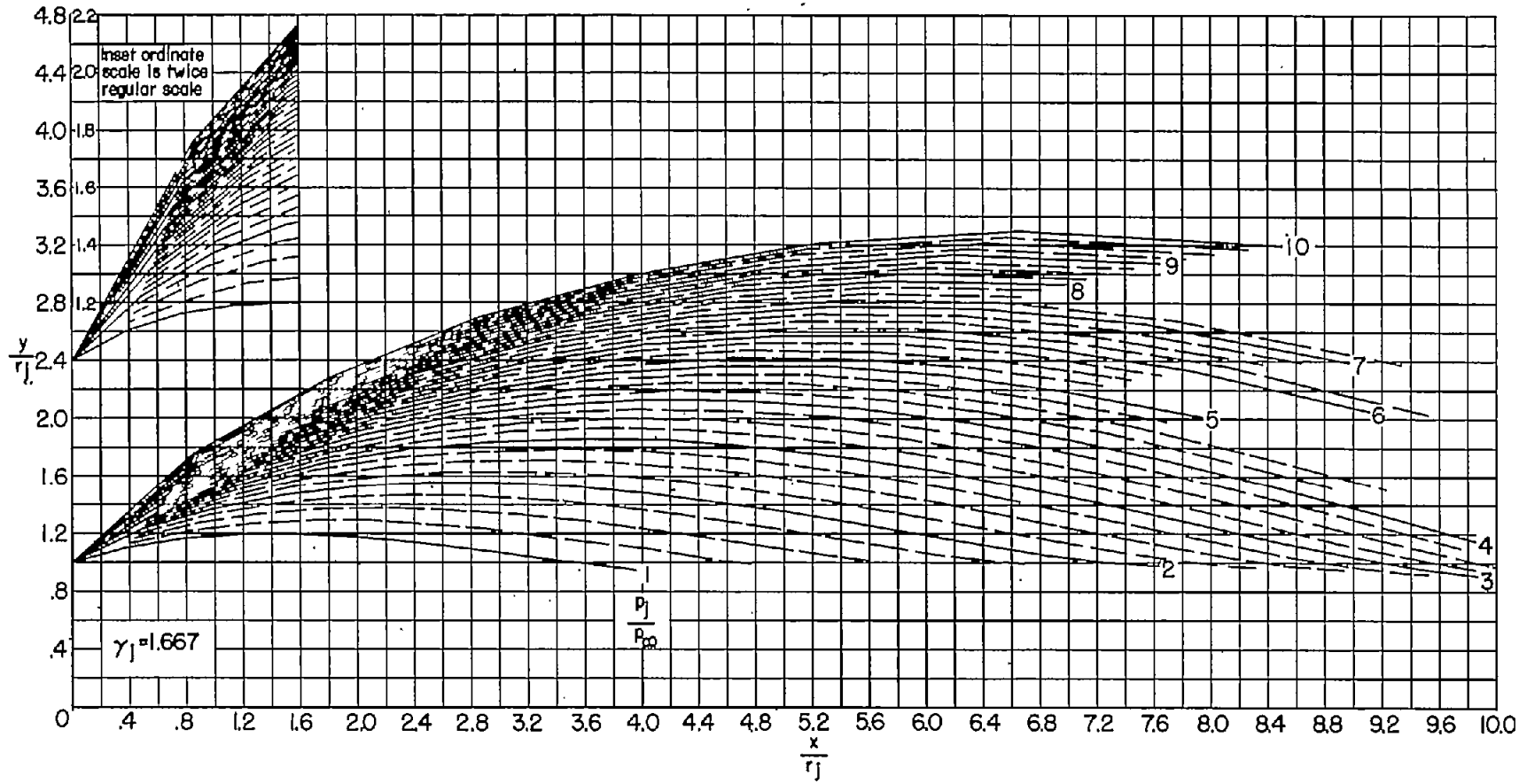


(c) $\theta_N = 15°$. Concluded.

Figure 3.- Continued.

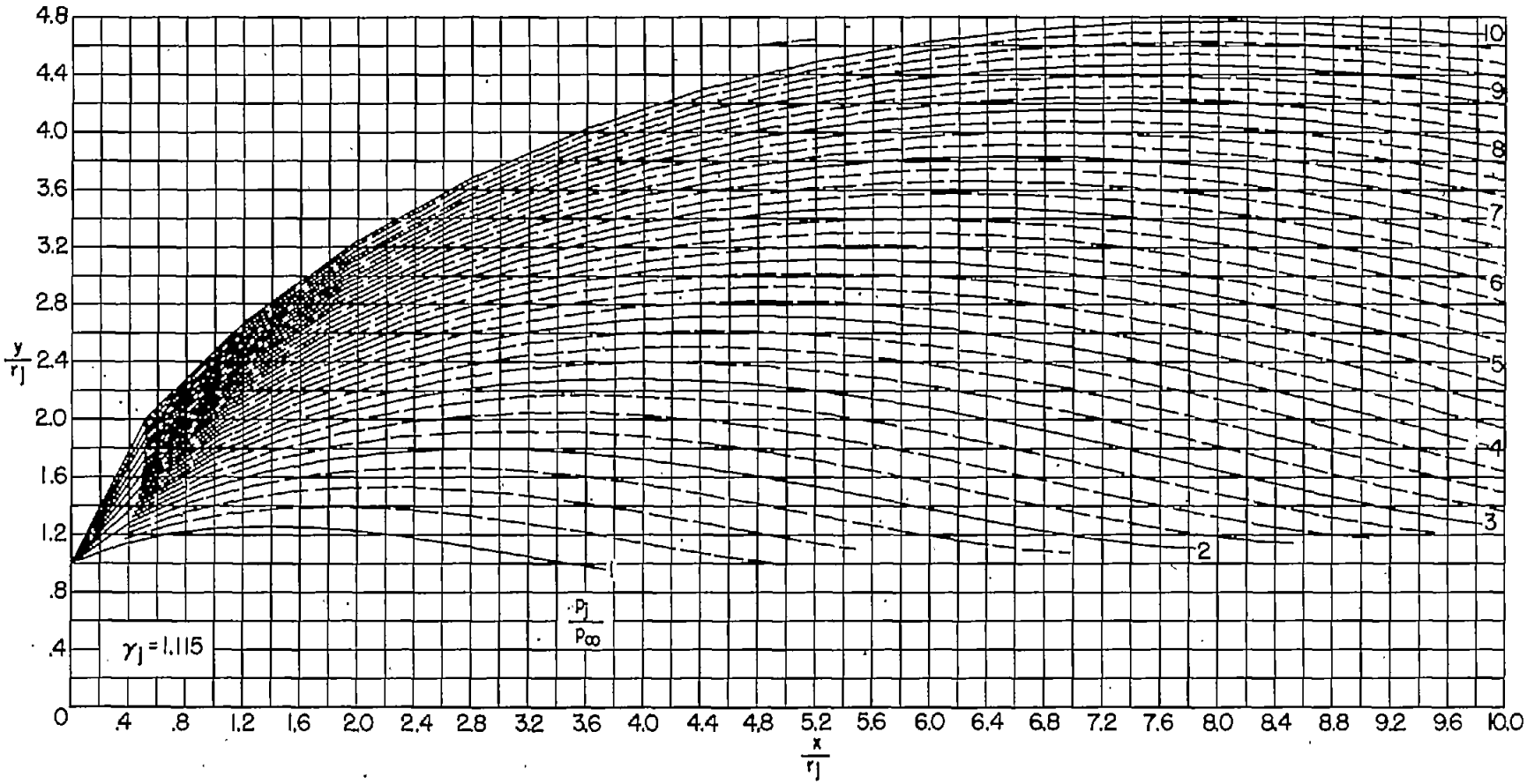


(d) $\theta_N = 20^\circ$.

Figure 3.- Continued.

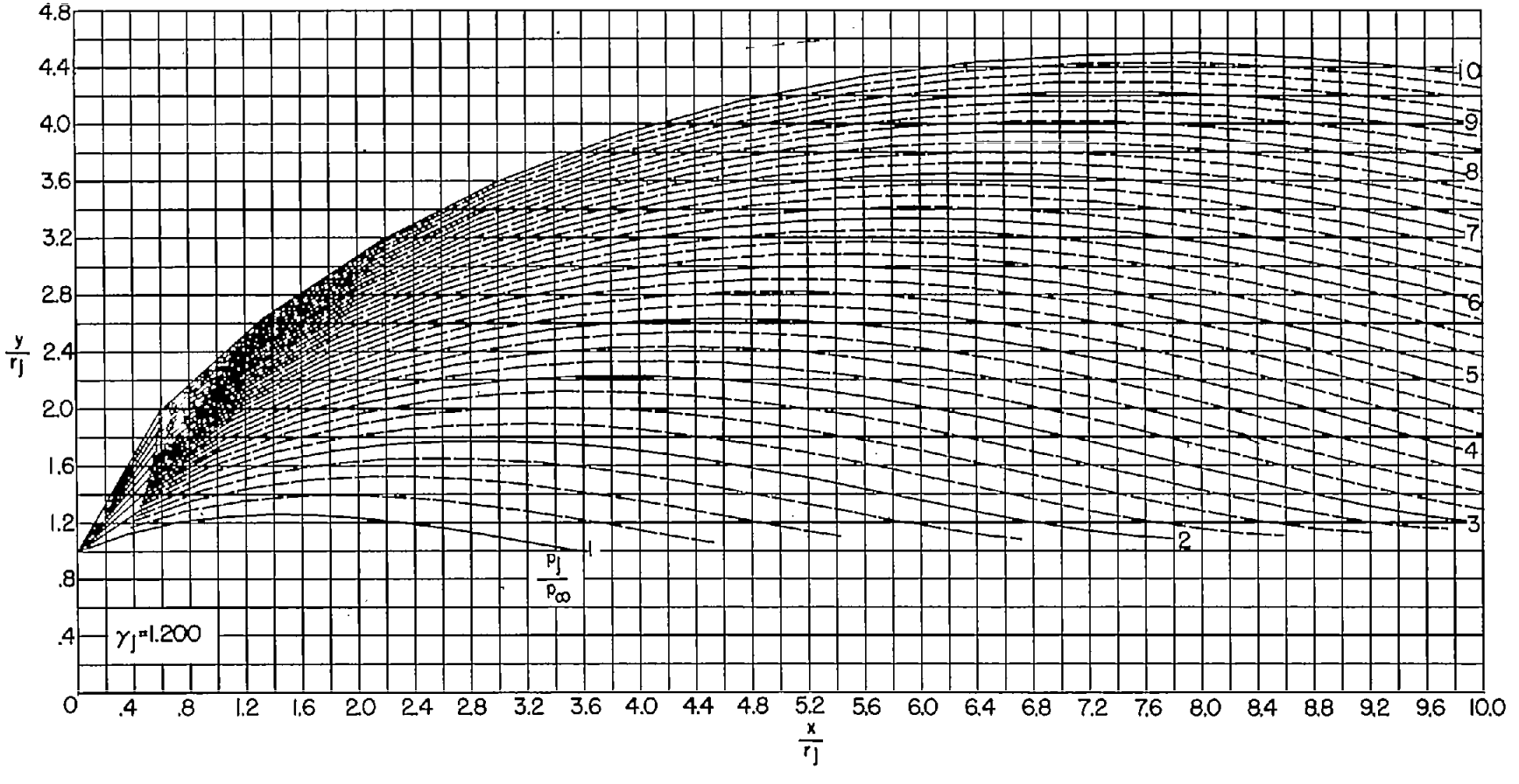


(d) $\theta_N = 20^\circ$. Continued.

Figure 3.- Continued.

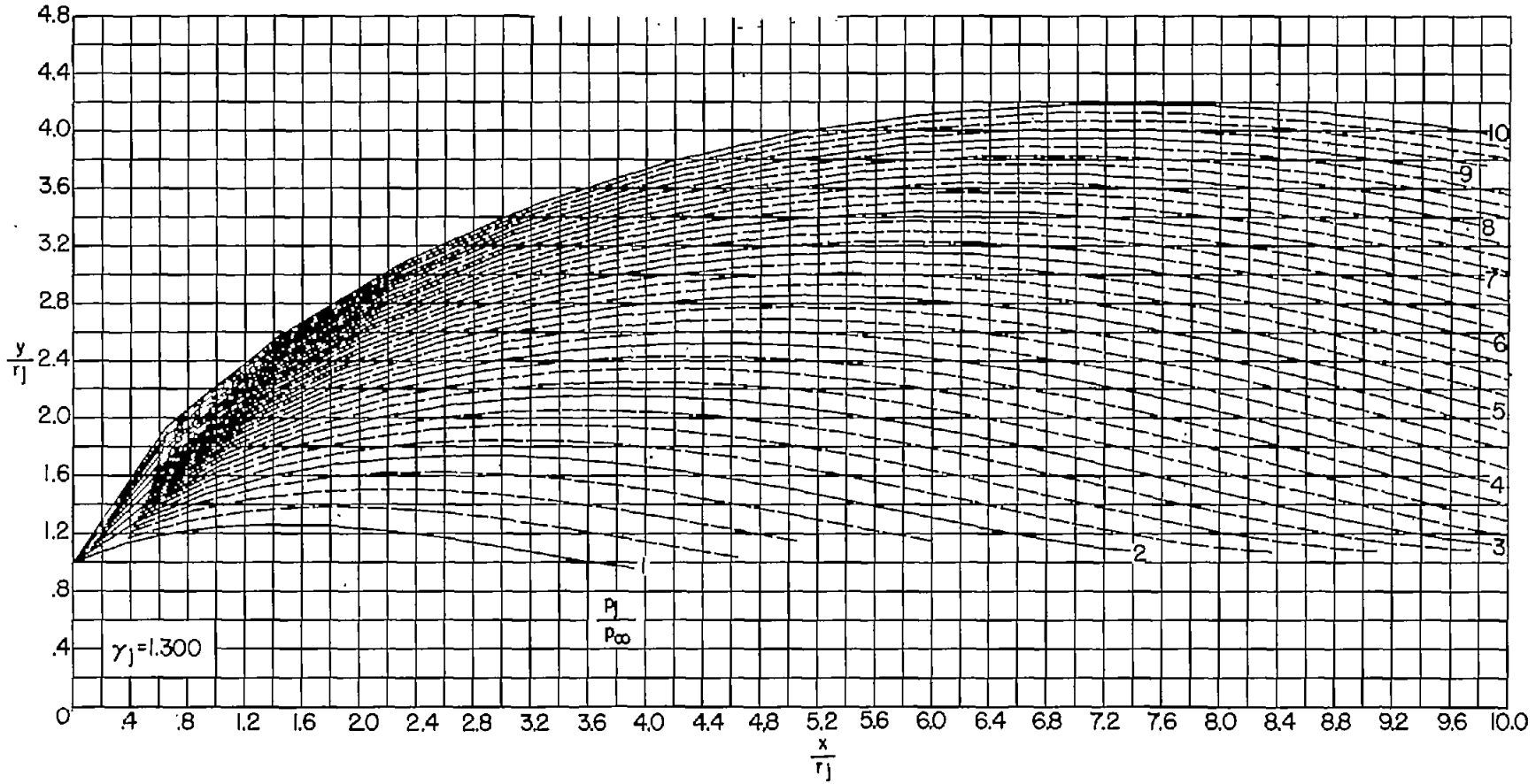


(d) $\theta_N = 20^\circ$. Continued.

Figure 3.- Continued.

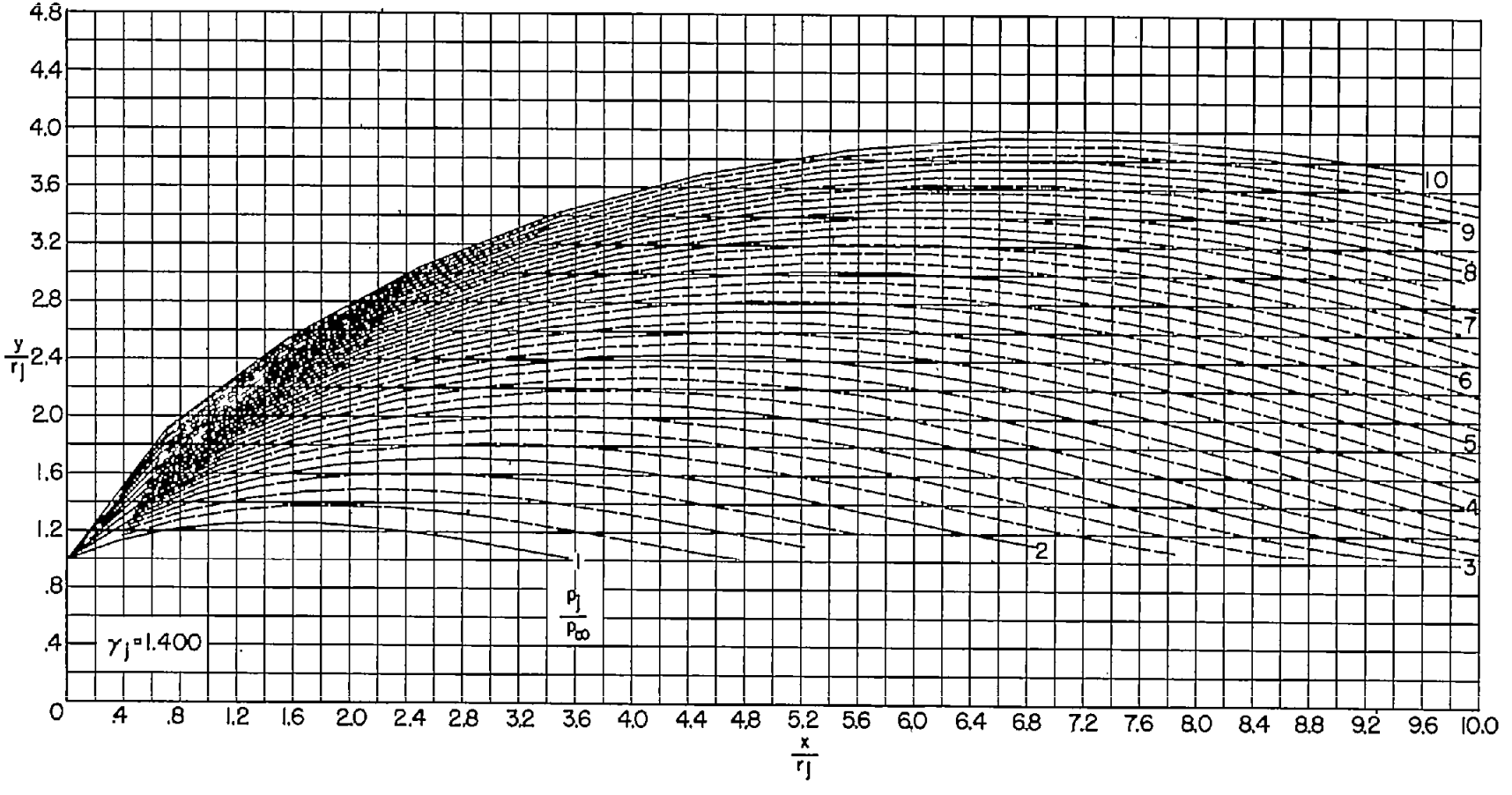


(d) $\theta_N = 20^\circ$. Continued.

Figure 3.- Continued.

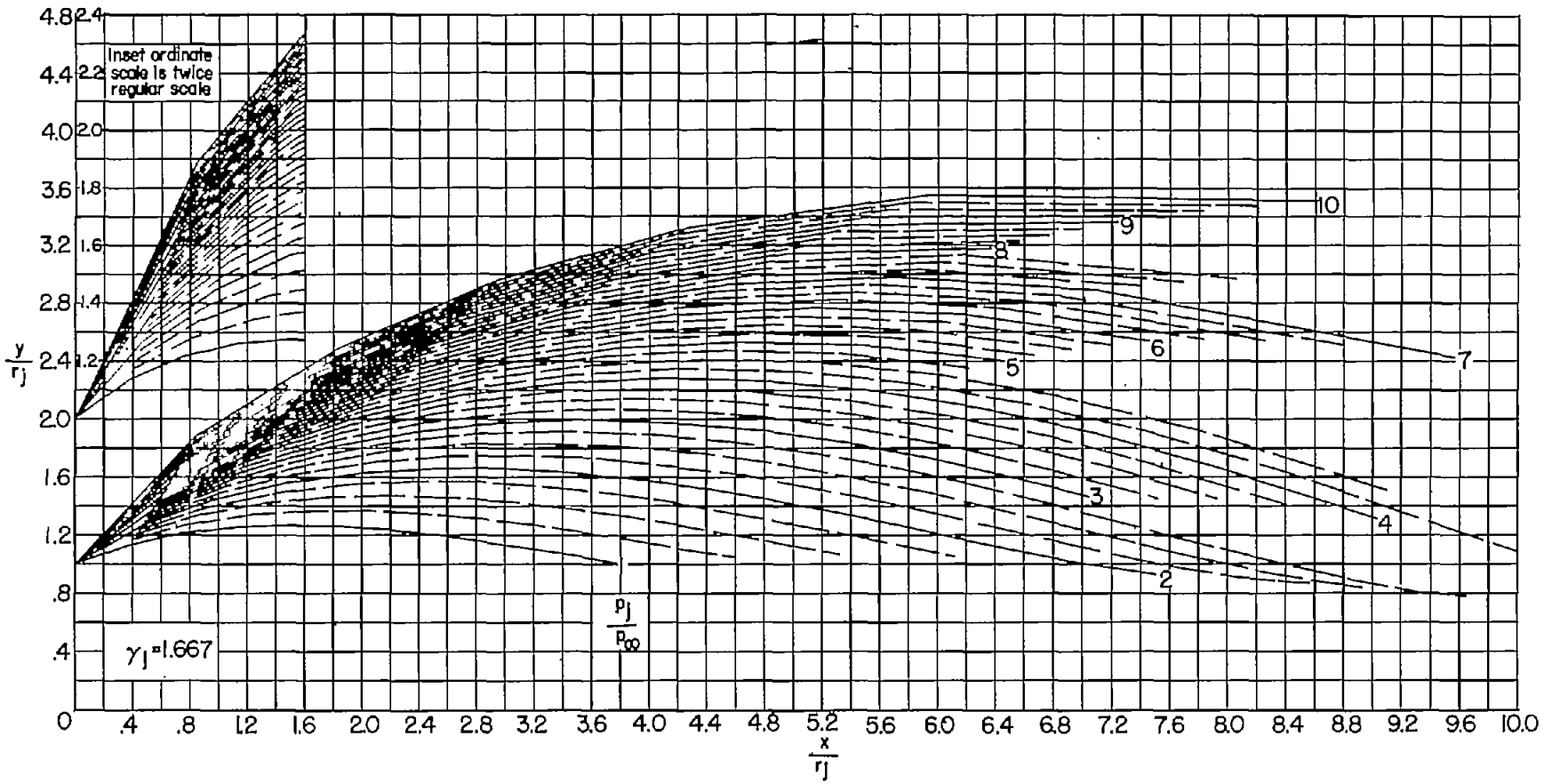


(d) $\theta_N = 20^\circ$. Concluded.

Figure 3.- Concluded.

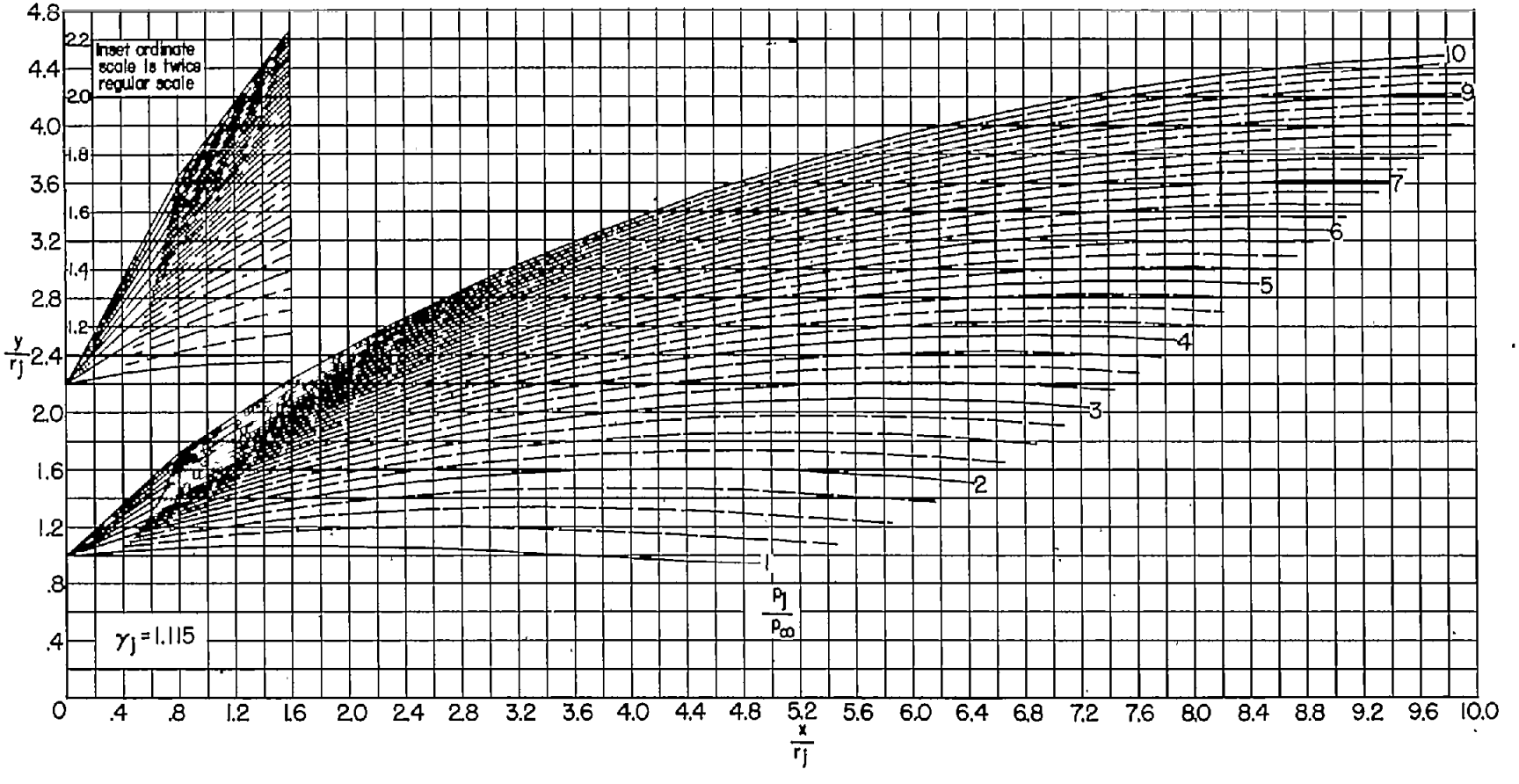


(a) $\theta_N = 5^\circ$.

Figure 4.- Jet boundaries at $M_j = 2.5$ for jet static-pressure ratios from 1 to 10. (Dashed boundaries denote changes in $p_j/p_\infty$ of 0.25.)

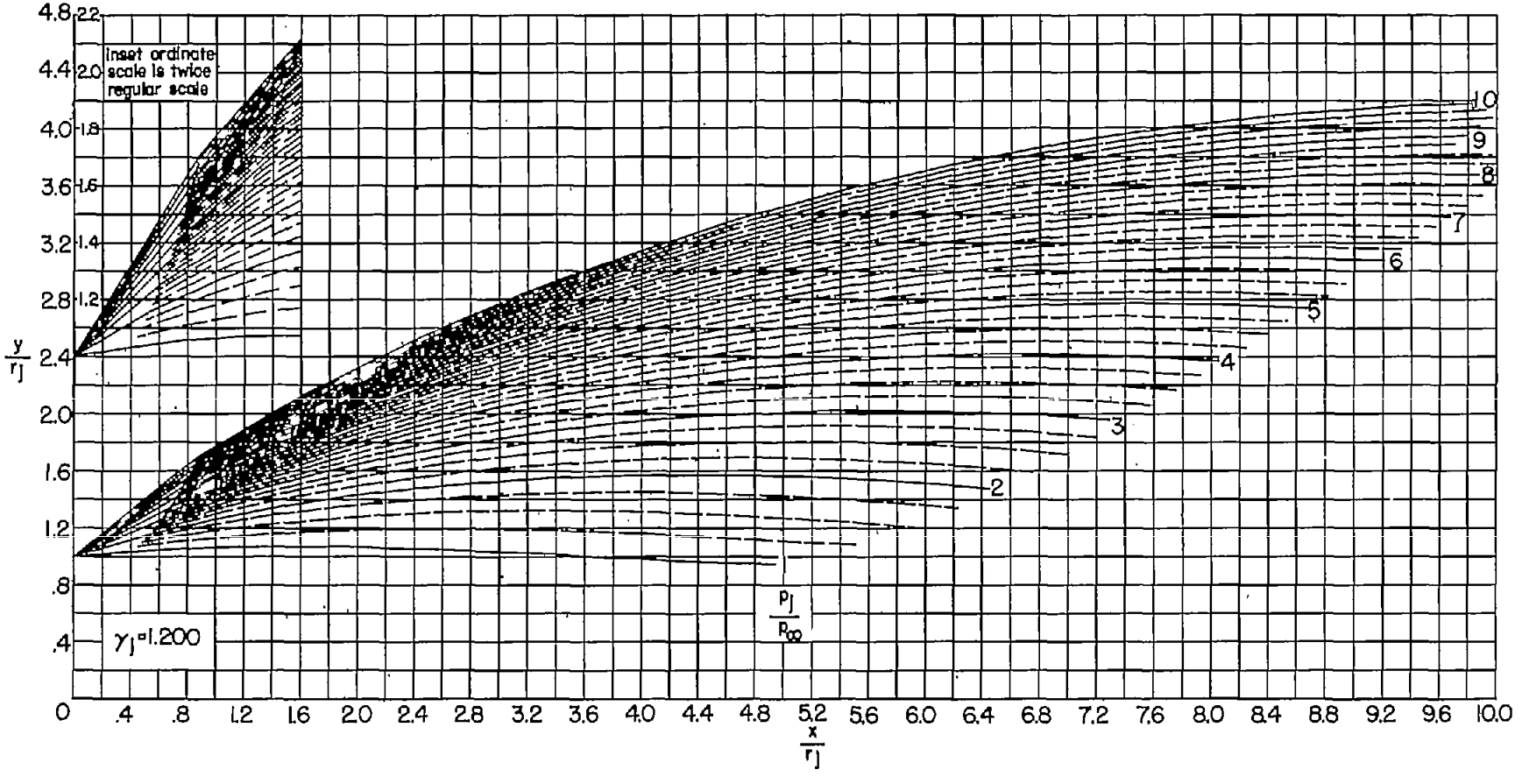


(a) $\theta_N = 5^\circ$. Continued.

Figure 4.- Continued.

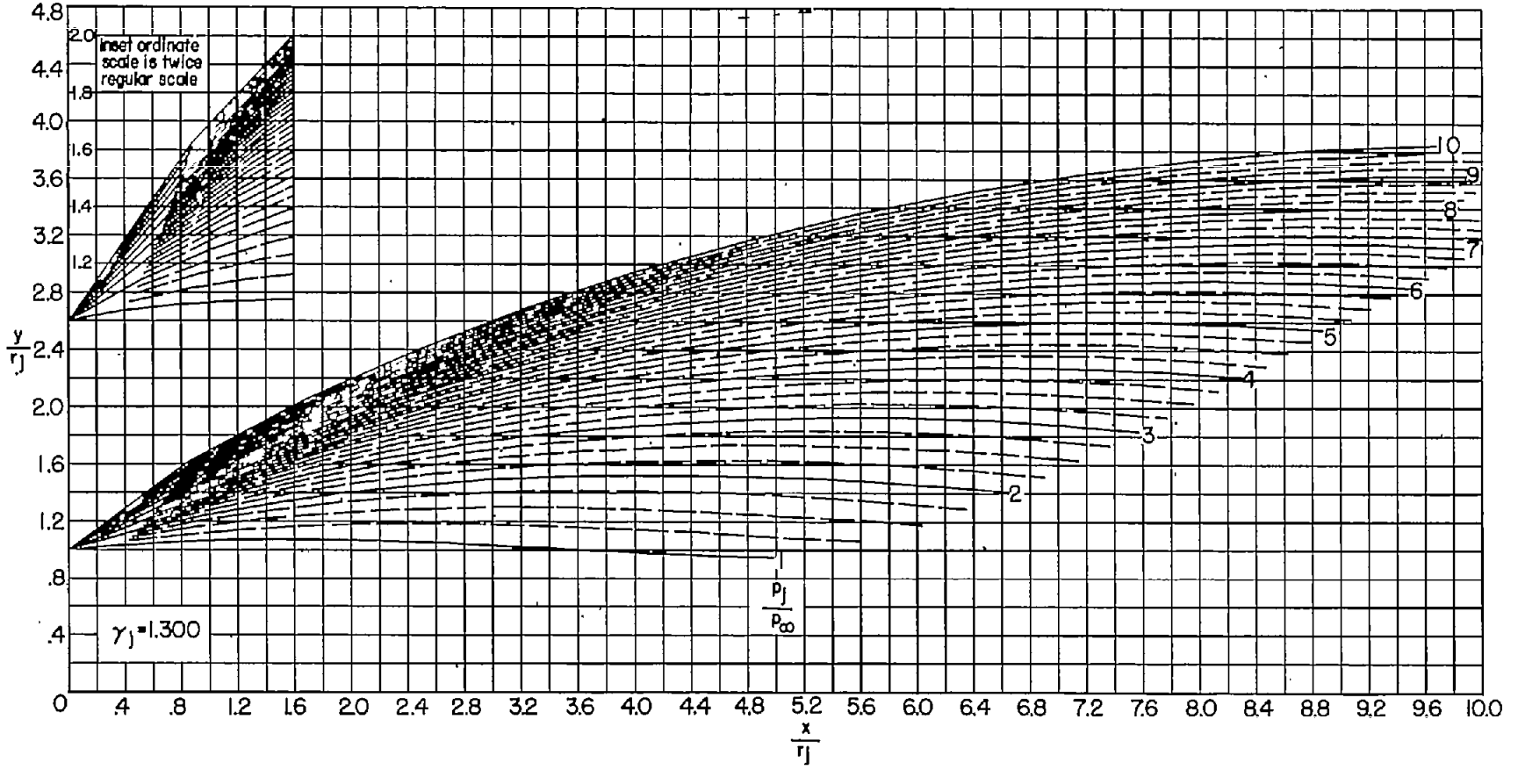


(a) $\theta_N = 5^\circ$. Continued.

Figure 4.- Continued.

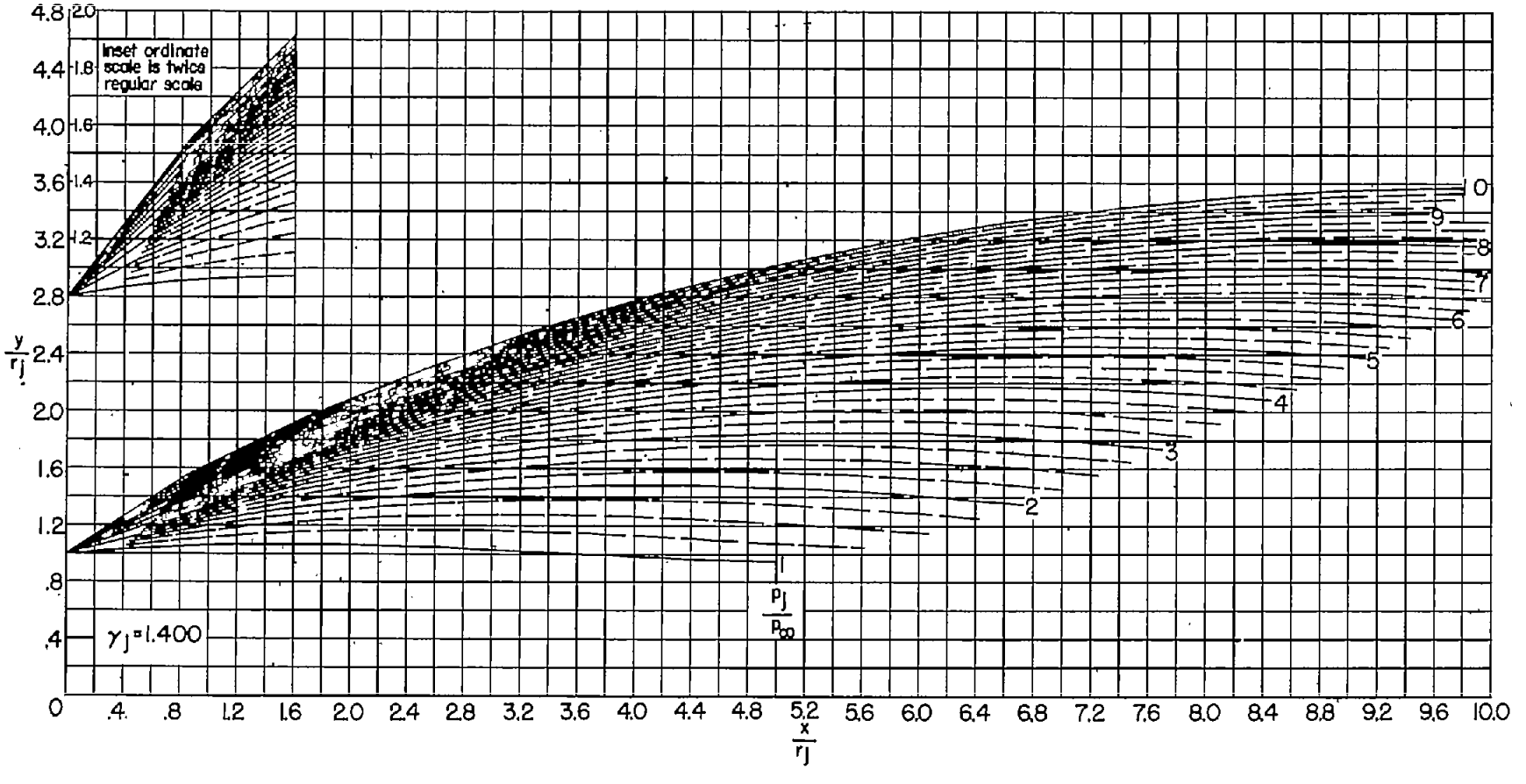


(a) $\theta_N = 5^\circ$. Continued.

Figure 4.- Continued.

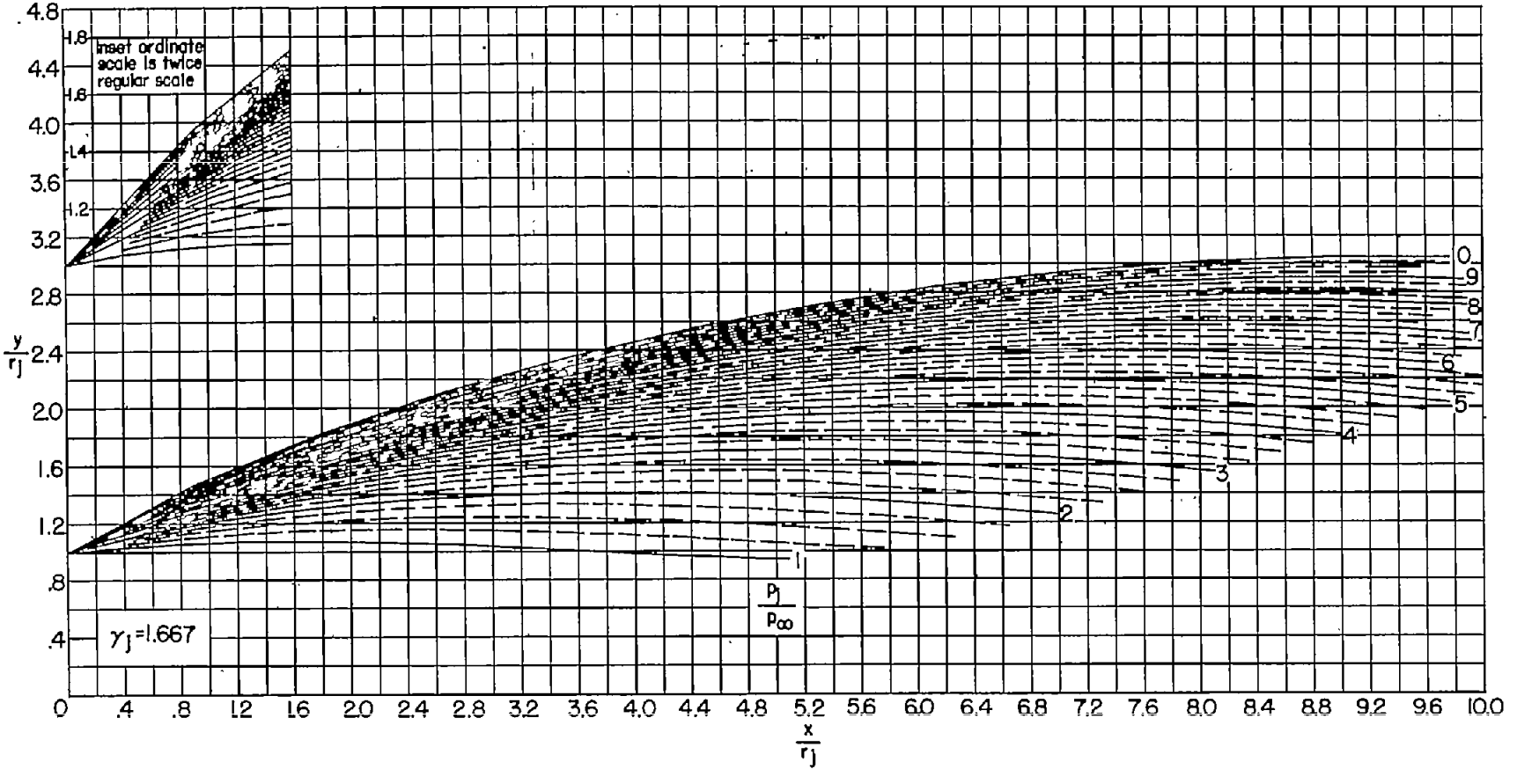


(a) $\theta_N = 5^\circ$. Concluded.

Figure 4.- Continued.

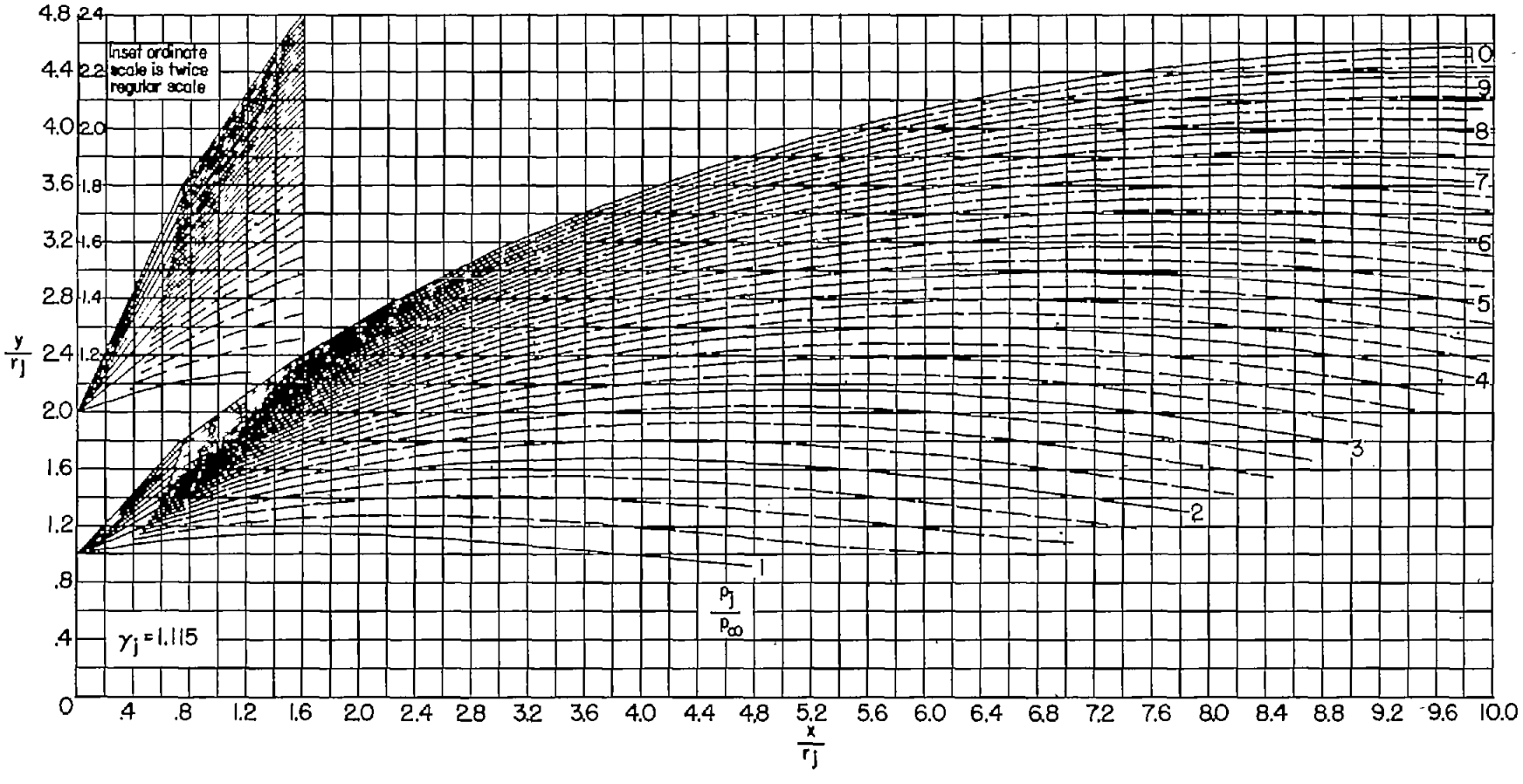


(b) $\theta_N = 10^\circ$.

Figure 4.- Continued.

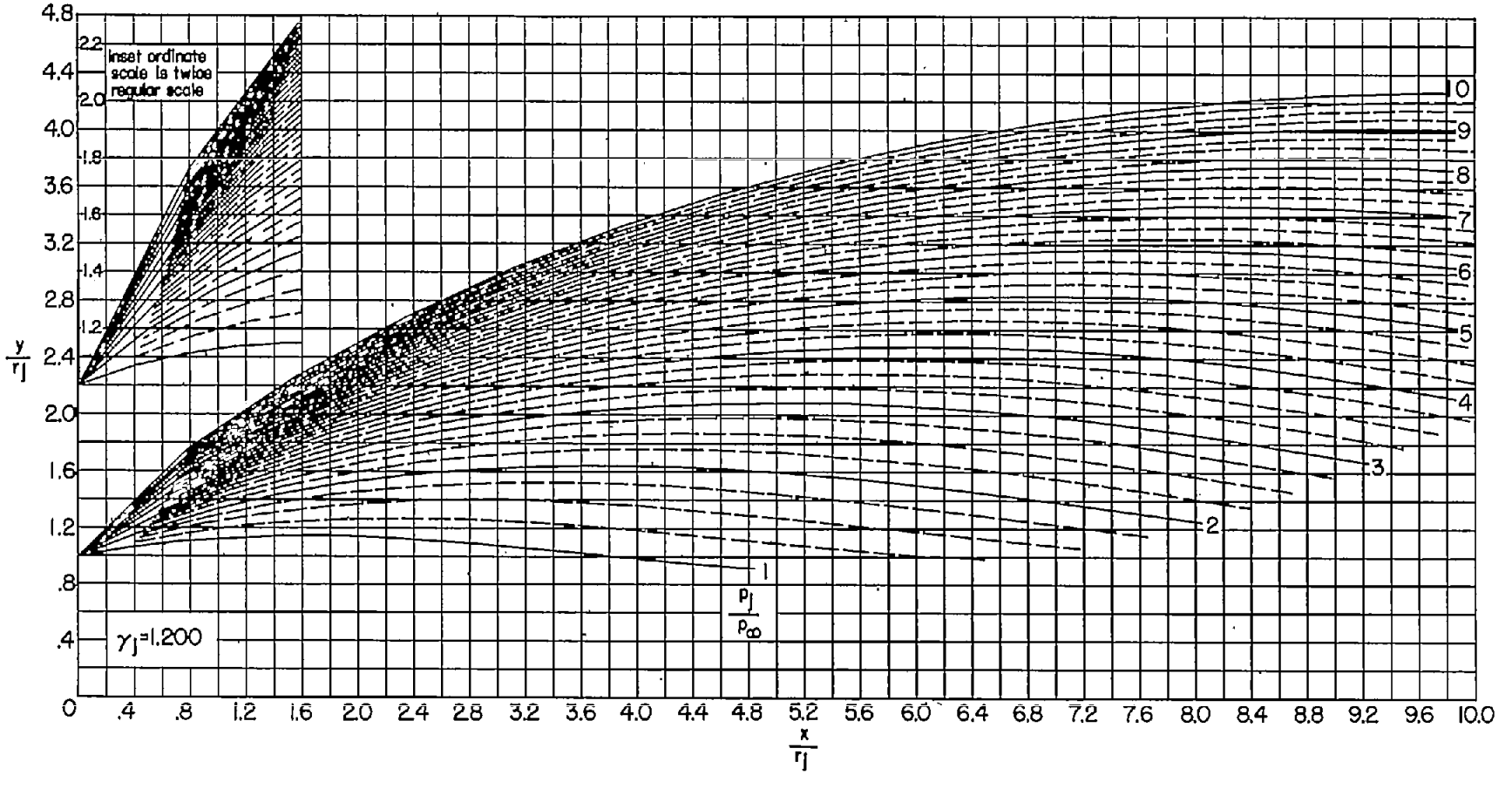


(b) $\theta_N = 10^\circ$. Continued.

Figure 4.- Continued.

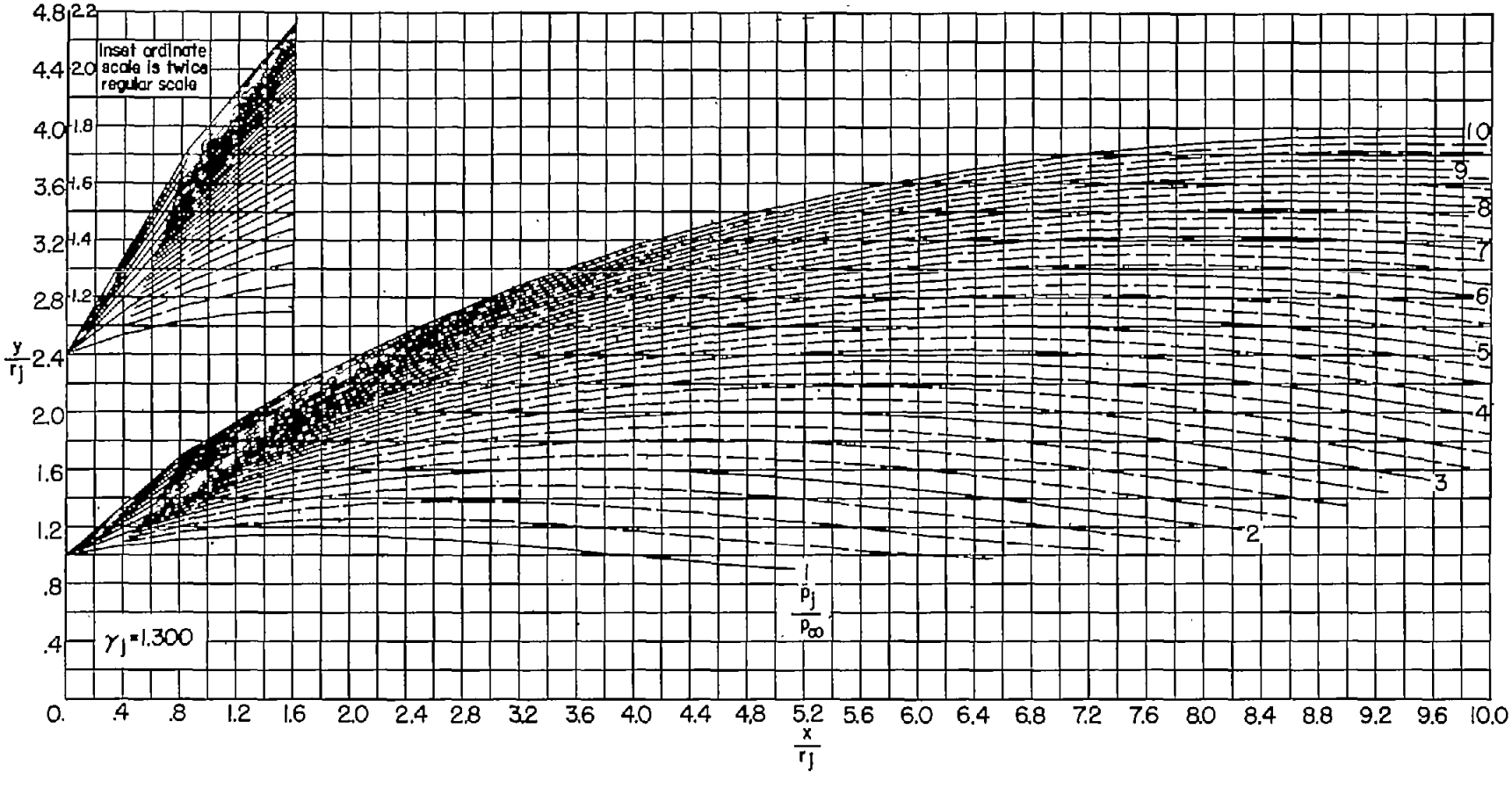


(b) $\theta_N = 10^\circ$. Continued.

Figure 4.- Continued.

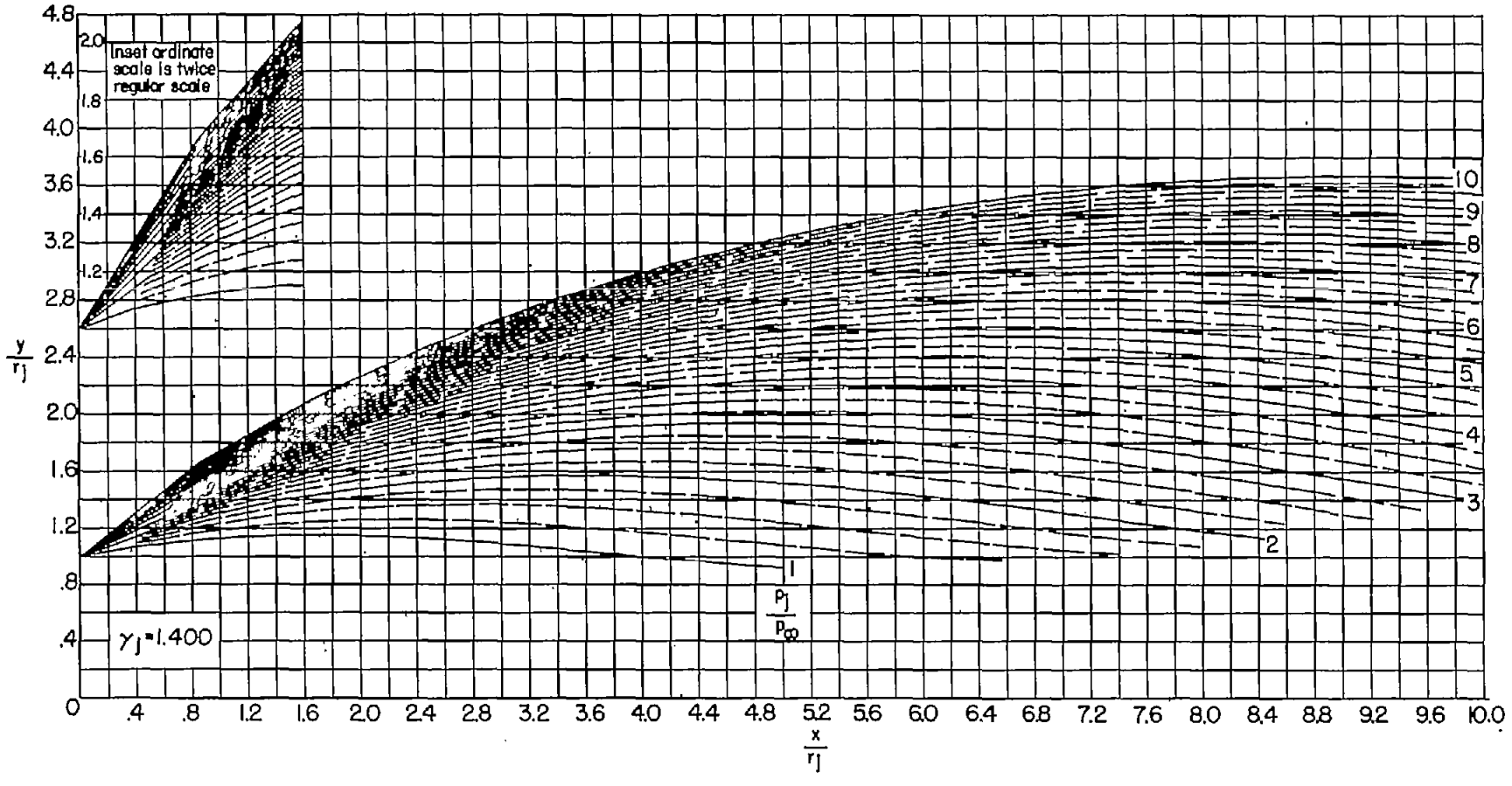


(b) $\theta_N = 10^\circ$. Continued.

Figure 4.- Continued.

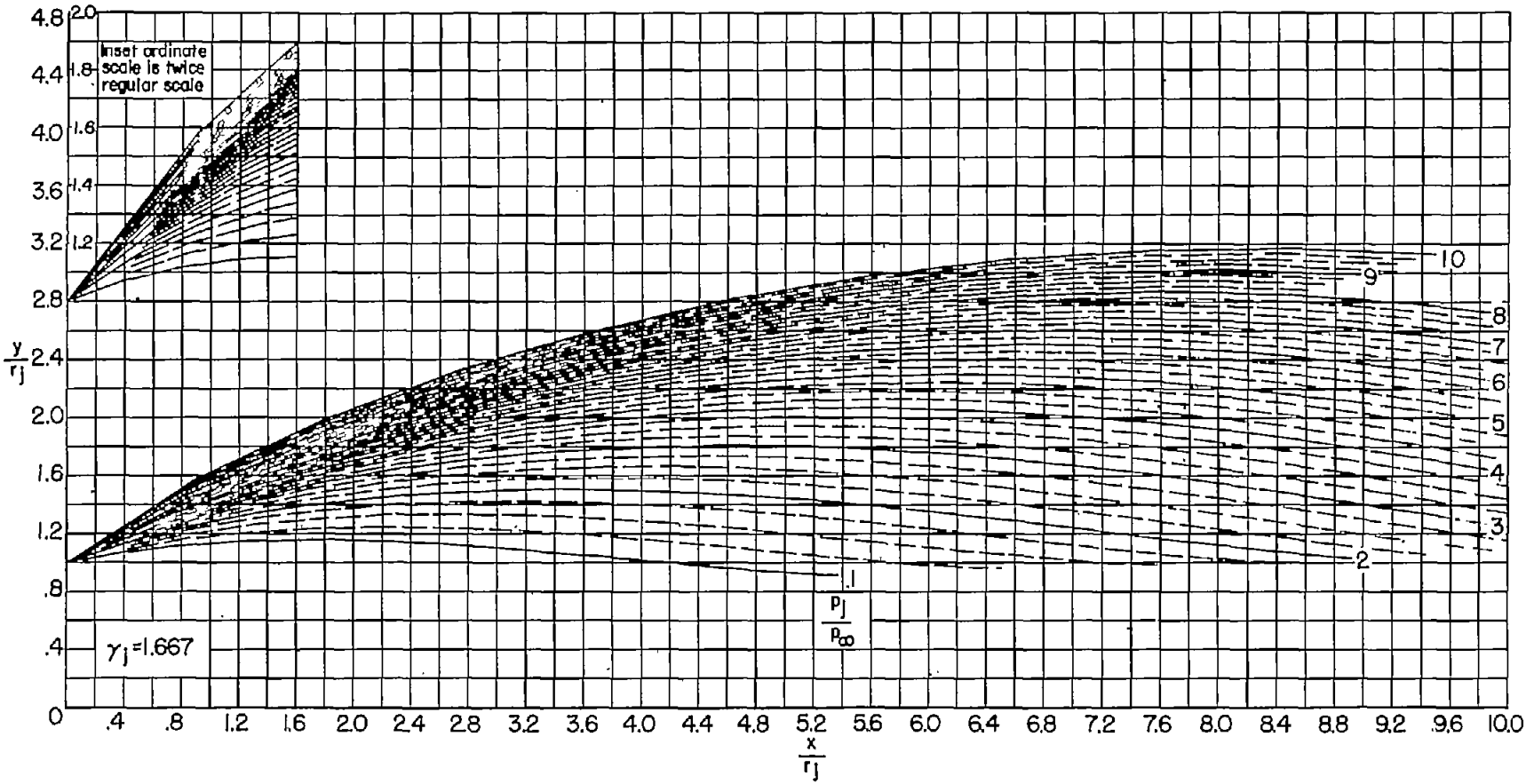


(b) $\theta_N = 10^\circ$. Concluded.

Figure 4.- Continued.

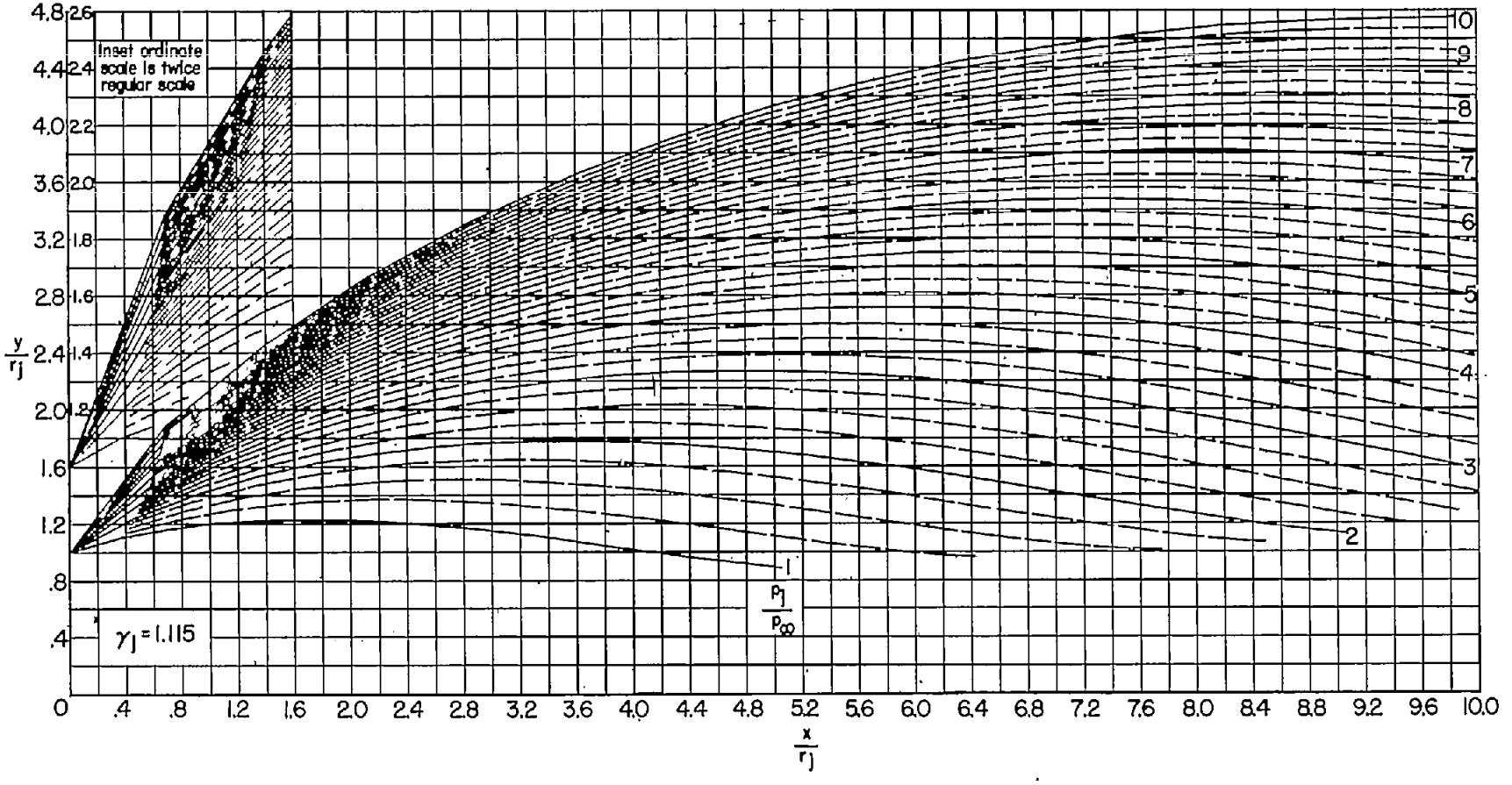


(c) $\theta_N = 15°$.

Figure 4.- Continued.

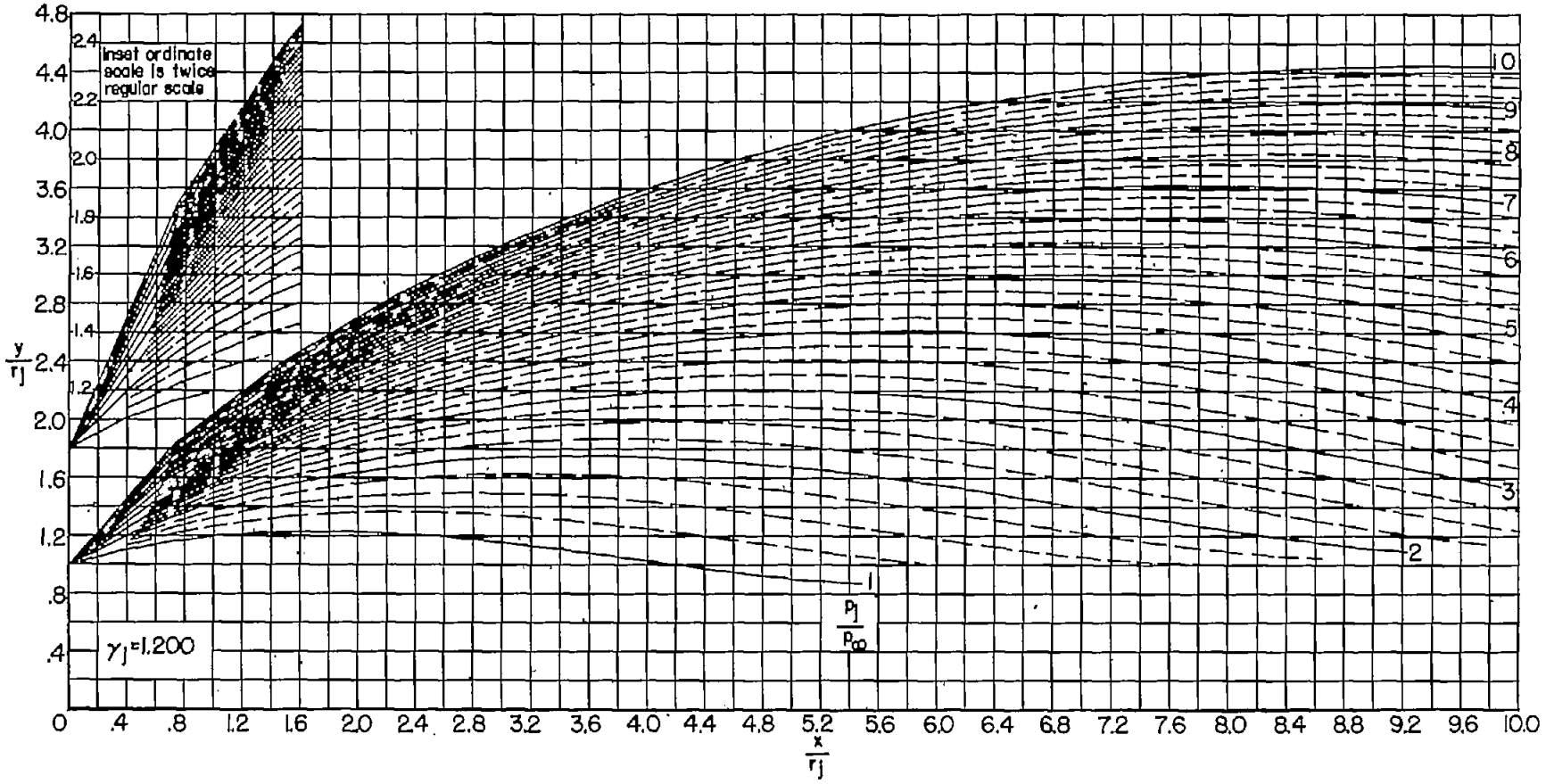


(c) $\theta_N = 15^\circ$. Continued.

Figure 4.- Continued.

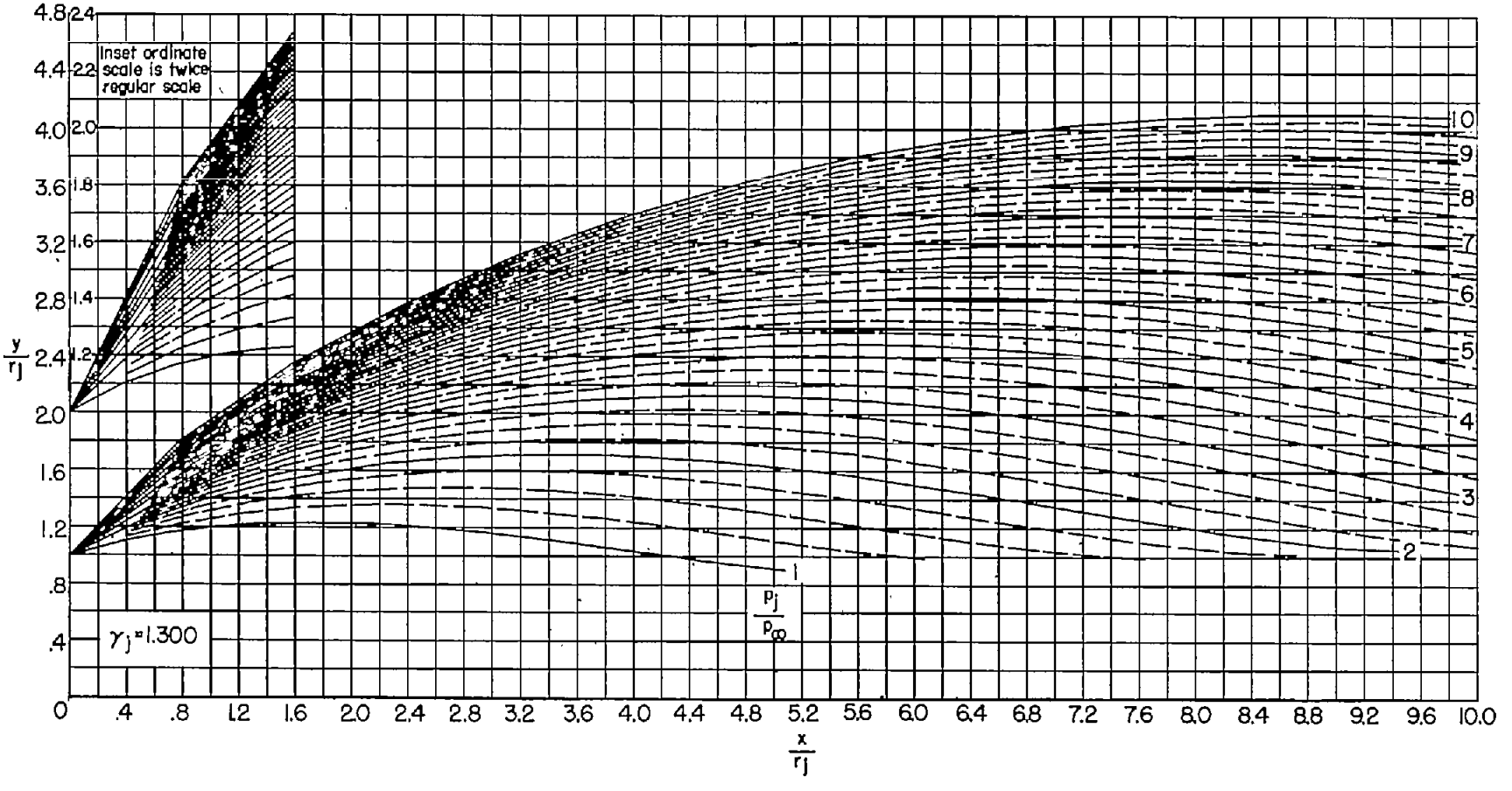


(c) $\theta_N = 15^\circ$. Continued.

Figure 4.- Continued.

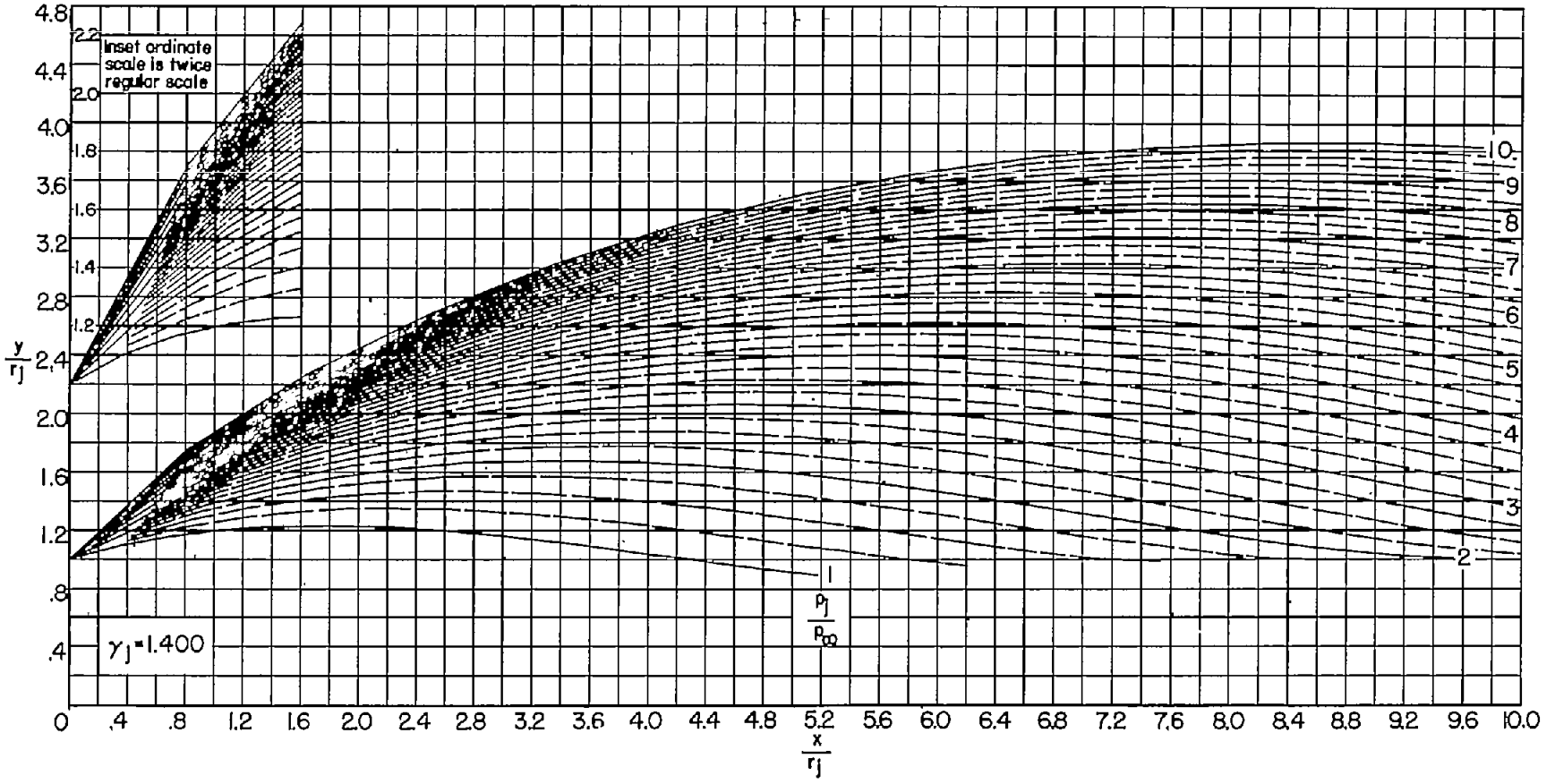


(c) $\theta_N = 15^\circ$. Continued.

Figure 4.- Continued.

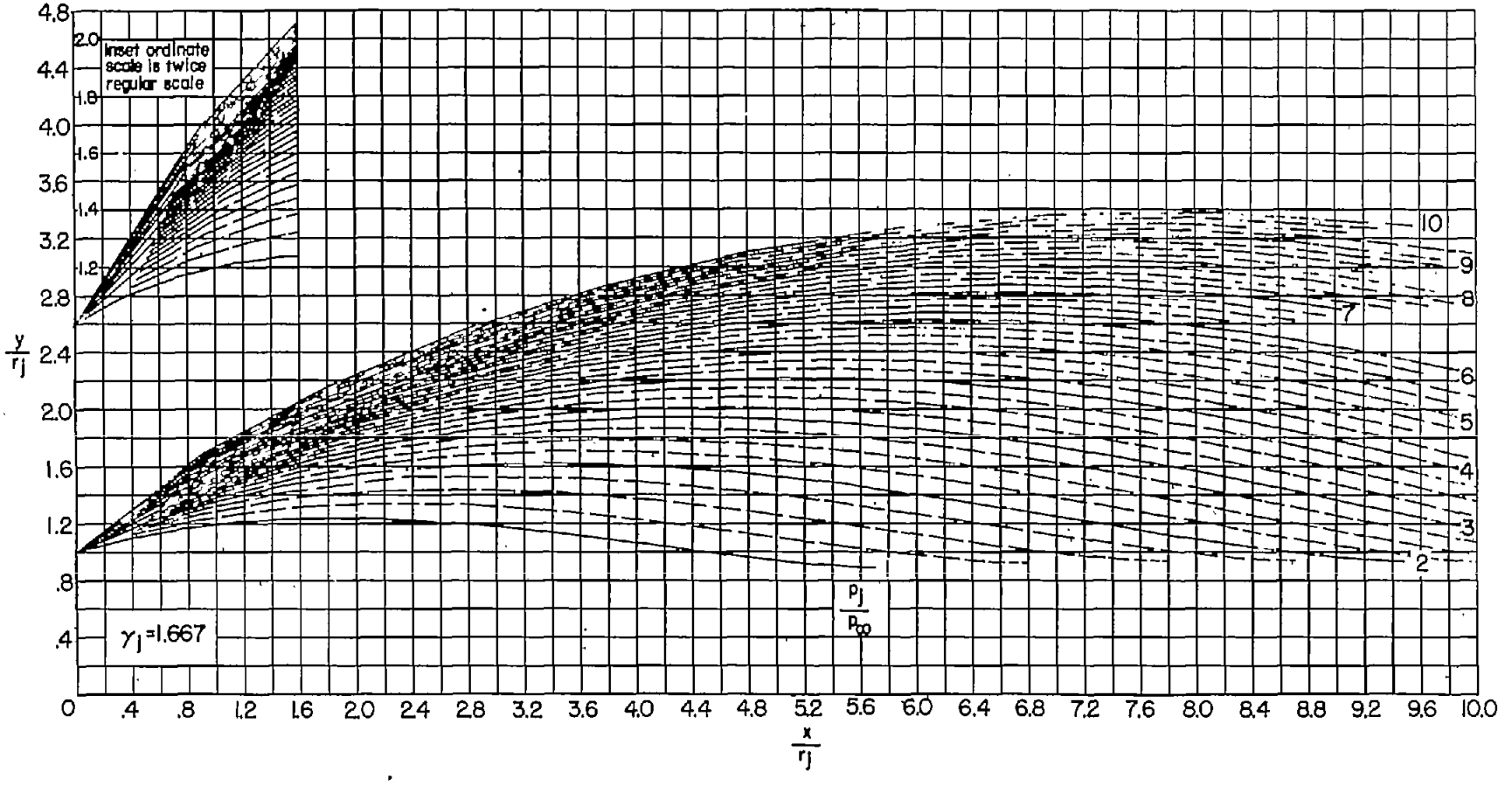


(c) $\theta_N = 15^\circ$. Concluded.

Figure 4.- Continued.

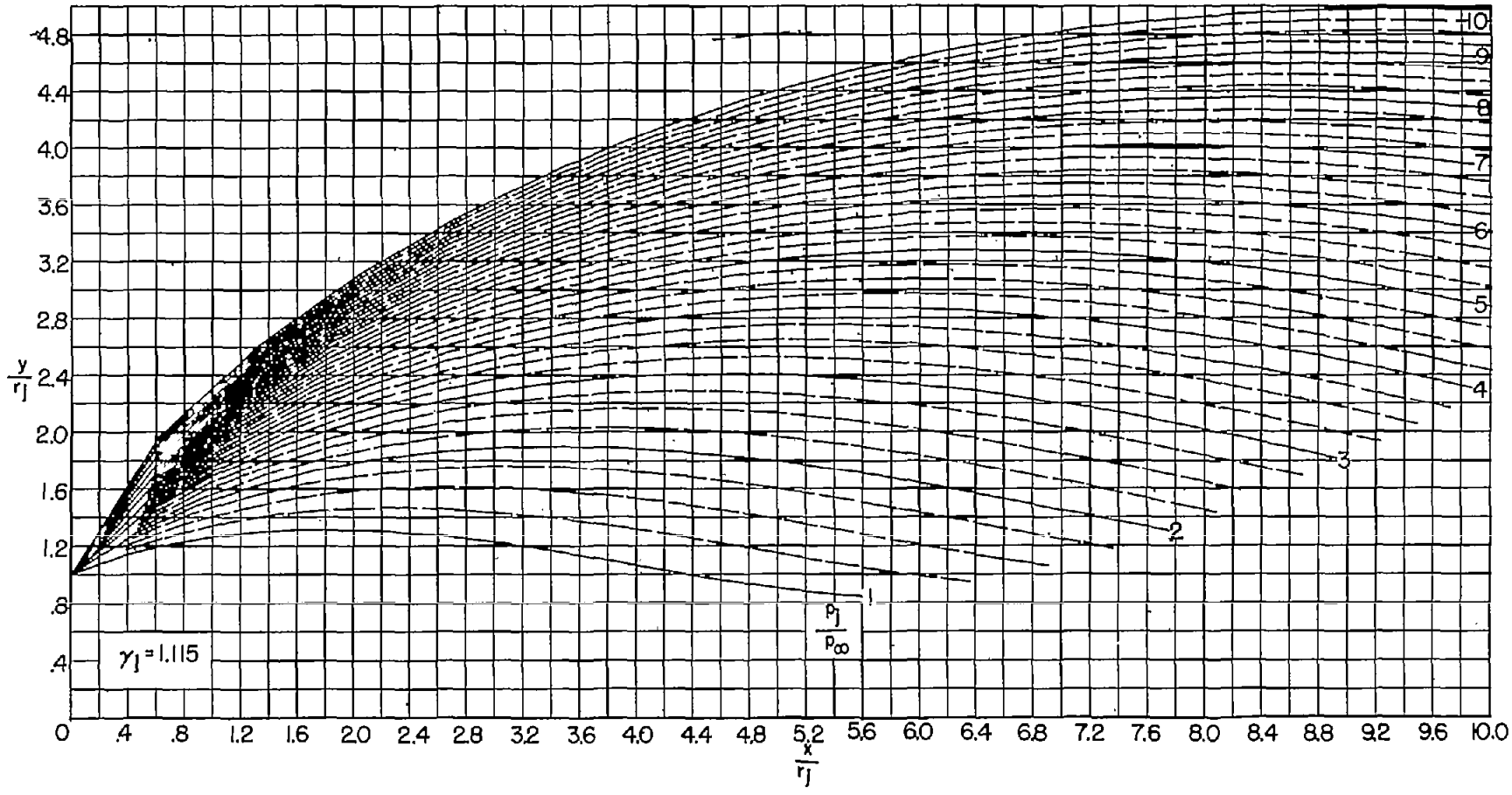


(d) $\theta_N = 20^\circ$.

Figure 4.- Continued.

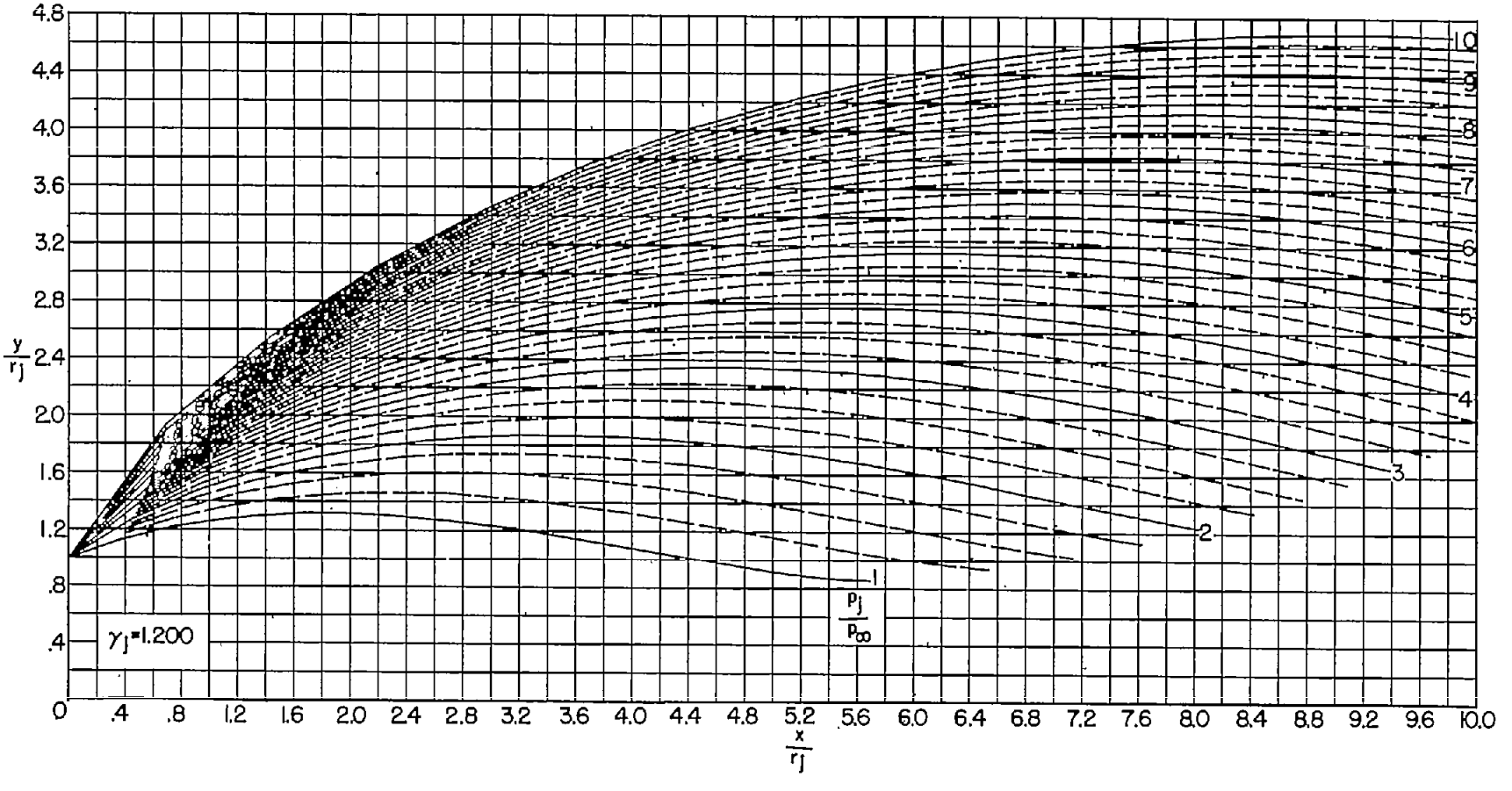


(d) $\theta_N = 20^\circ$. Continued.

Figure 4.- Continued.

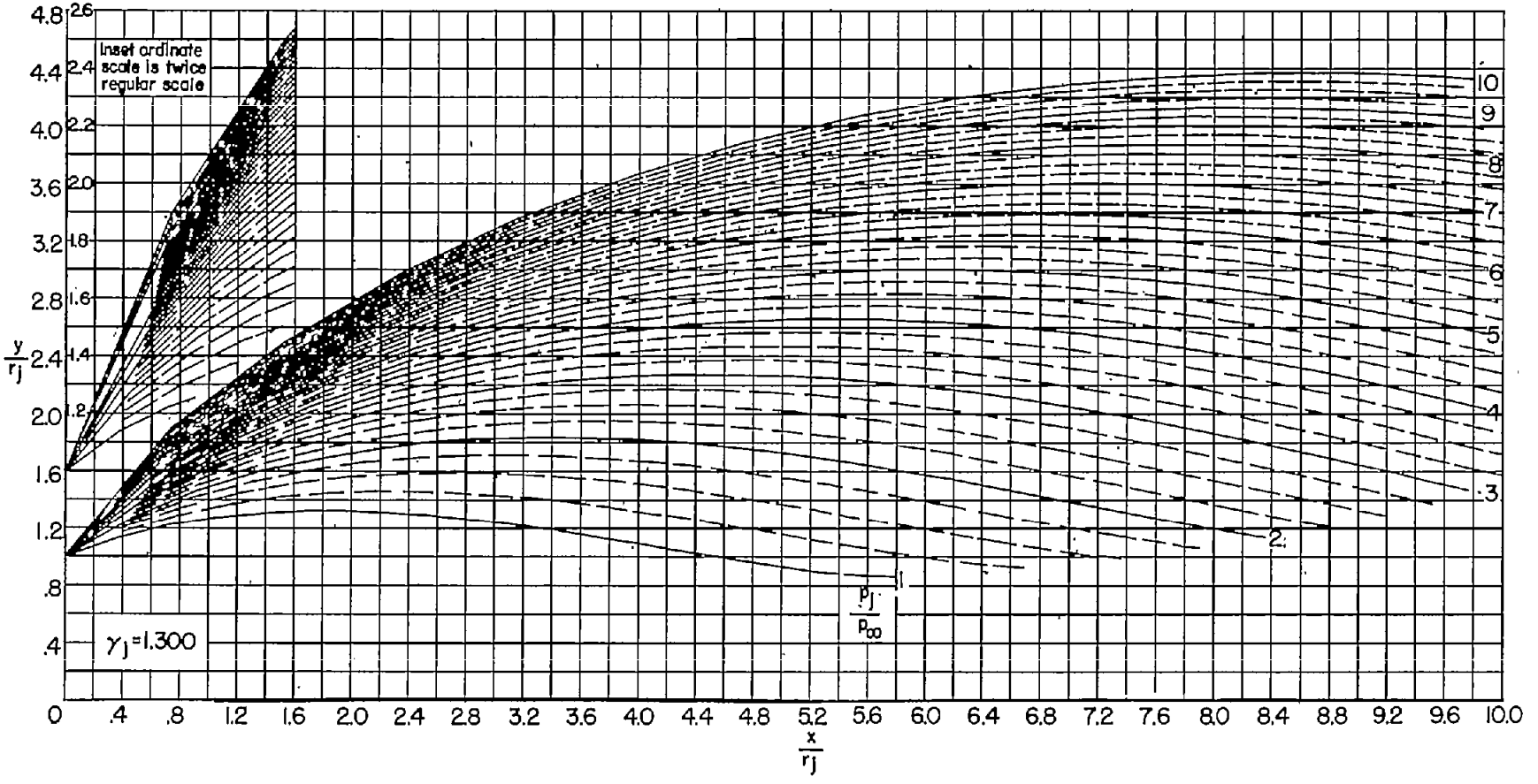


(d) $\theta_N = 20°$. Continued.

Figure 4.- Continued.

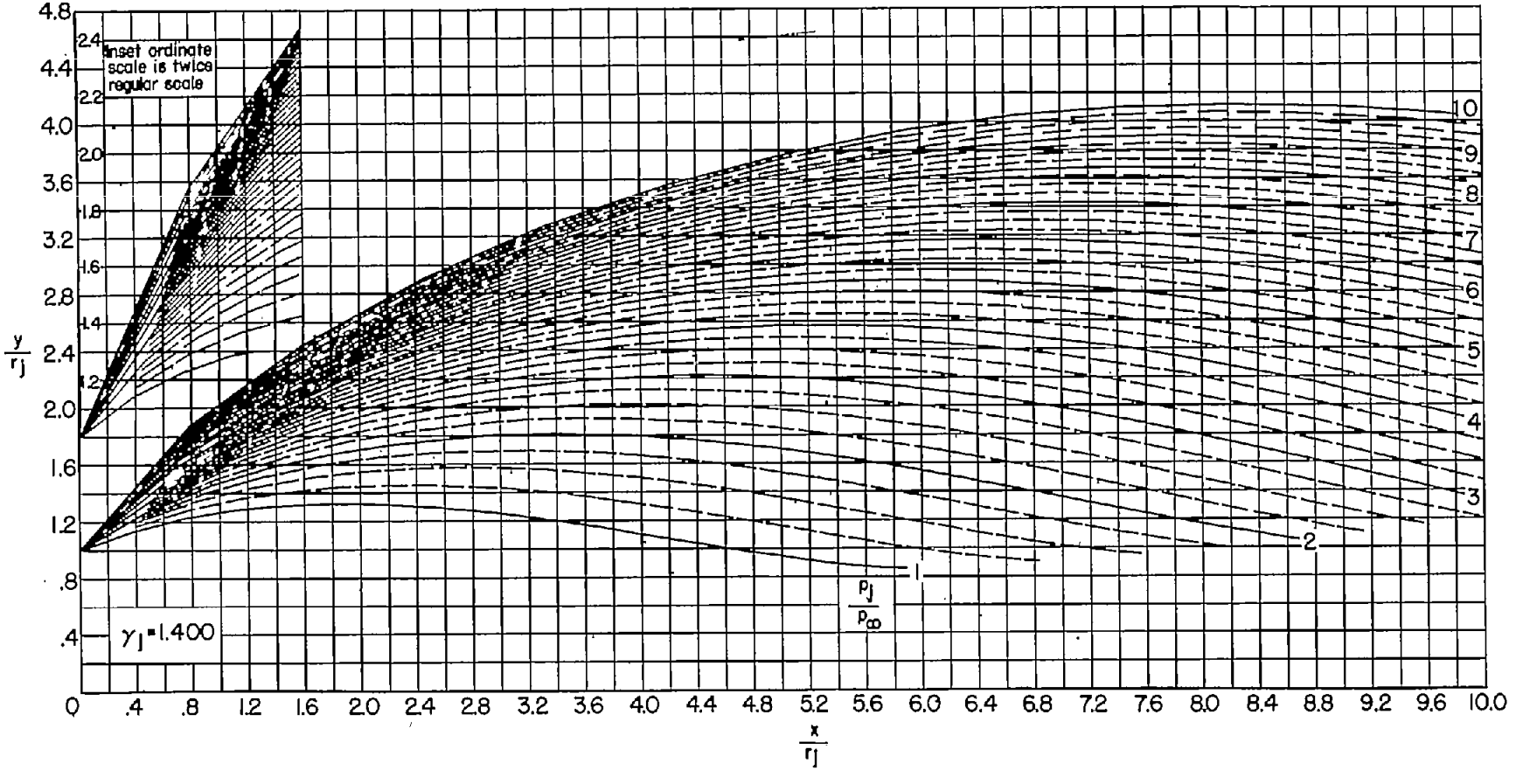


(d) $\theta_N = 20^\circ$. Continued.

Figure 4.- Continued.

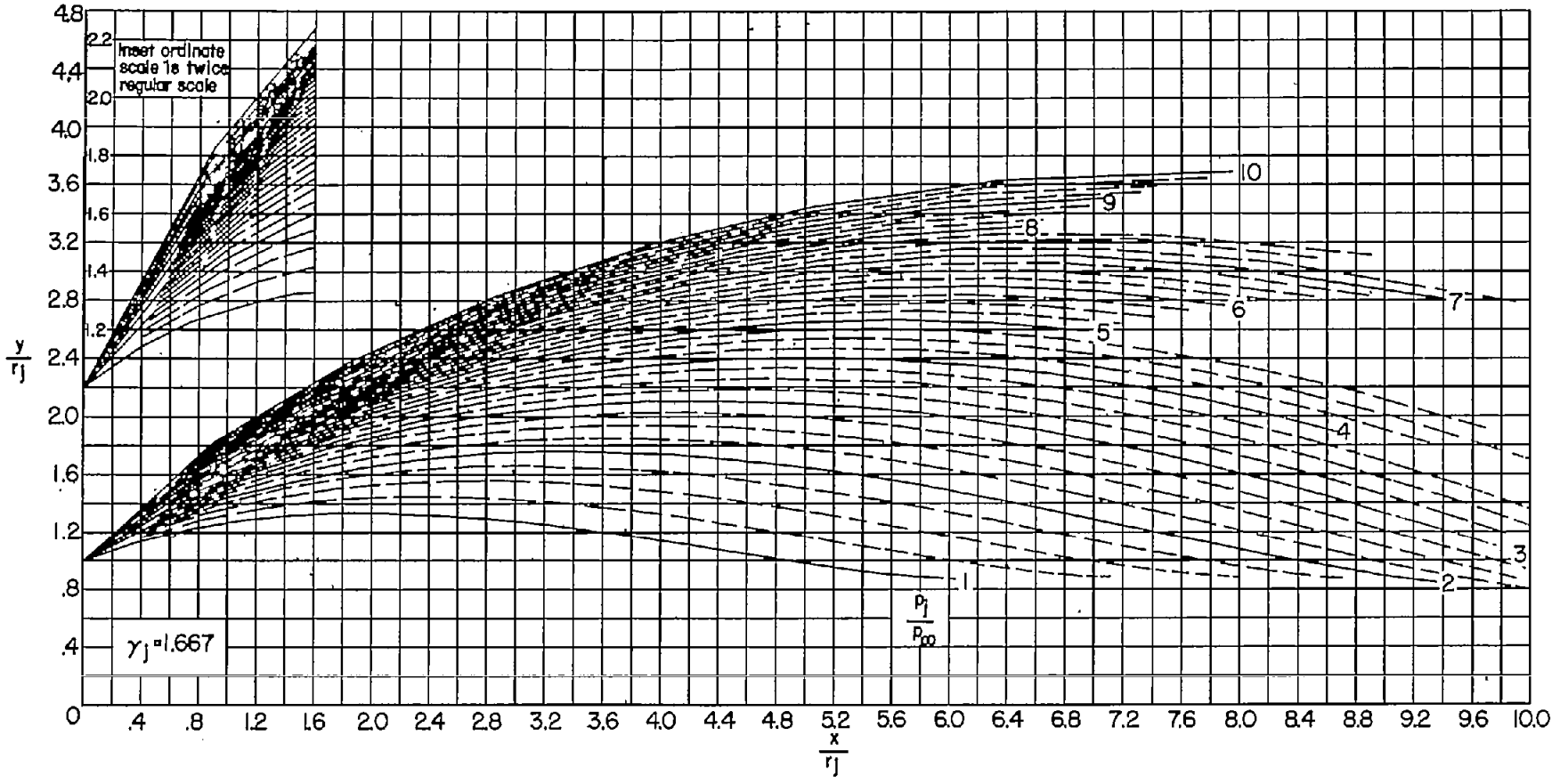


(d) $\theta_N = 20^\circ$. Concluded.

Figure 4.- Concluded.

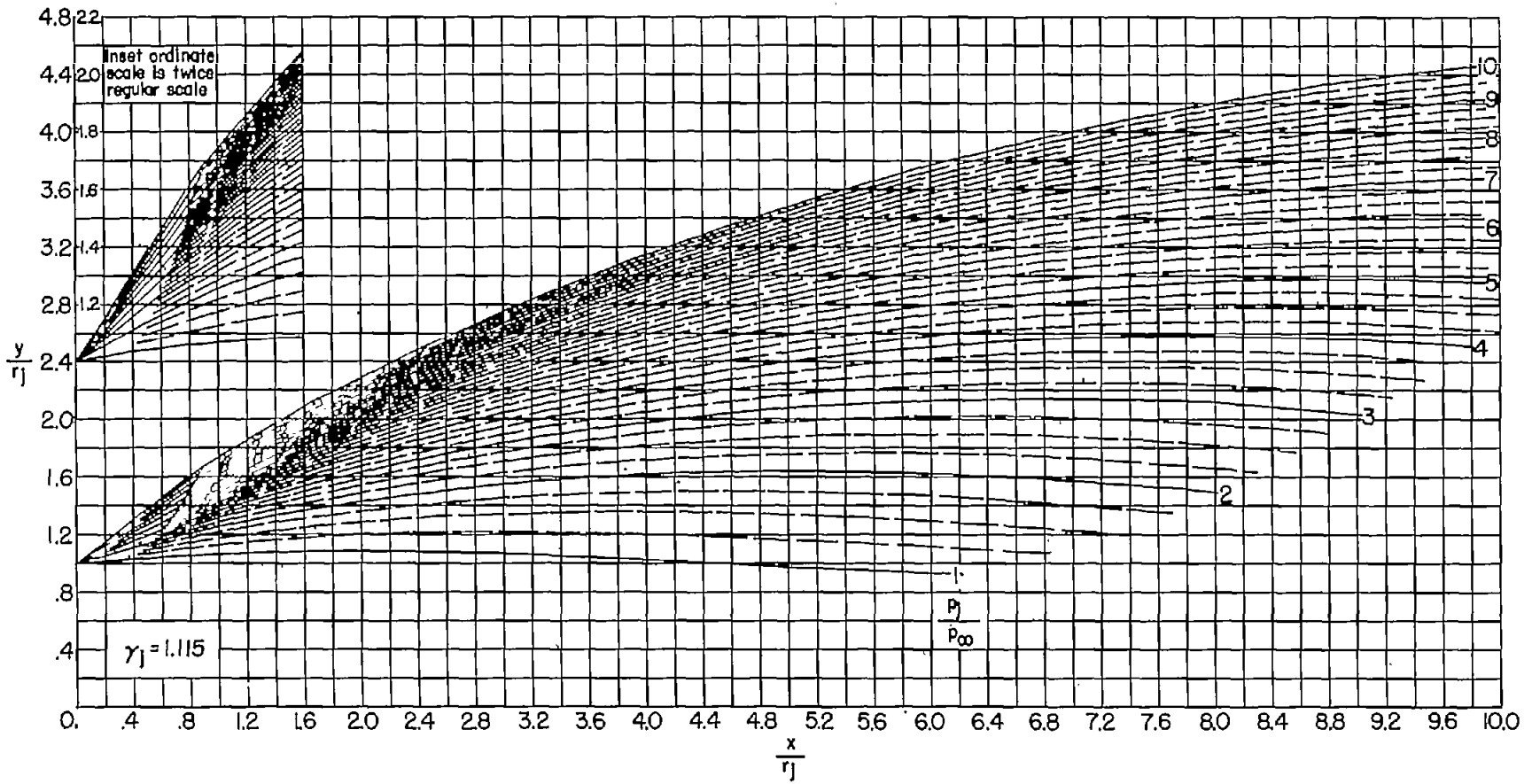


(a) $\theta_N = 5^\circ$.

Figure 5.- Jet boundaries at $M_j = 3.0$ for jet static-pressure ratios from 1 to 10. (Dashed boundaries denote changes in $p_j/p_\infty$ of 0.25.)

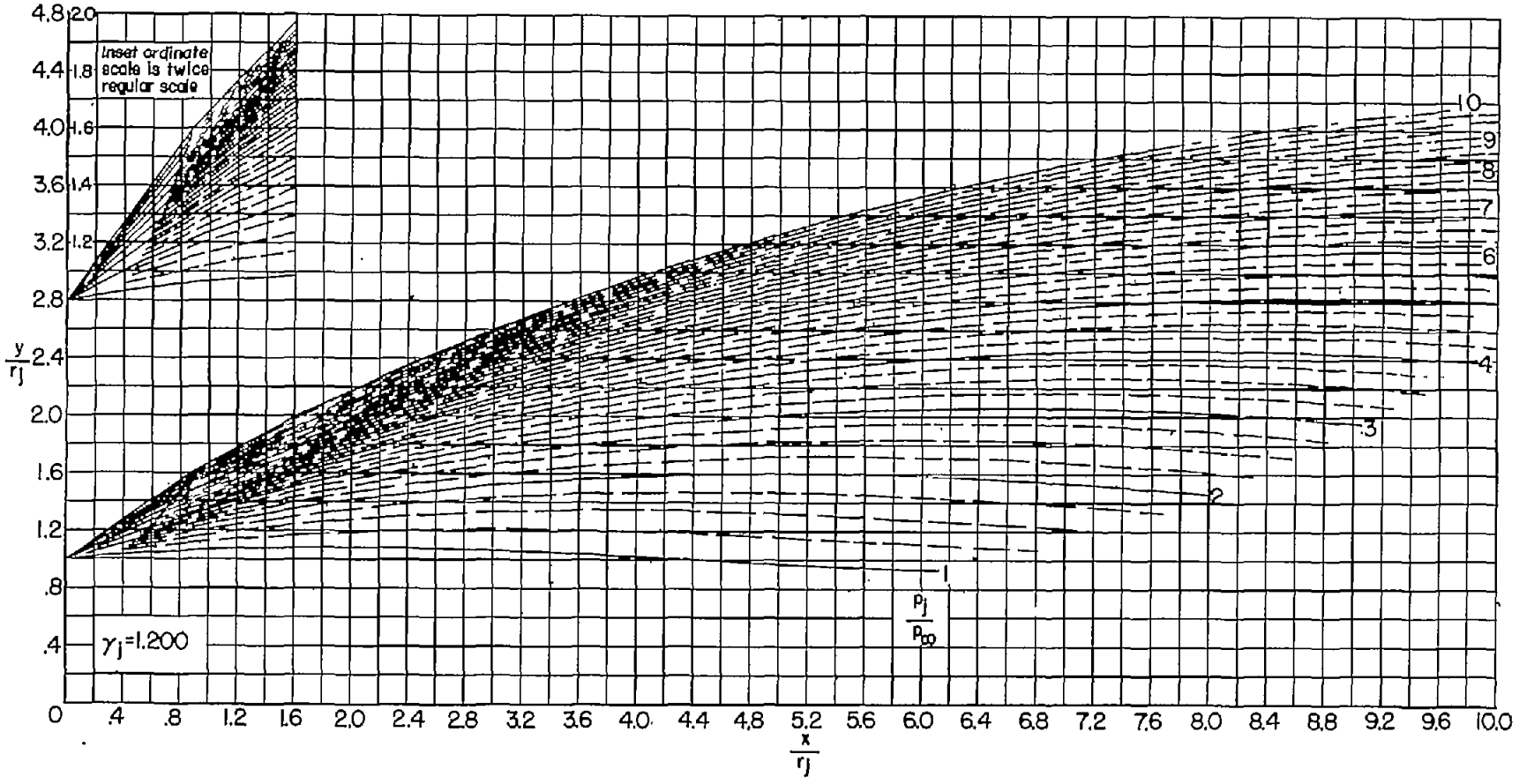


(a) $\theta_N = 5^\circ$. Continued.

Figure 5.- Continued.

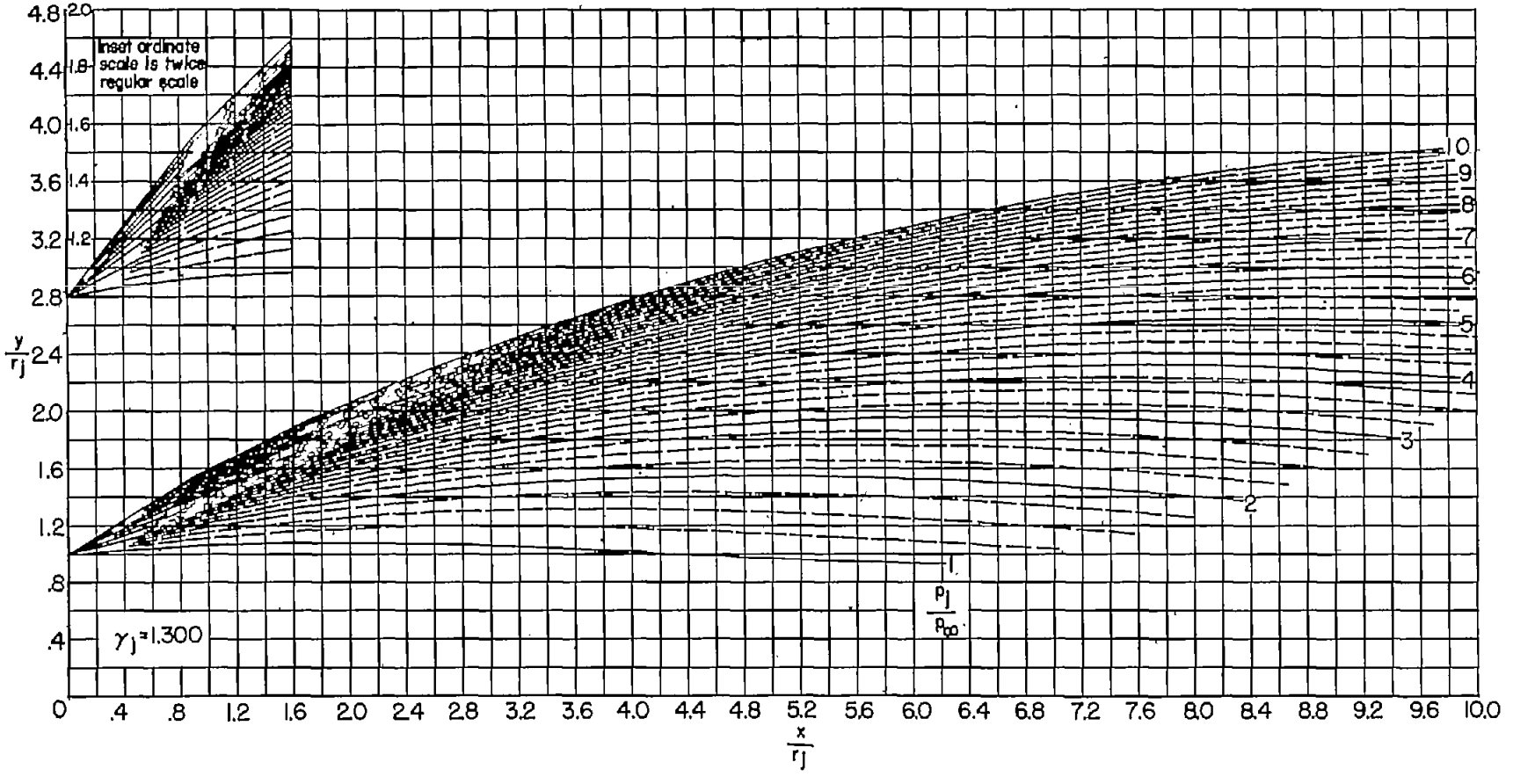


(a) $\theta_N = 5^\circ$. Continued.

Figure 5.- Continued.

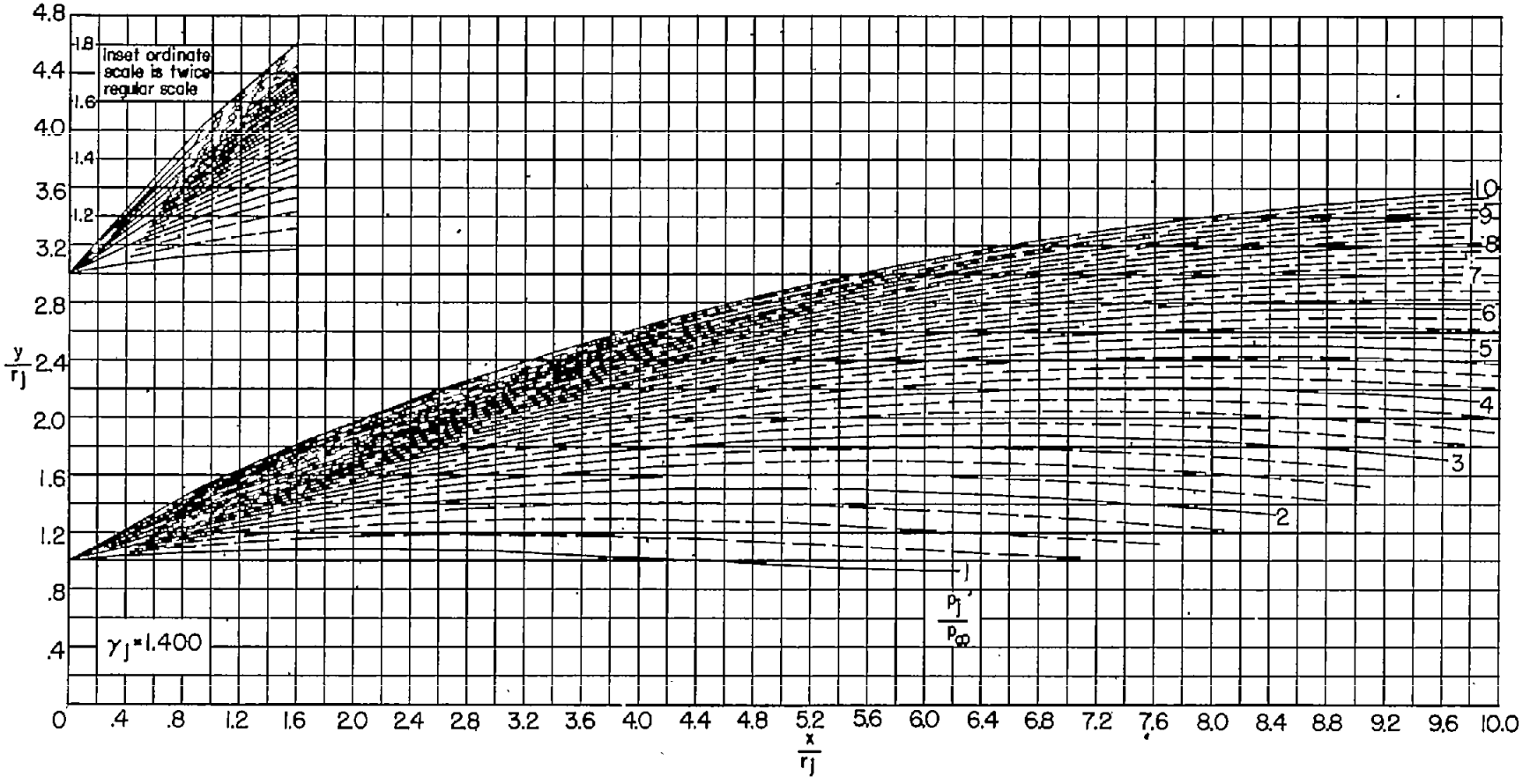


(a) $\theta_N = 5^\circ$. Continued.

Figure 5.- Continued.

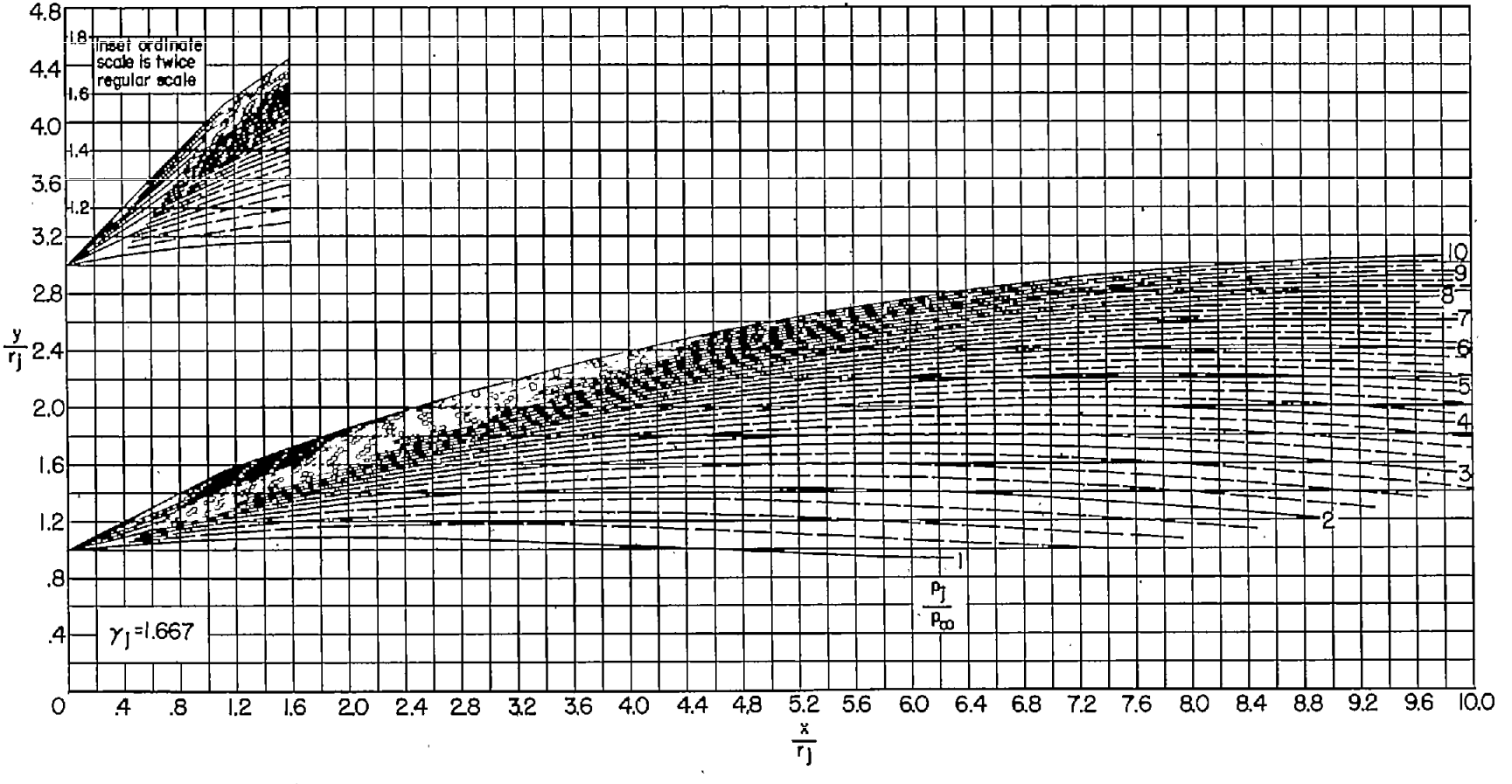


(a) $\theta_N = 5^\circ$. Concluded.

Figure 5.- Continued.

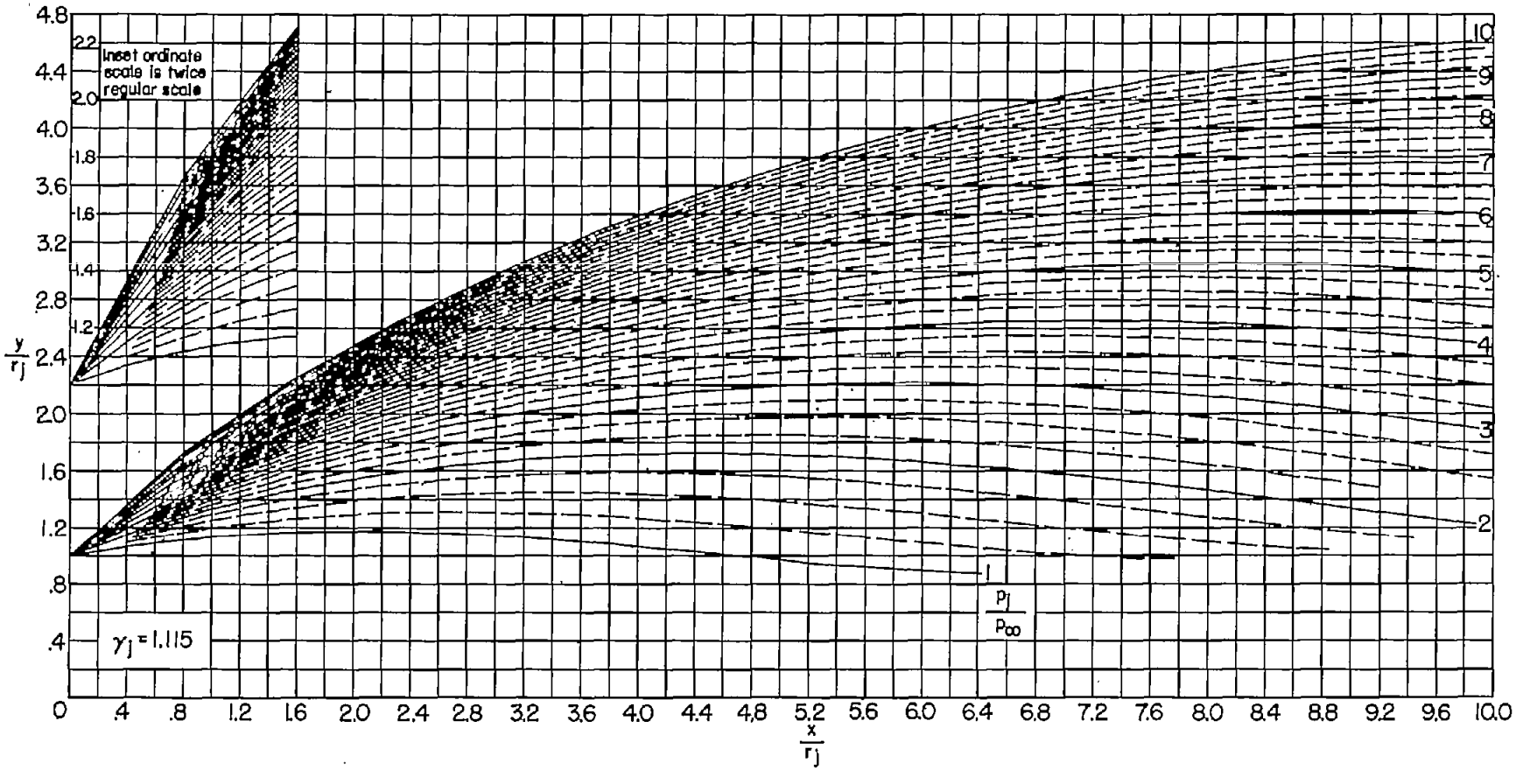


(b) $\theta_N = 10^\circ$.

Figure 5.- Continued.

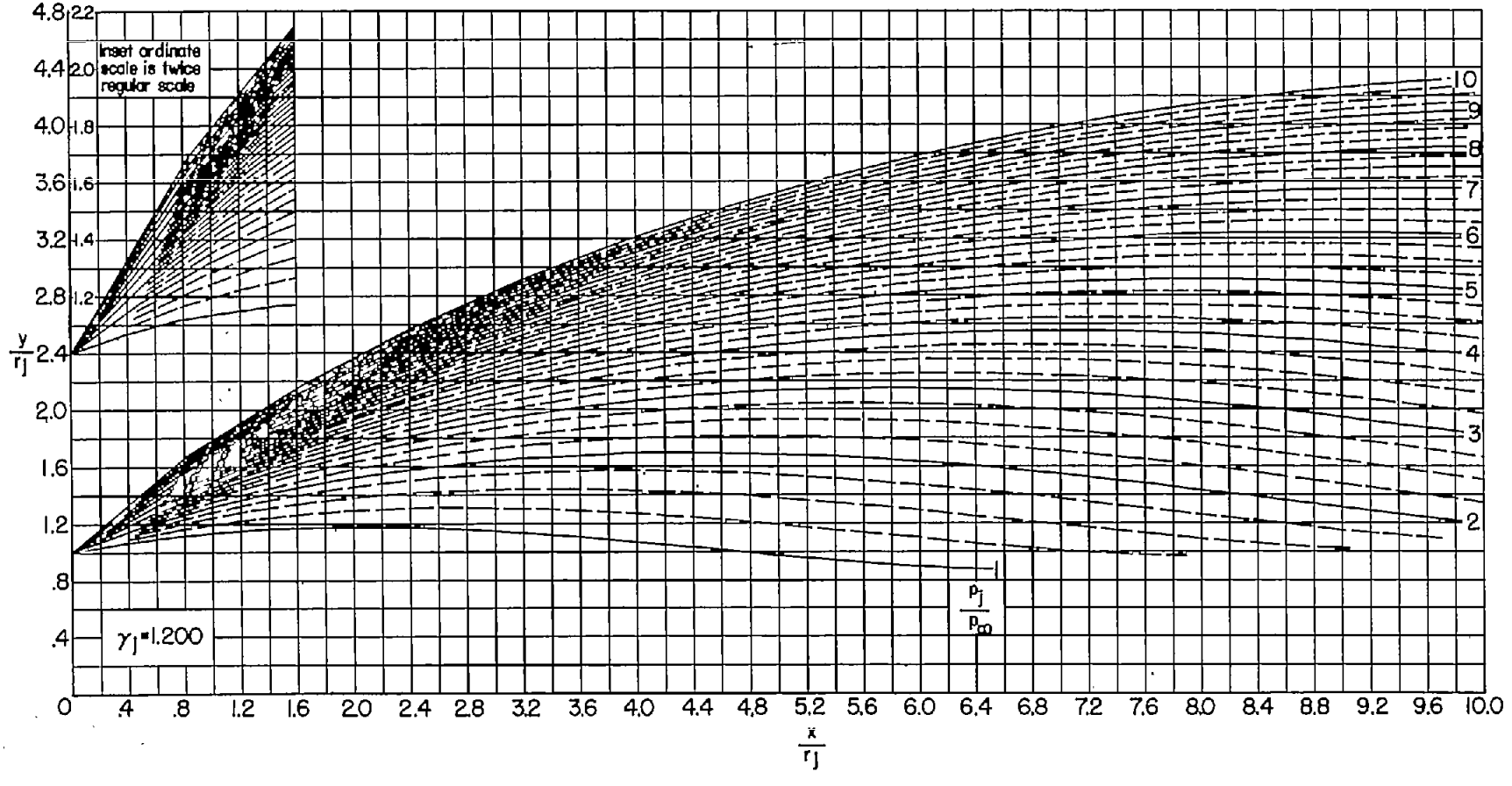


(b) $\theta_N = 10^\circ$. Continued.

Figure 5.- Continued.

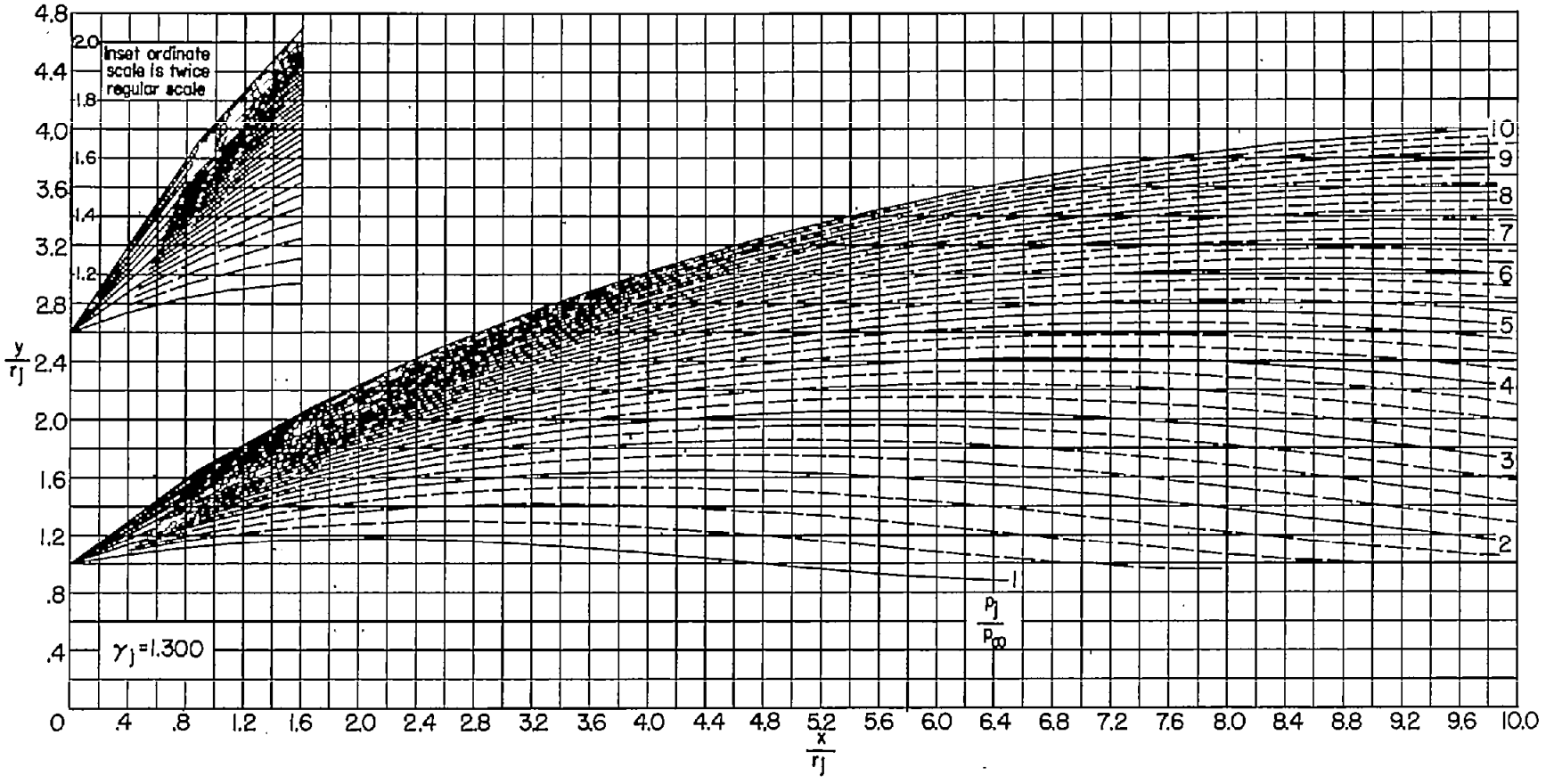


(b) $\theta_N = 10^\circ$. Continued.

Figure 5.- Continued.

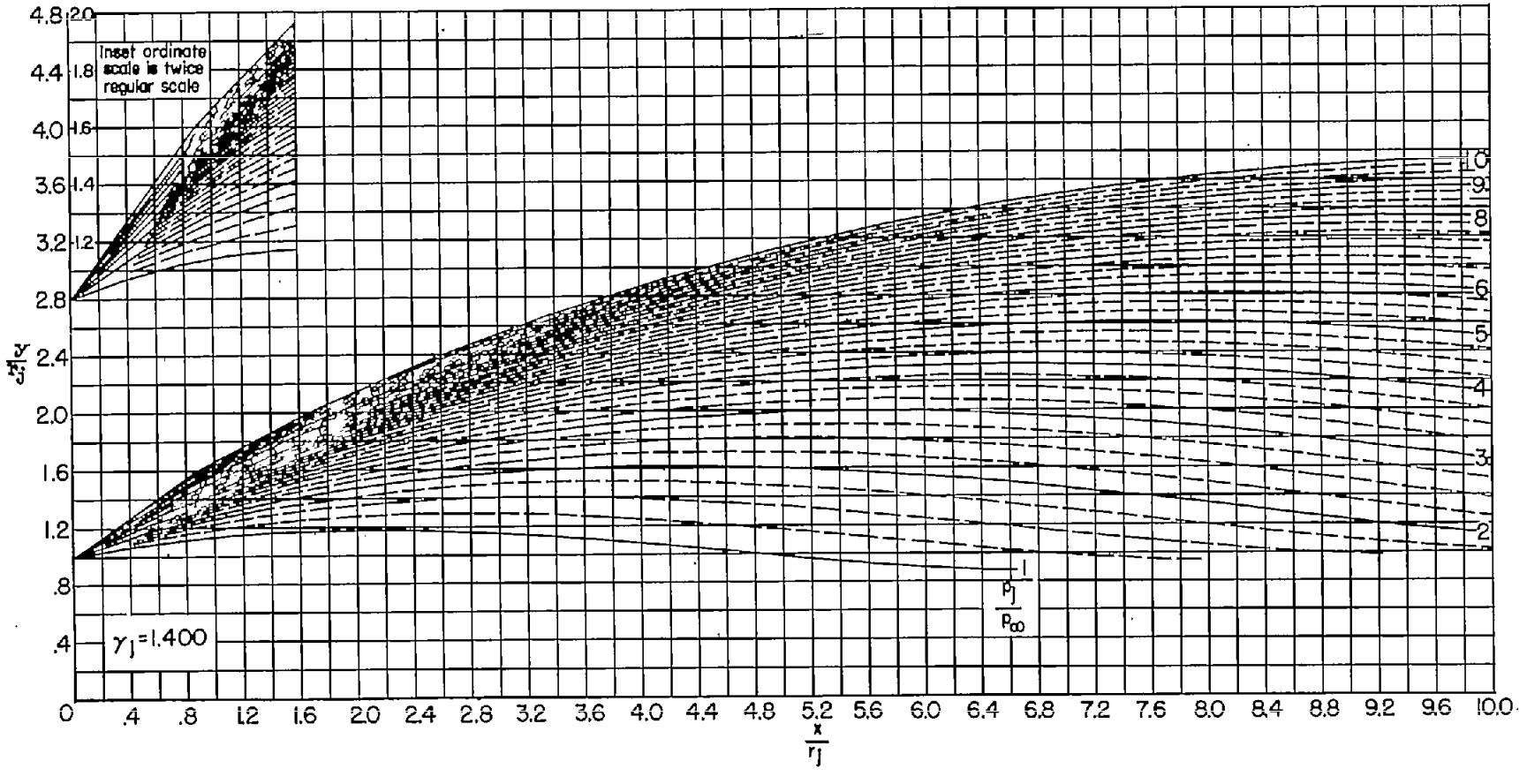


(b) $\theta_N = 10^\circ$. Continued.

Figure 5.- Continued.

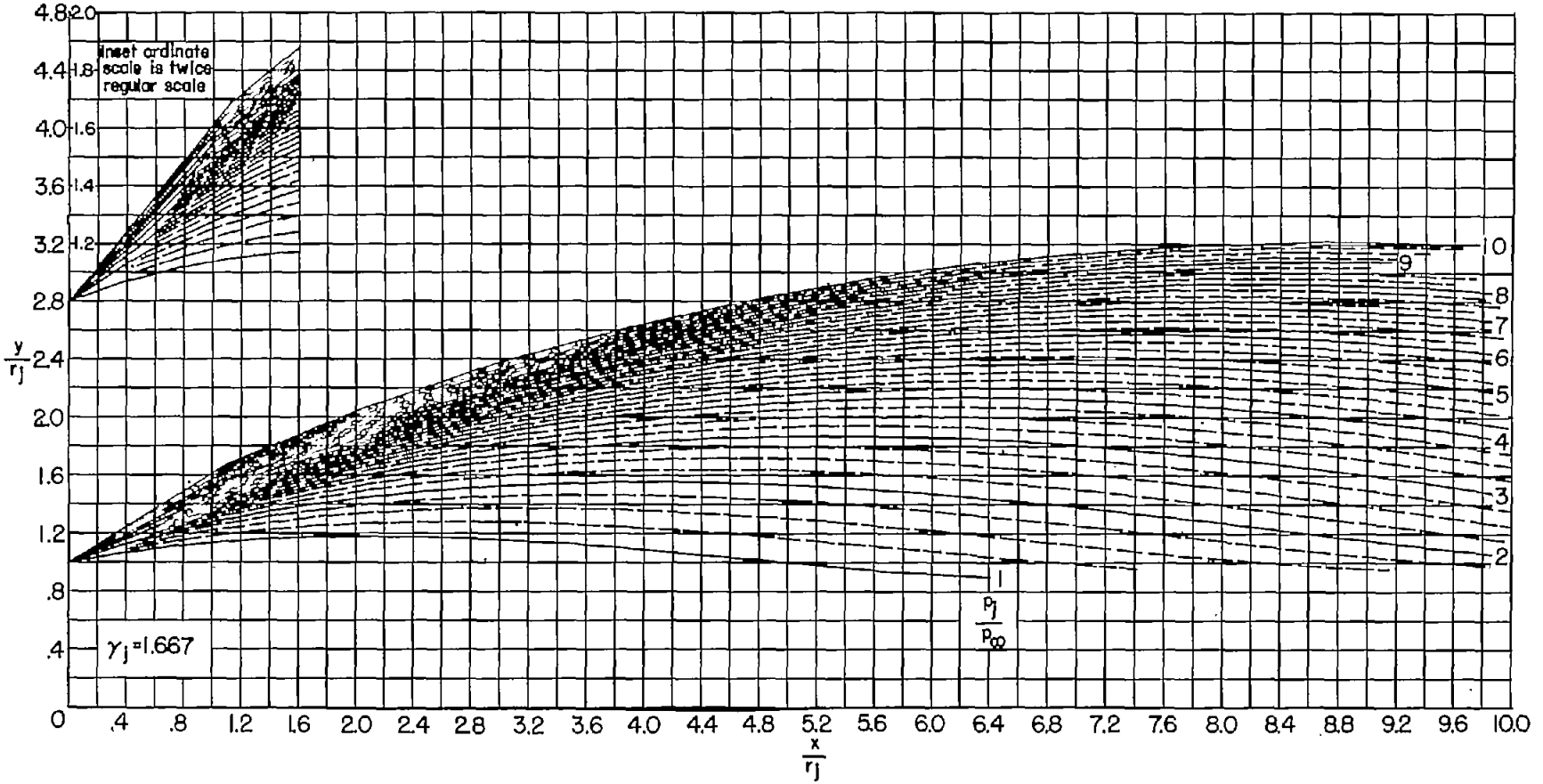


(b) $\theta_N = 10^\circ$. Concluded.

Figure 5.- Continued.

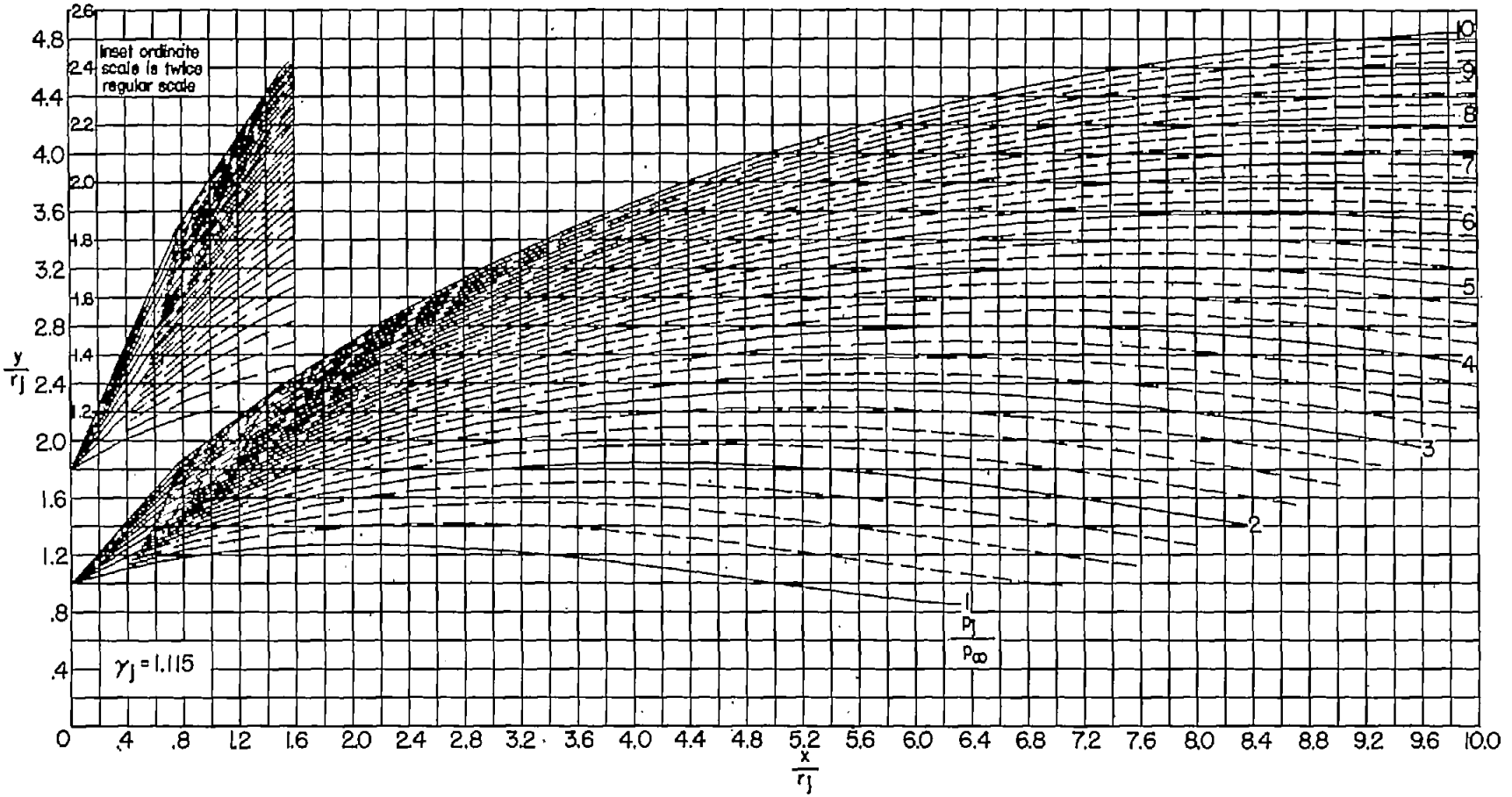


(c) $\theta_N = 15^\circ$.

Figure 5.- Continued.

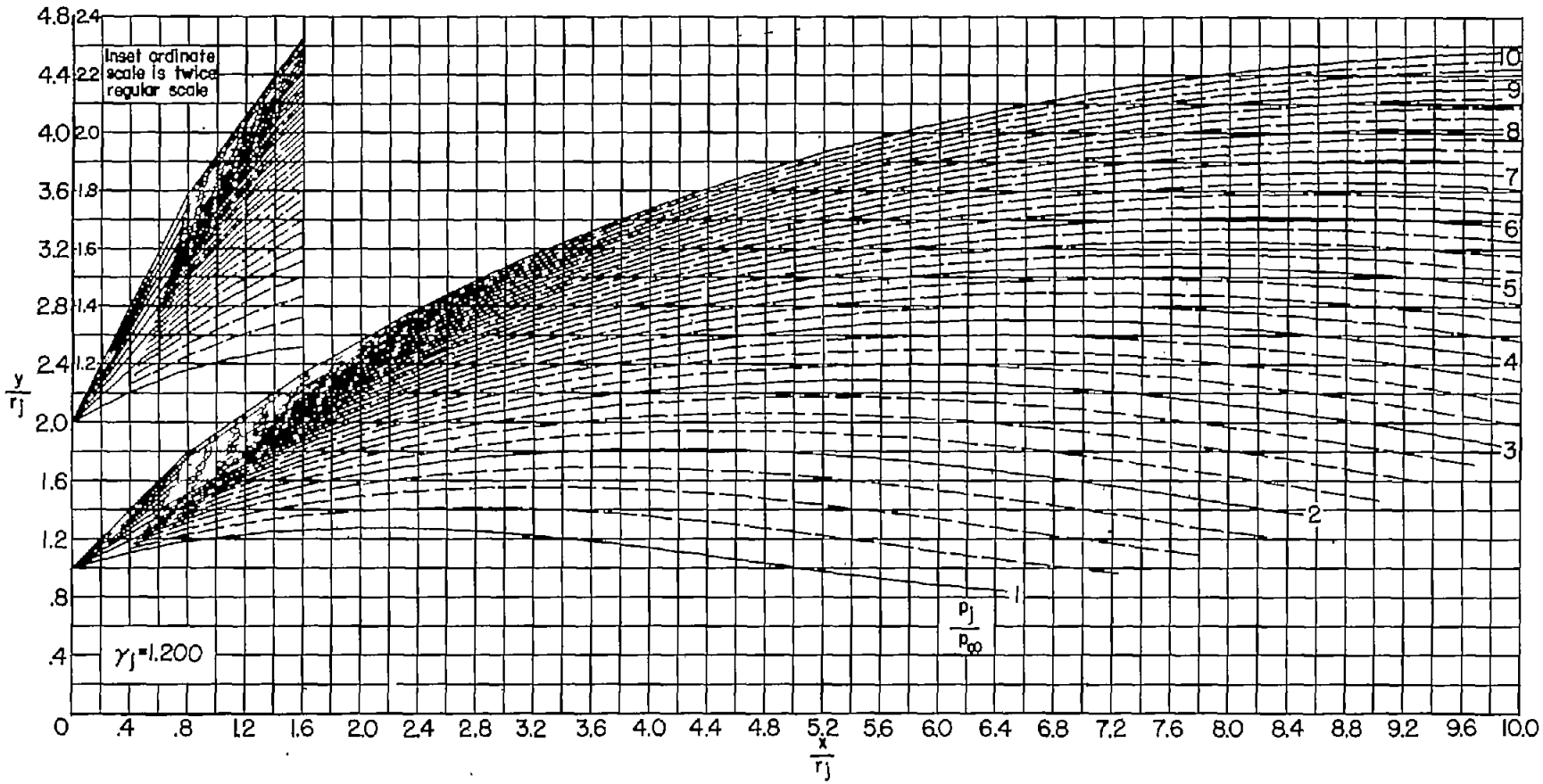


(c) $\theta_N = 15^\circ$. Continued.

Figure 5.- Continued.

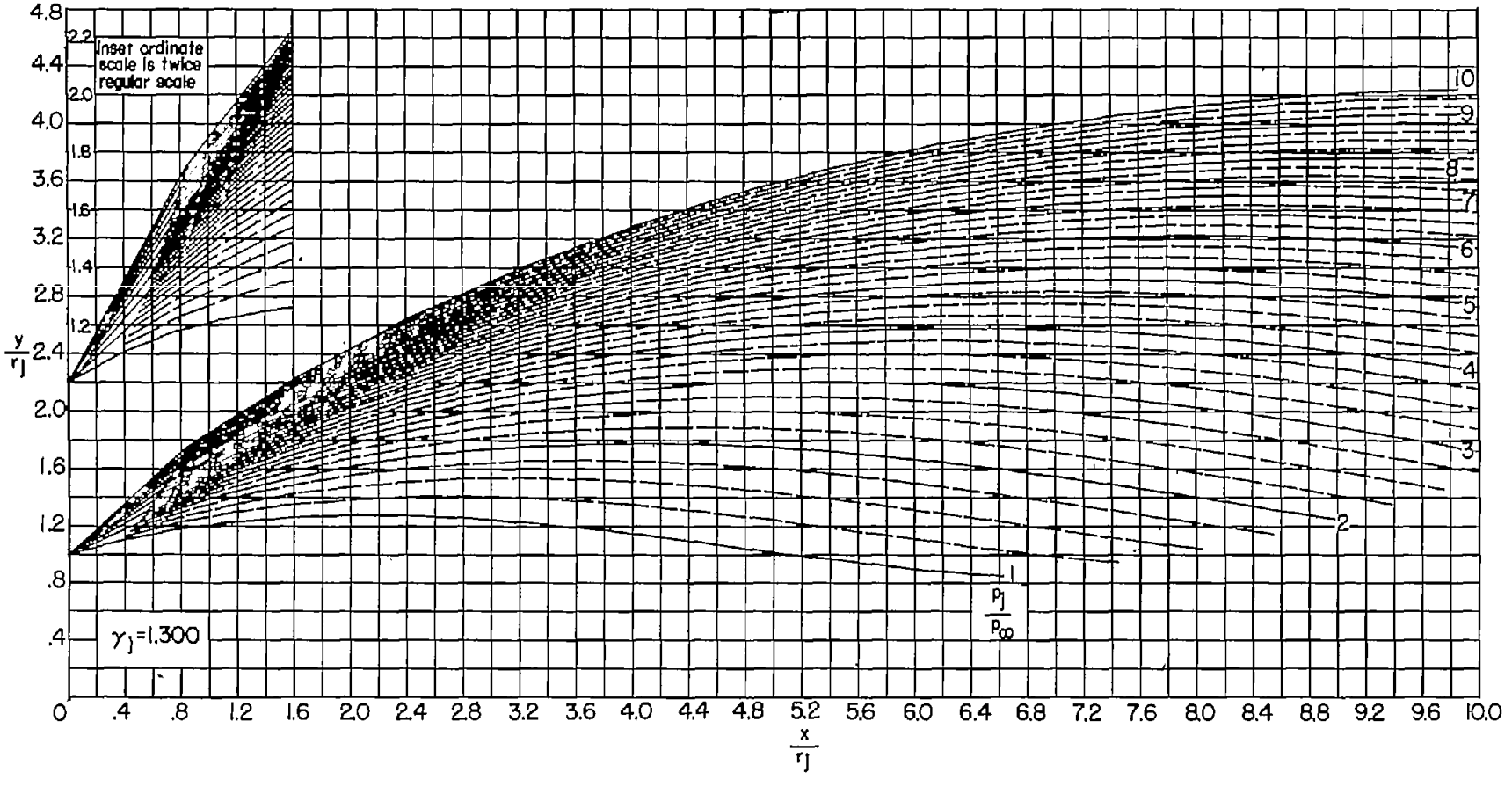


(c) $\theta_N = 15^\circ$. Continued.

Figure 5.- Continued.

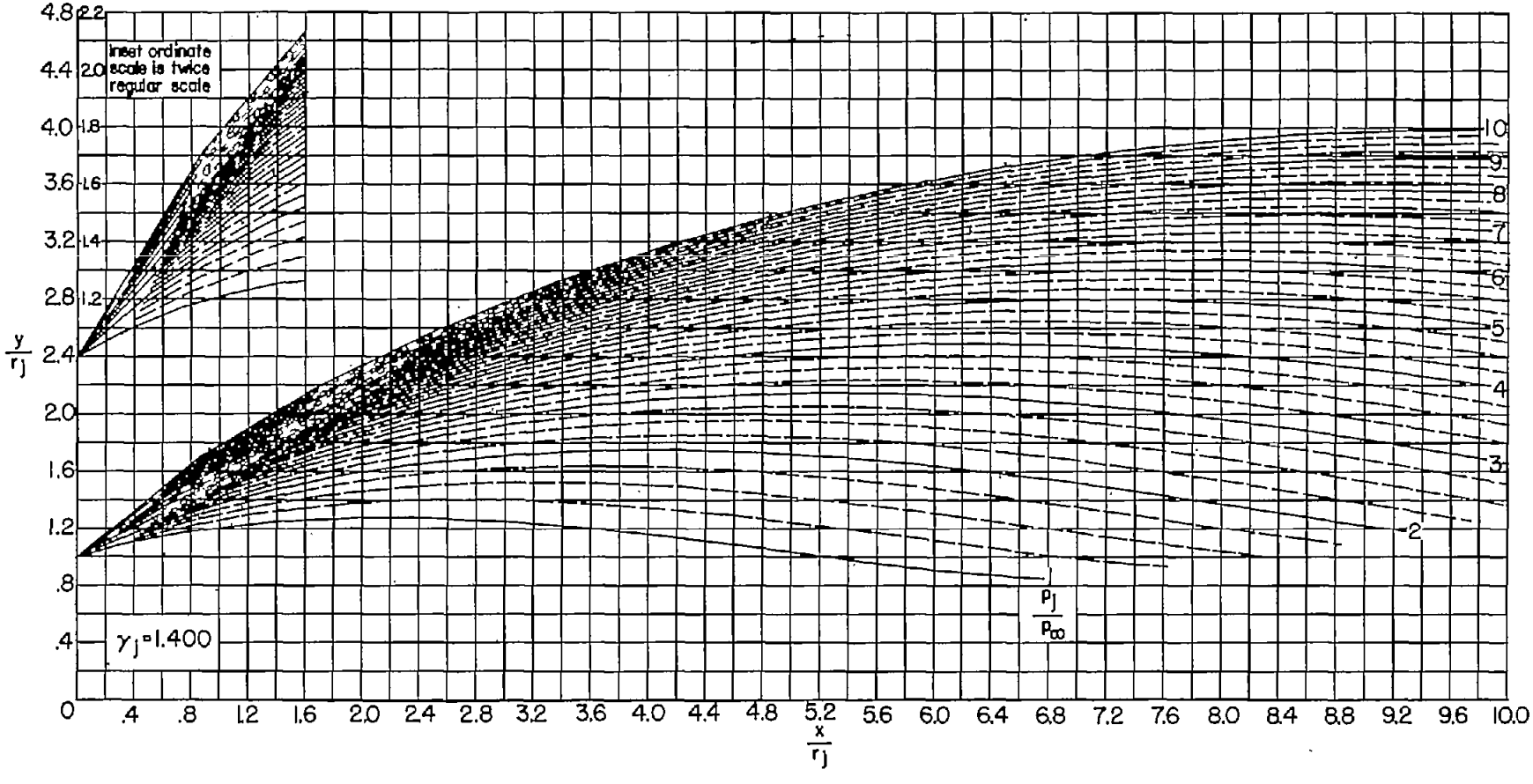


(c) $\theta_N = 15°$. Continued.

Figure 5.- Continued.

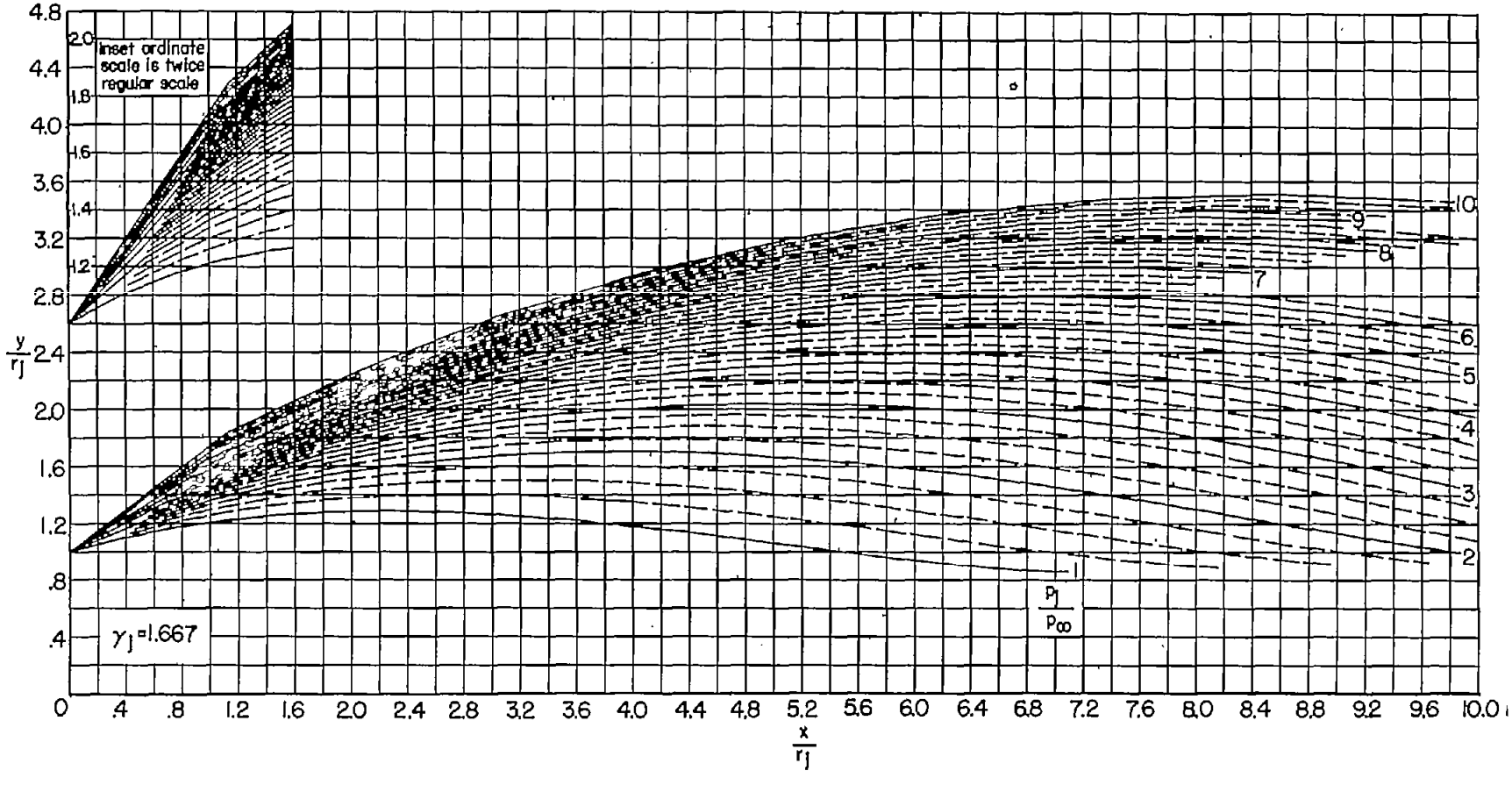


(c) $\theta_N = 15°$. Concluded.

Figure 5.- Continued.

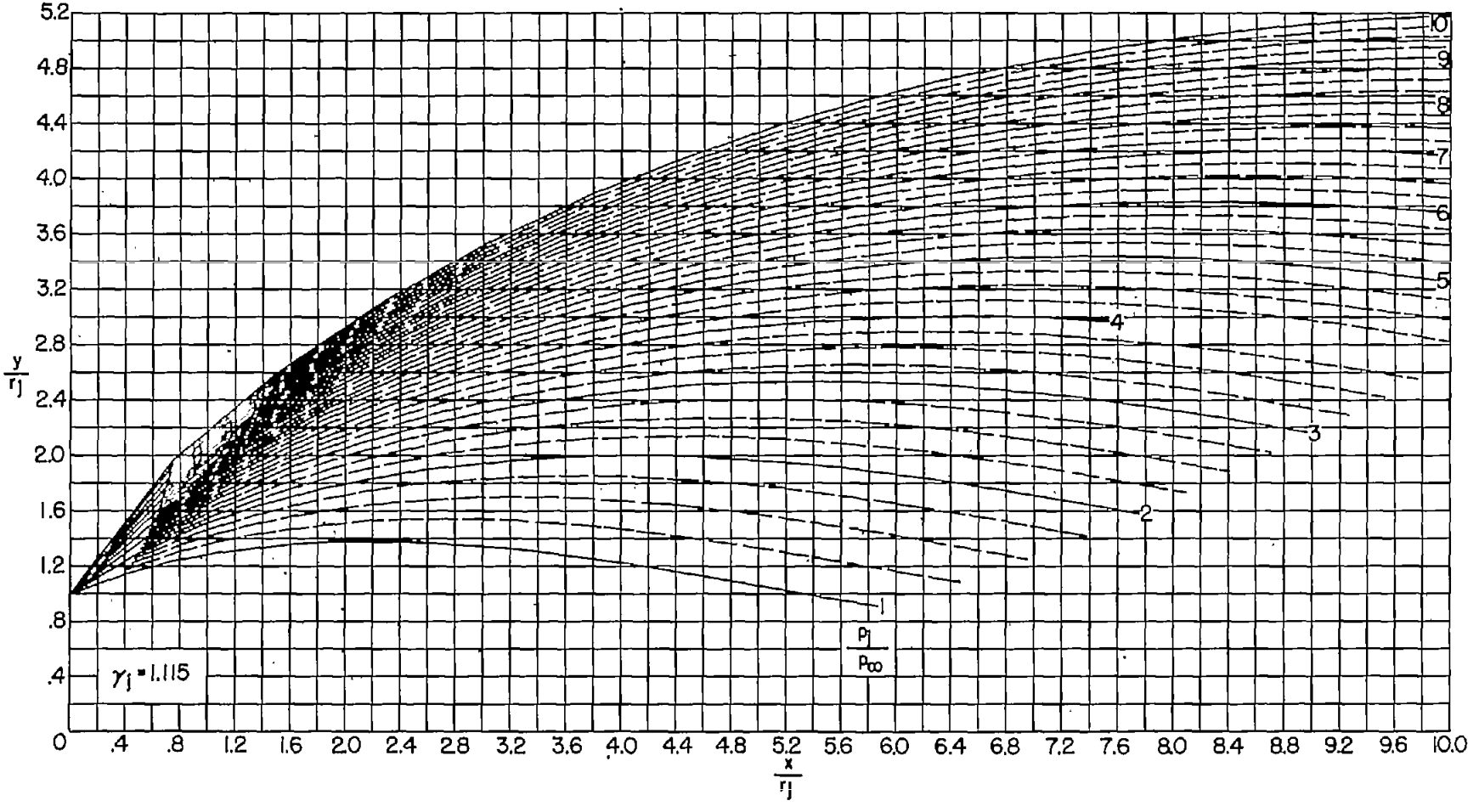


(d) $\theta_N = 20^\circ$.

Figure 5.- Continued.

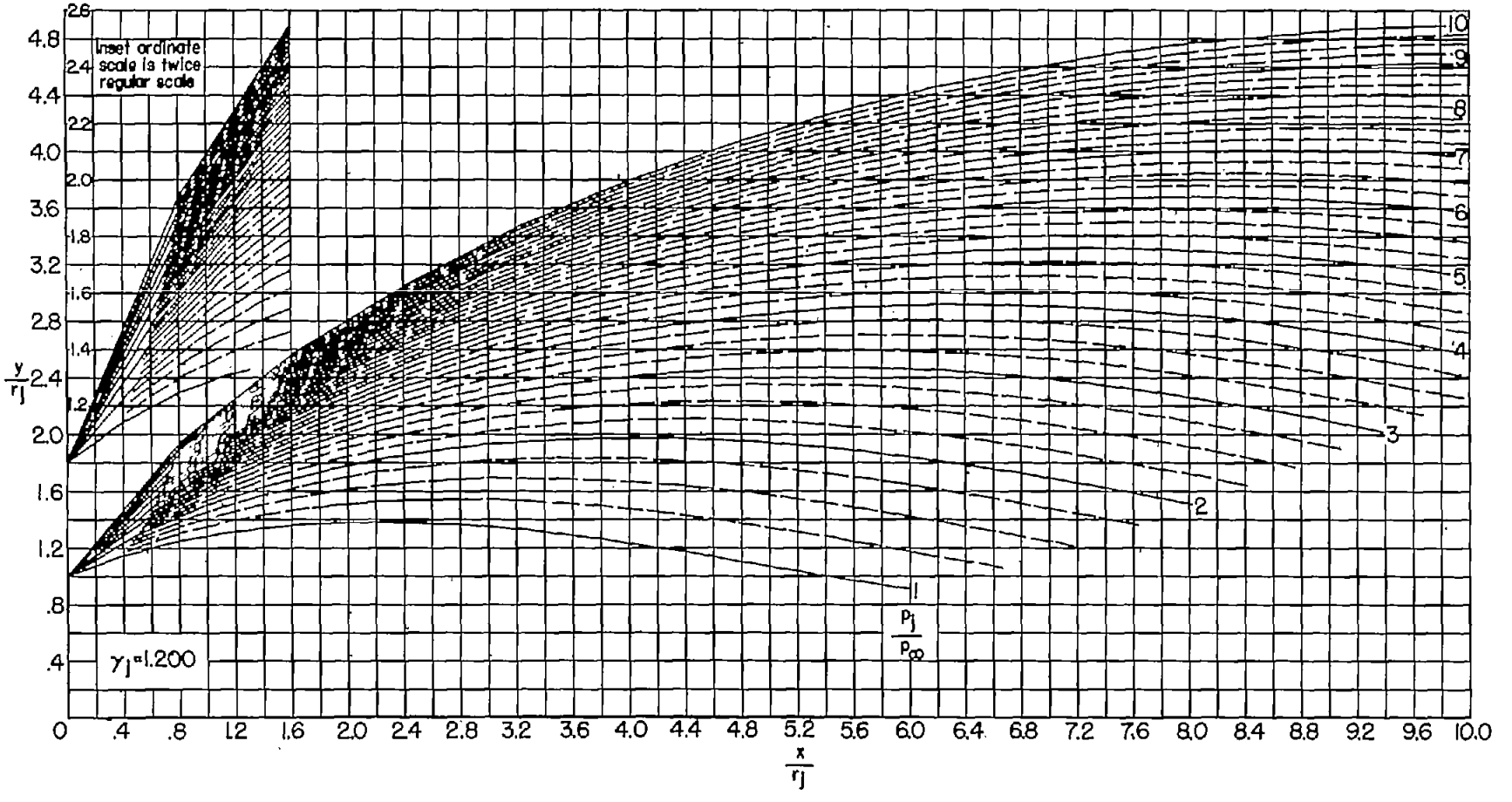


(d) $\theta_N = 20^\circ$. Continued.

Figure 5.- Continued.

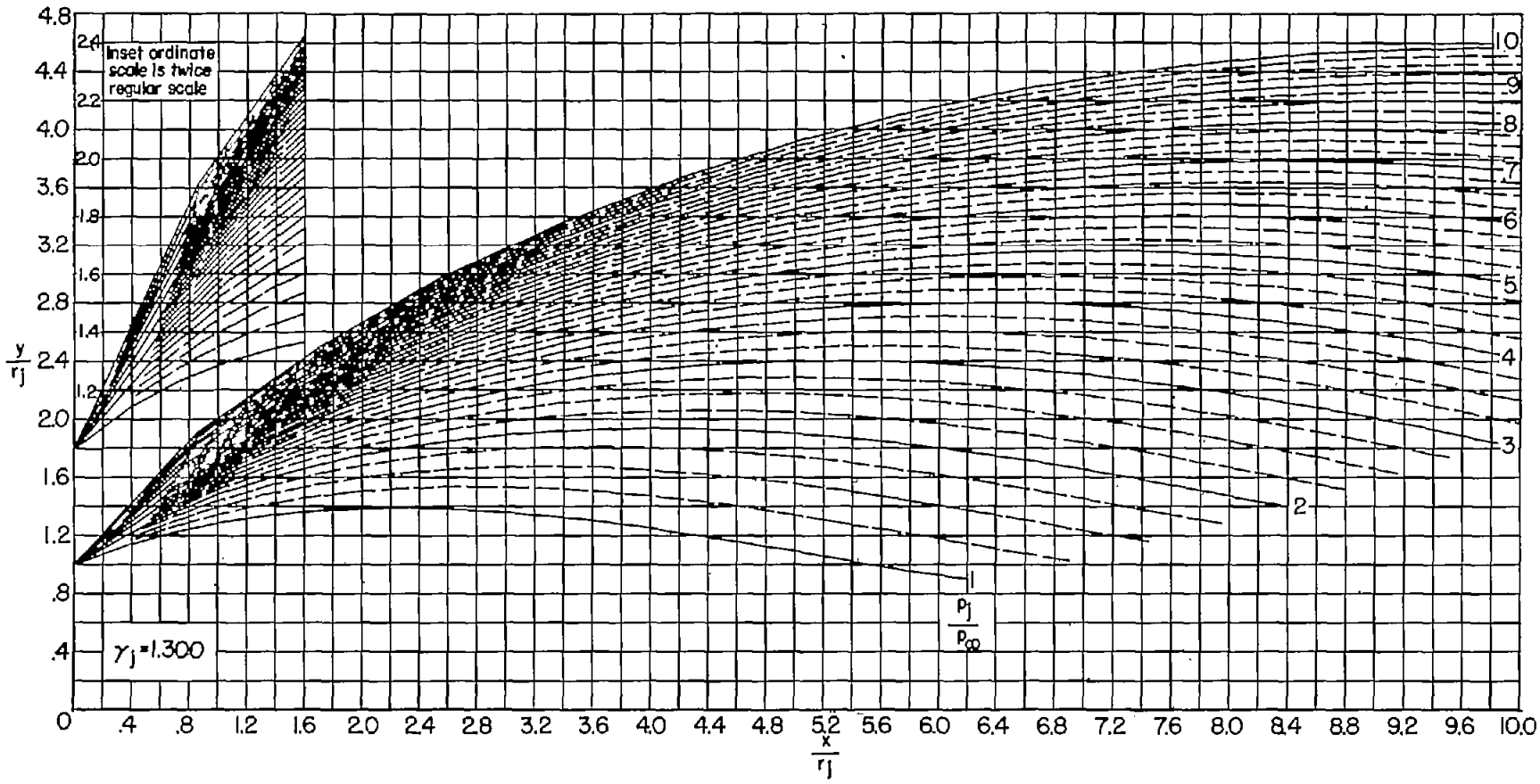


(d) $\theta_N = 20^\circ$. Continued.

Figure 5.- Continued.

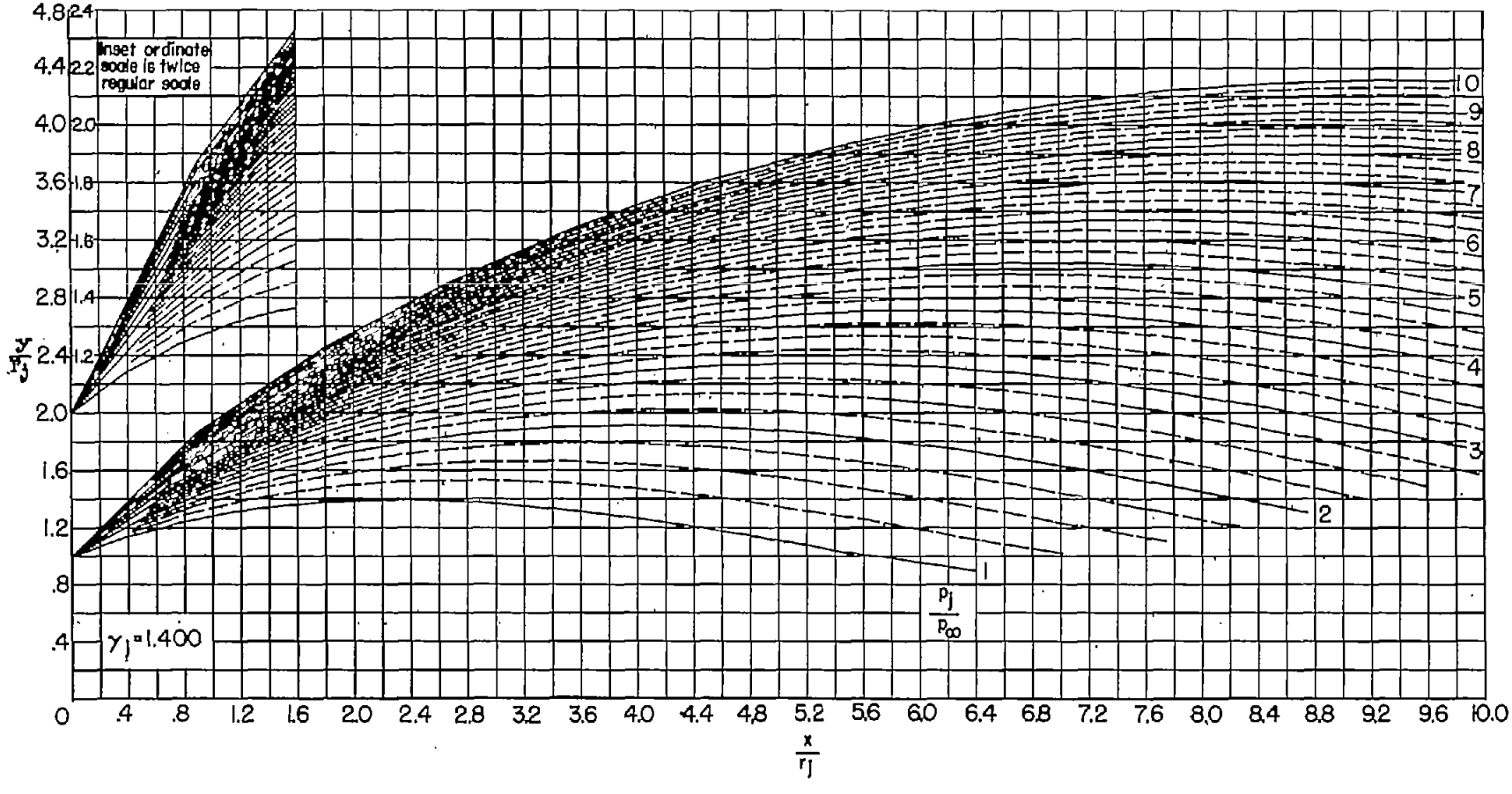


(d) $\theta_N = 20^\circ$. Continued.

Figure 5.- Continued.

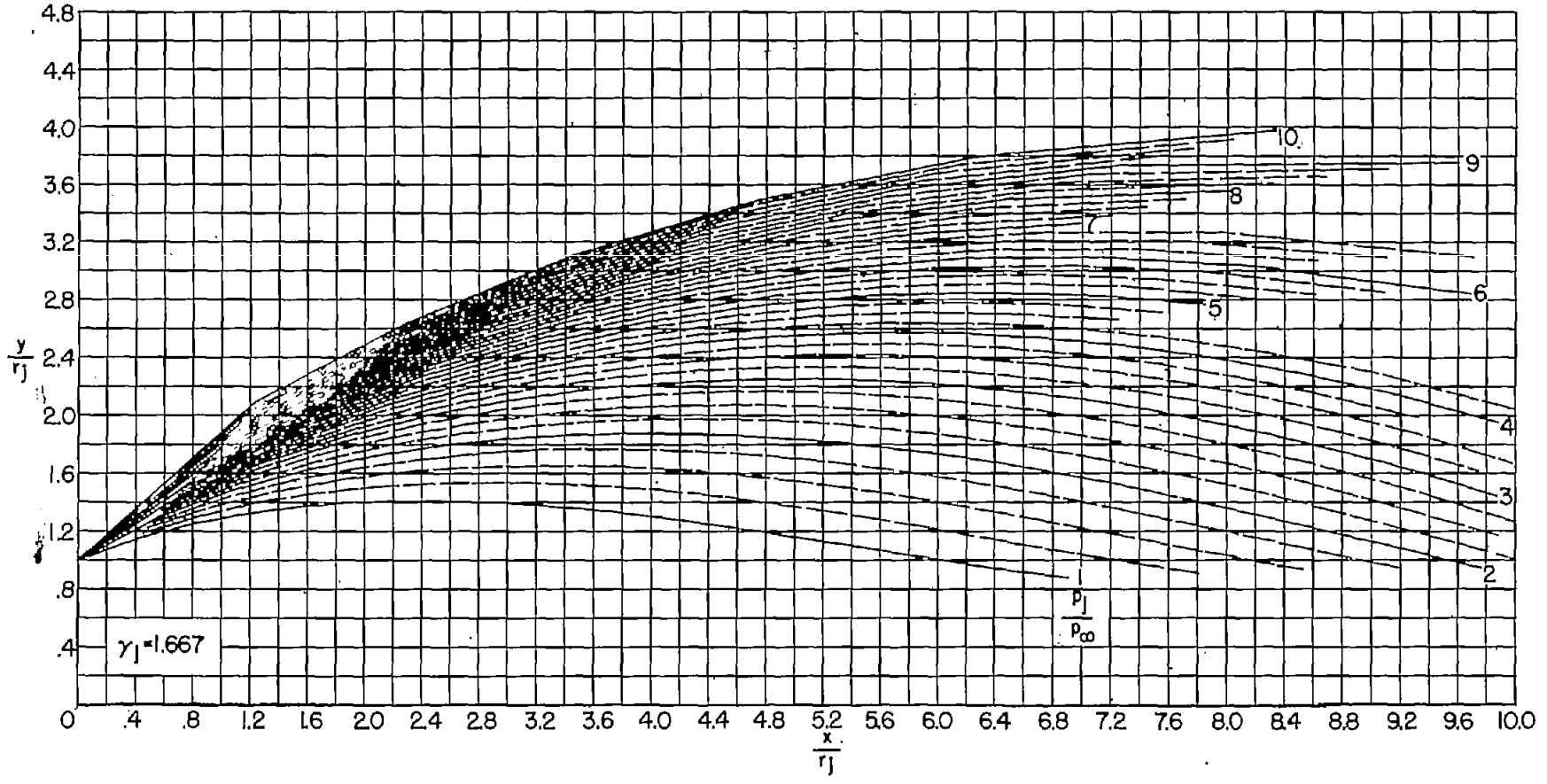


(d) $\theta_N = 20^\circ$. Concluded.

Figure 5.- Concluded.

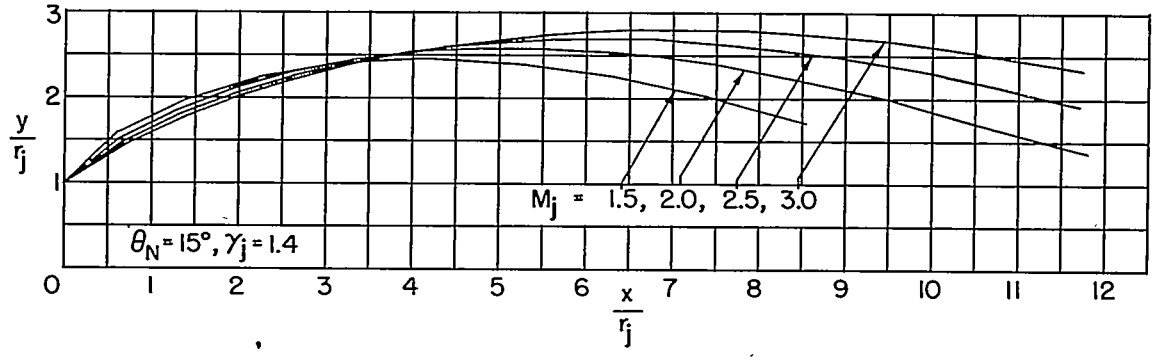


(a) Effect of $M_j$.

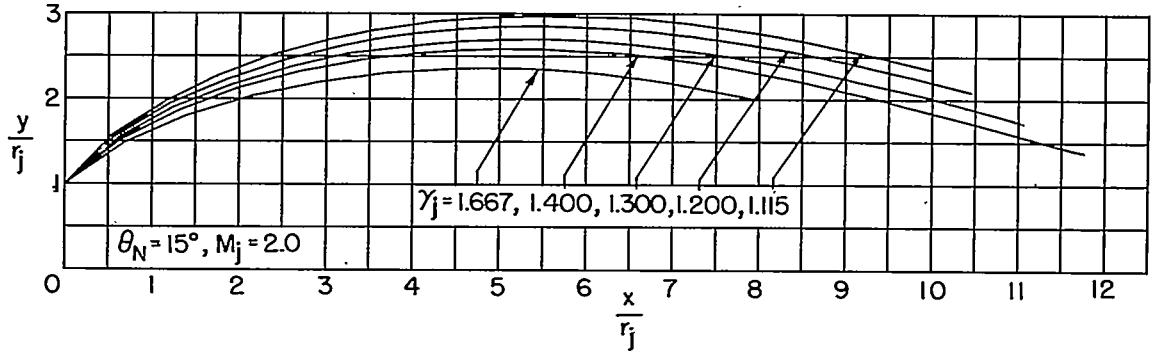


(b) Effect of $\gamma_j$.

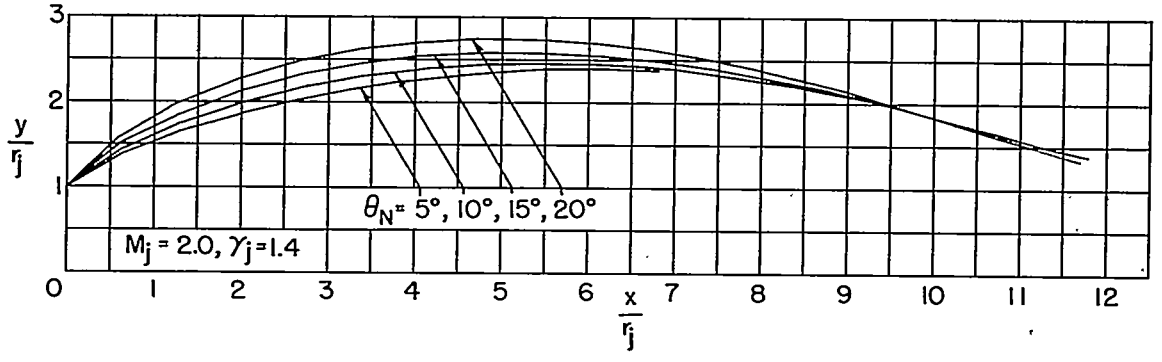


(c) Effect of $\theta_N$.

Figure 6.- Example of the effects of jet Mach number, ratio of specific heats of the jet, and nozzle divergence angle upon the shape of the jet boundary. $p_j/p_\infty = 5$.

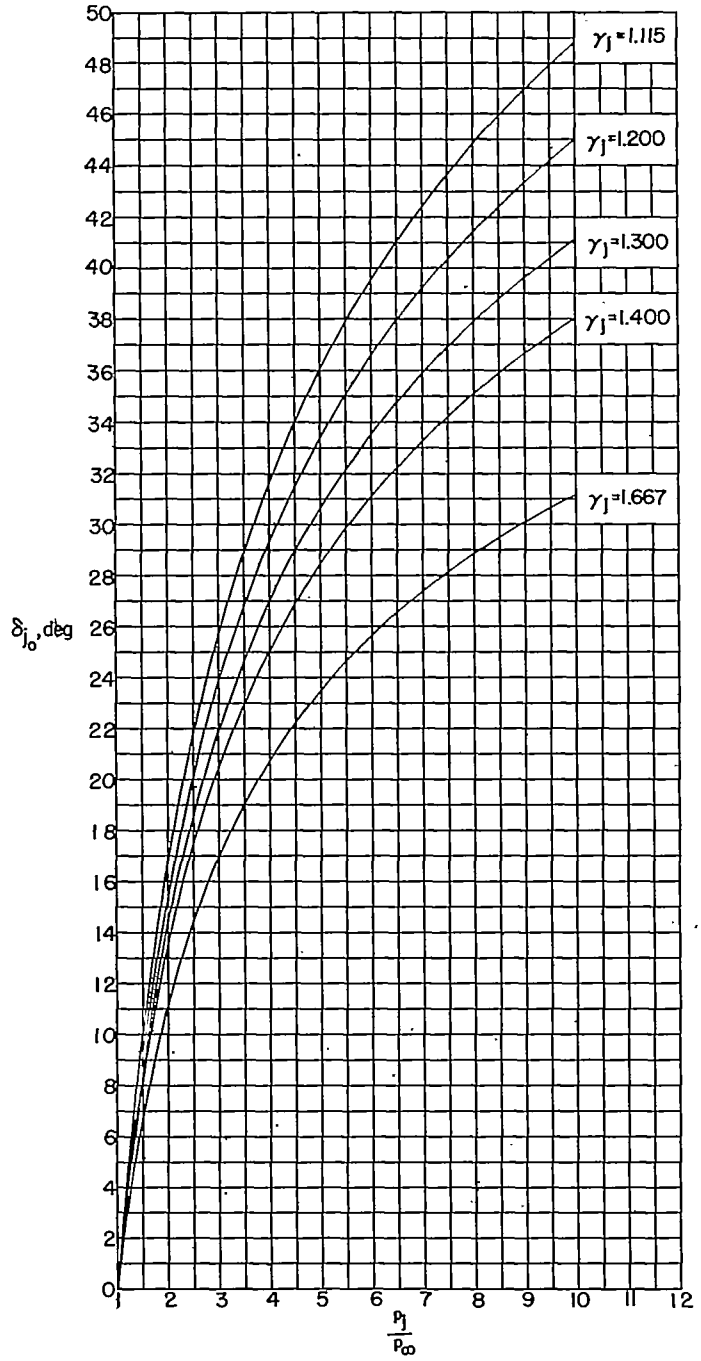


(a) $M_j = 1.5$.

Figure 7.- Effect of jet static-pressure ratio upon the initial inclination of the jet boundary for $\theta_N = 0^\circ$.

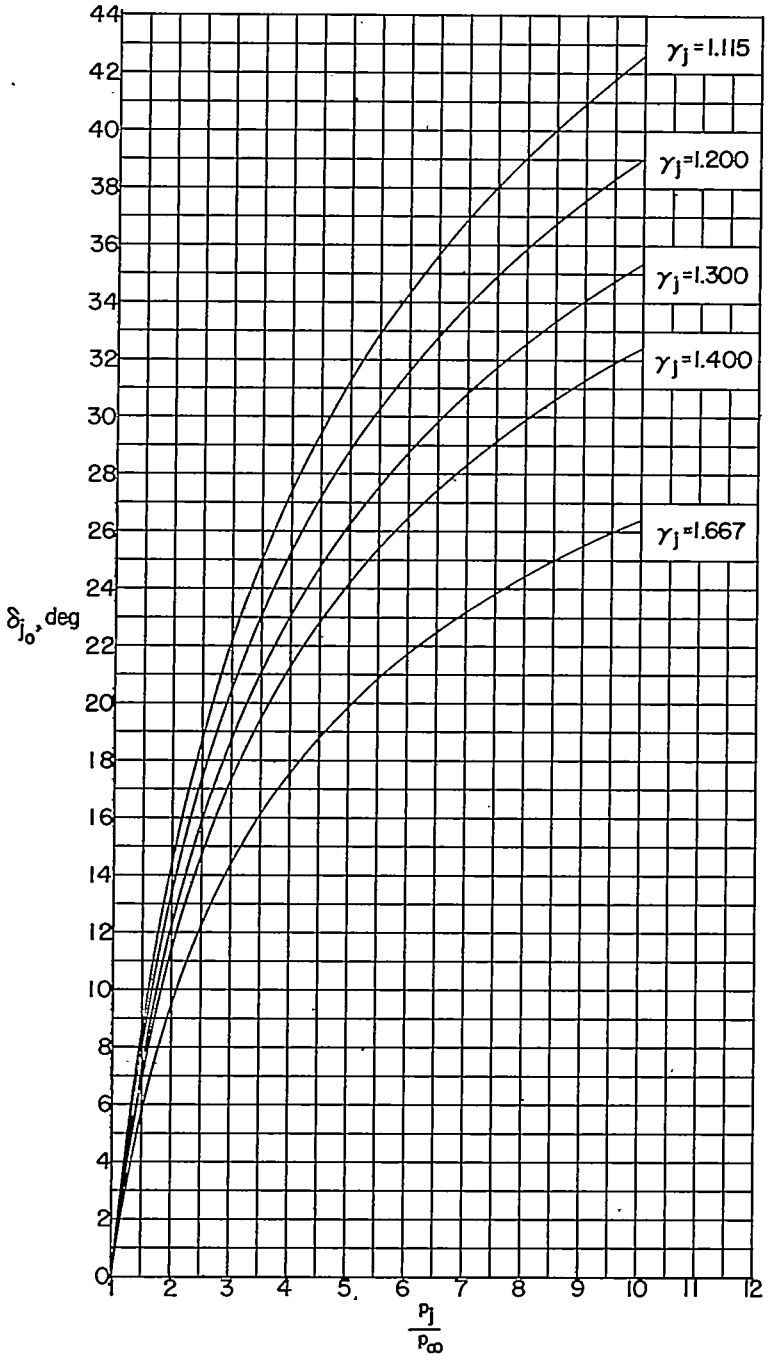


(b) $M_j$ = 2.0.

Figure 7.- Continued.

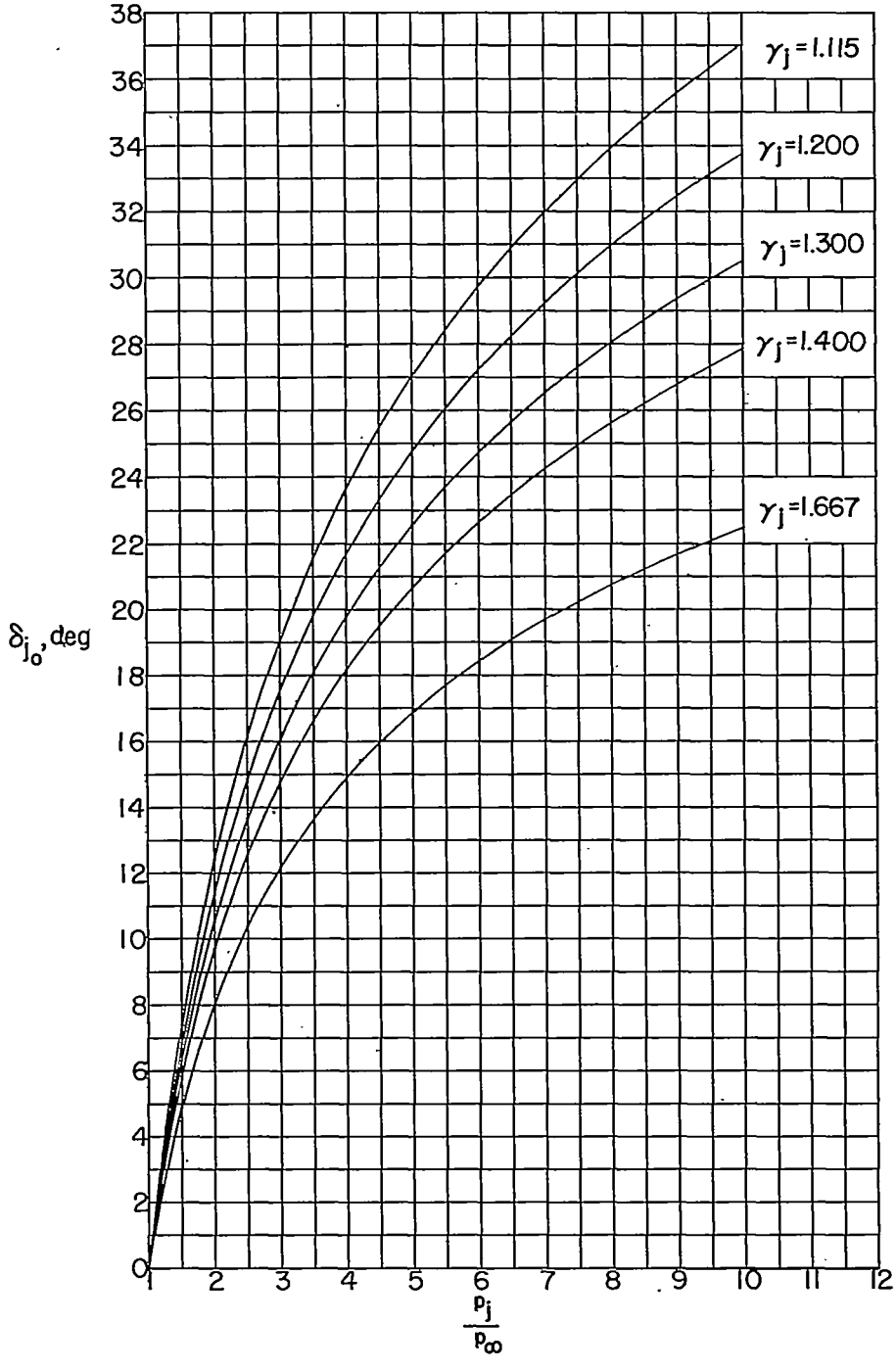


(c) $M_j$ = 2.5.

Figure 7.- Continued.

[redacted]

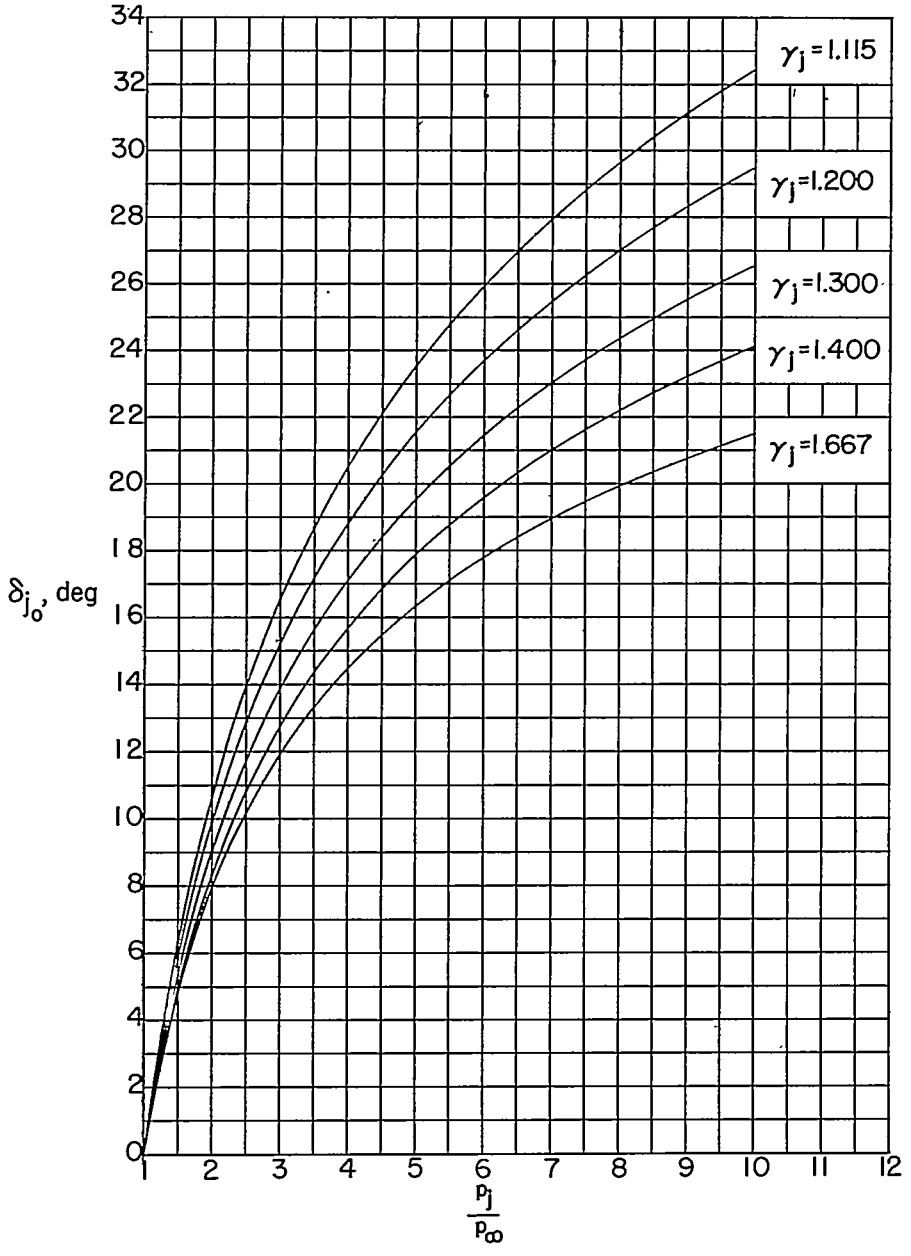


(d) $M_j = 3.0$

Figure 7.- Concluded.

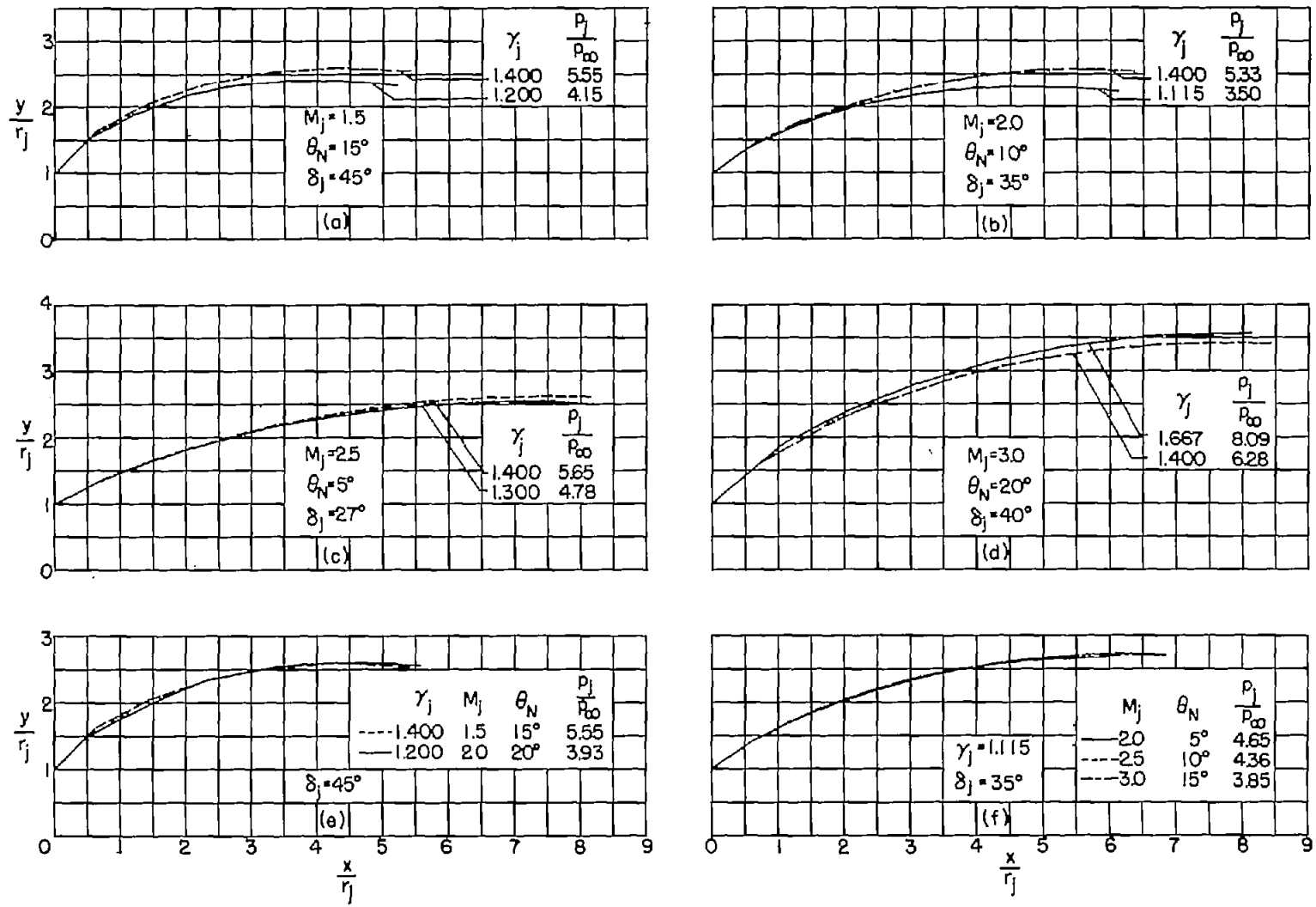


Figure 8.- Examples of jet boundary simulation.

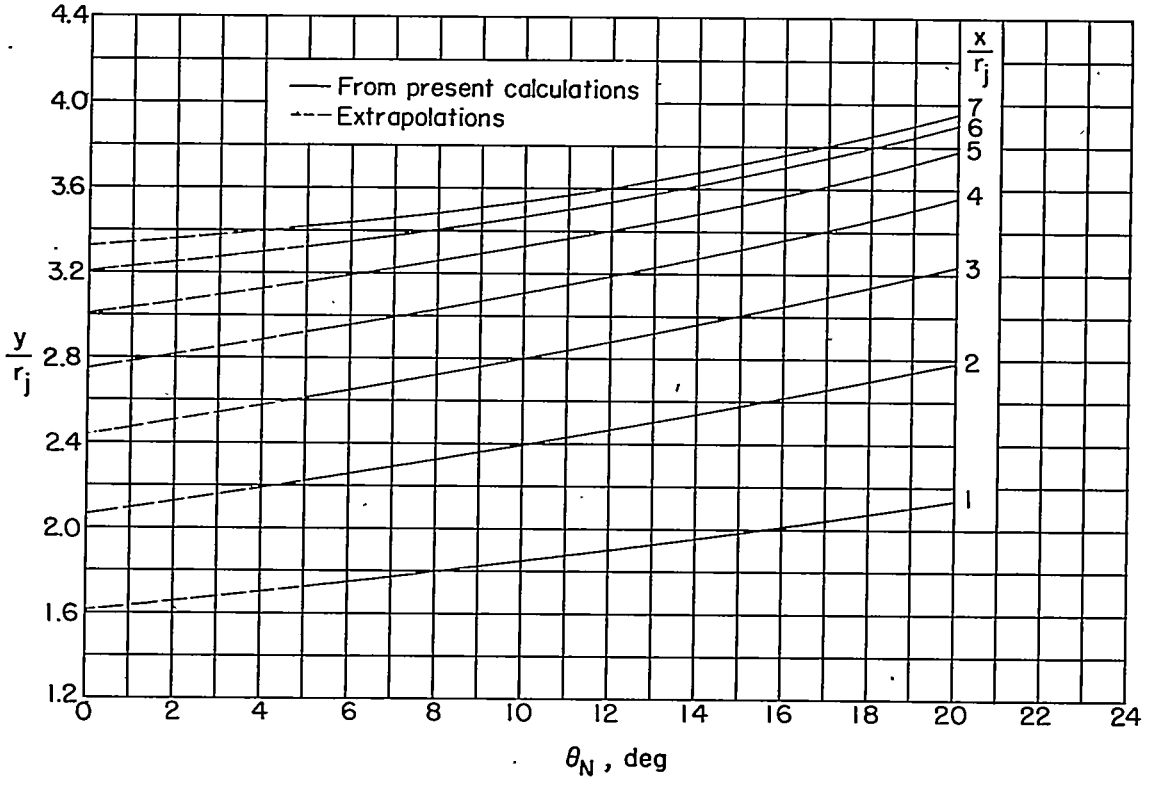


(a) Extrapolation to $\theta_N = 0^\circ$.

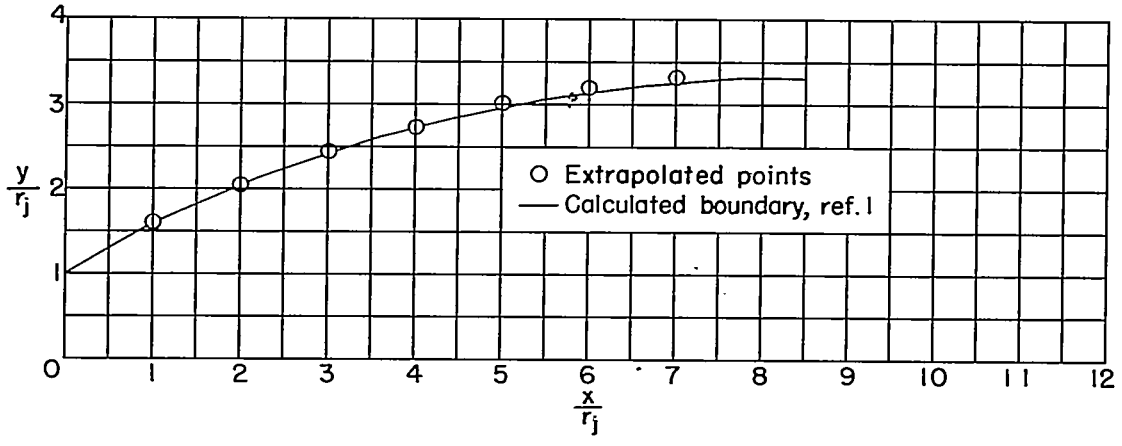


(b) Comparison of extrapolated and calculated boundary.

Figure 9.- Example of extrapolation to $\theta_N = 0^\circ$. $M_j = 2.0$; $\gamma_j = 1.400$; and $p_j/p_\infty = 10$.



NACA - Langley Field, Va.